nature portfolio

https://doi.org/10.1038/s41563-021-01020-4

Supplementary information

Programmable icosahedral shell system for virus trapping

In the format provided by the authors and unedited

Supplementary information

Programmable icosahedral shell system for virus trapping

Christian Sigl[1], Elena M. Willner[1], Wouter Engelen[1], Jessica A. Kretzmann[1], Ken Sachenbacher[1], Anna Liedl[1], Fenna Kolbe[2,3], Florian Wilsch[2,3], S. Ali Aghvami[4], Ulrike Protzer[2,3], Michael F. Hagan[4], Seth Fraden[4], Hendrik Dietz[1]*

[1] Department of Physics, Technical University of Munich, Garching near Munich, Germany
[2] Institute of Virology, School of Medicine, Technical University of Munich, and Helmholtz Zentrum München, Munich, Germany
[3] German Center for Infection Research (DZIF), Munich partner site, Munich, Germany
[4] Department of Physics, Brandeis University, Waltham, MA, United States

*Please address correspondence to: dietz@tum.de

Content:

Supplementary Figures

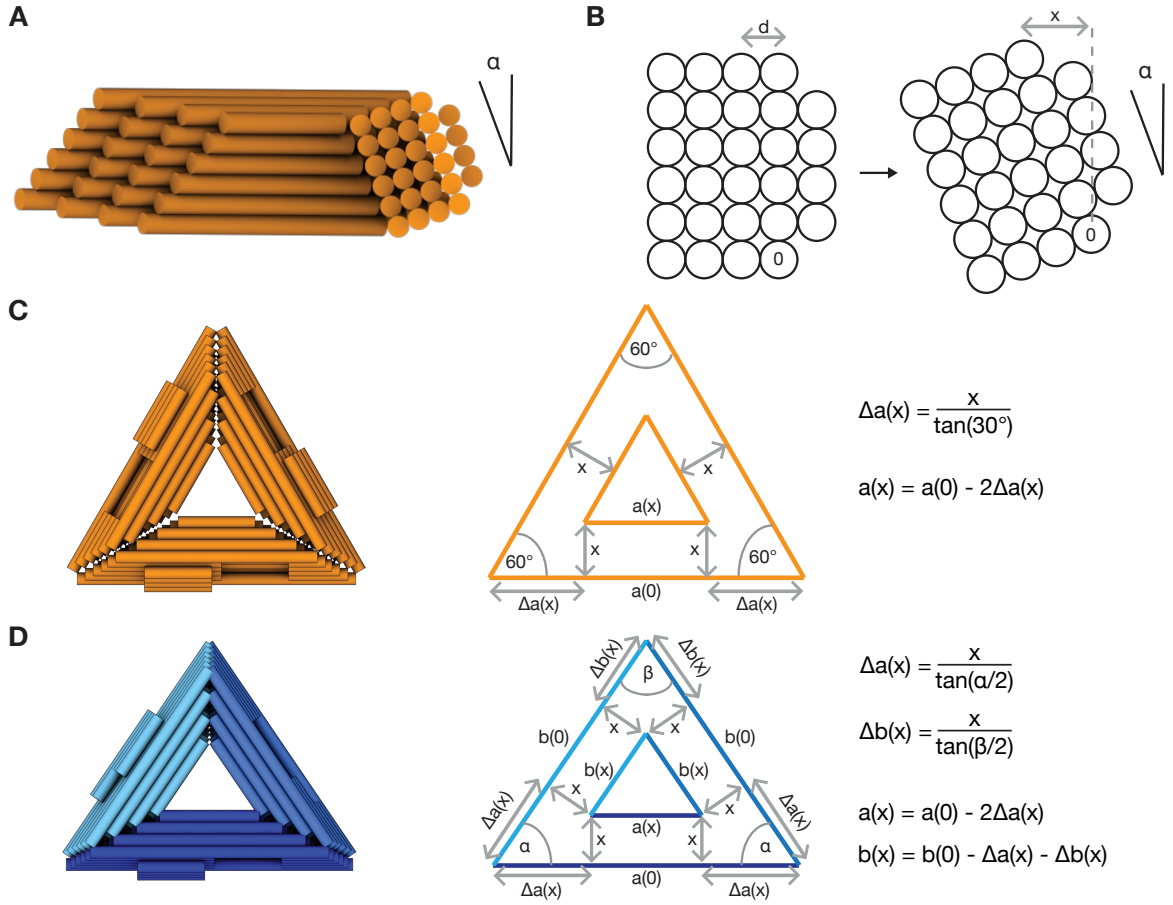

Supplementary Figure 1 | Design principle of triangular subunits. (**A**) Schematics of T=1 triangle design with a bevel angle alpha. (**B**) Cross-section of a triangle's side consisting of 4x6 helices in square-lattice packing without (left) and with (right) a bevel angle. The side is turned around the longest helix indicated by '0'. d is the distance between the center of two neighboring helices (2.6 nm) and x the radial distance of any helix to helix '0'. To transform nm in base pairs we used a rise of 0.34 nm per base pair. (**C** and **D**) Schematic illustrating the calculation of helix lengths. Left, cylindrical model of a triangle. Middle, schematics of the lengths a(x) and b(x) of different helices within the triangle depending on the distance x to helix '0'. Right, formulas to calculate the length differences of individual helices. To compensate for geometrical conflicts arising from mismatched backbone positions at the vertices, we include one single stranded scaffold bases and five single stranded thymine bases for each staple at the corners.

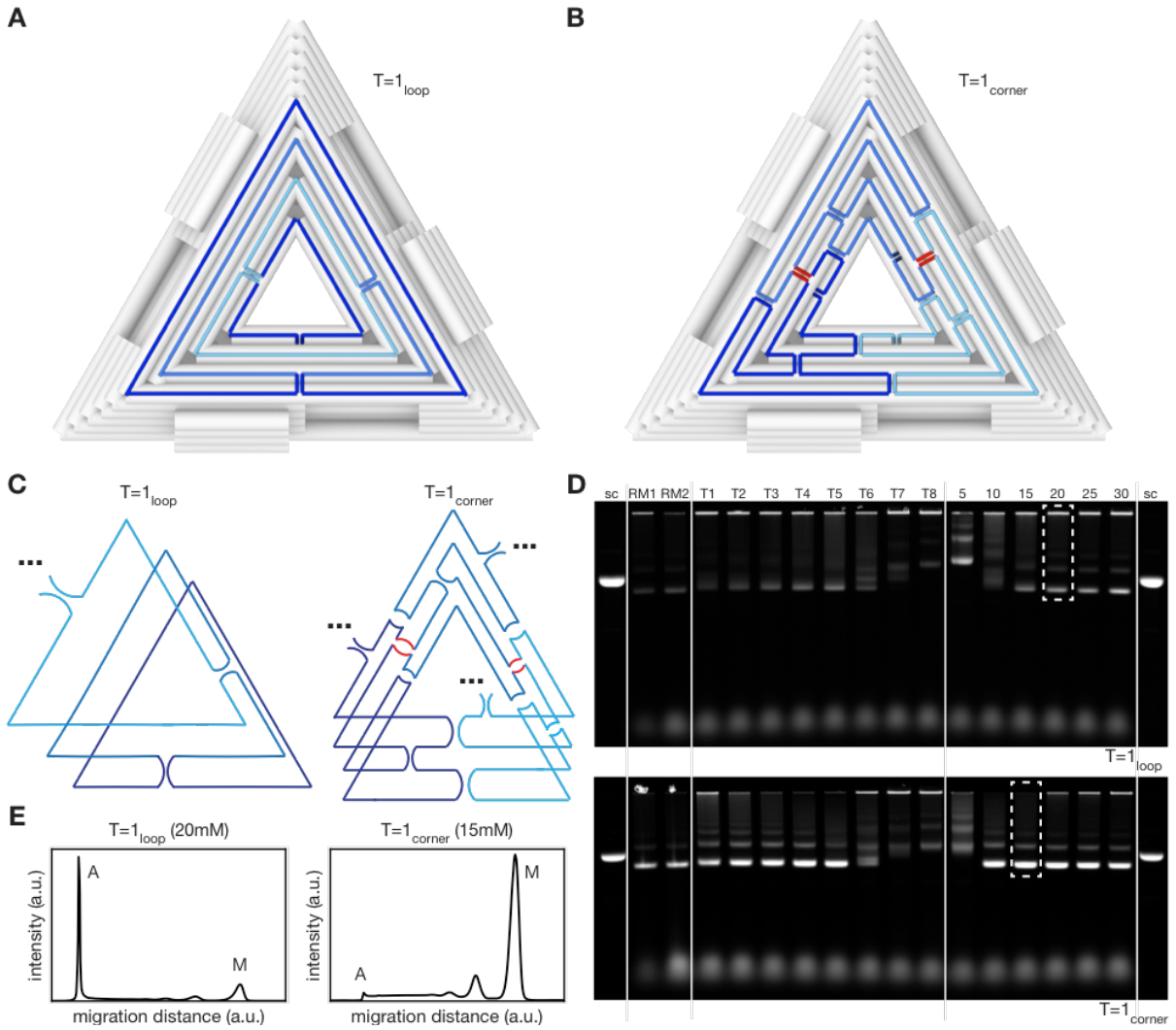

Supplementary Figure 2 | Routing of the scaffold strand through the triangular subunits. (**A**)+(**B**) Cylindrical model of the T=1 triangle with an exemplary routing of the scaffold strand for the first four helices. (A) The scaffold forms a loop around the whole triangle before connecting to the next helix. (B) Each corner is built by a certain scaffold domain (different blues) and is only connected by one cross-over (red) to a neighboring corner. (**C**) Schematic scaffold routing through the triangular structure. Left, routing for $T=1_{loop}$ like in (A). Here, the first three helices are shown exemplarily. Right, routing for $T=1_{corner}$ like in (B). Here, the first four helices are shown exemplarily. (**D**) 1.5% agarose gel containing 0.5xTBE buffer and 5.5 mM $MgCl_2$ showing initial folding screens according to (*47*). sc: M13-8064 scaffold strand as reference. (**E)** Integrated lane profiles of the two lanes indicated by the dotted squares in (D). $T=1_{loop}$ forms a lot of aggregates and less well-formed triangles. Changing the scaffold routing to $T=1_{corner}$ clearly improves the folding yield. Subsequently, all triangles presented in this work are designed with the improved scaffold routing of $T=1_{corner}$. A: malformed aggregates, M: correctly folded monomers.

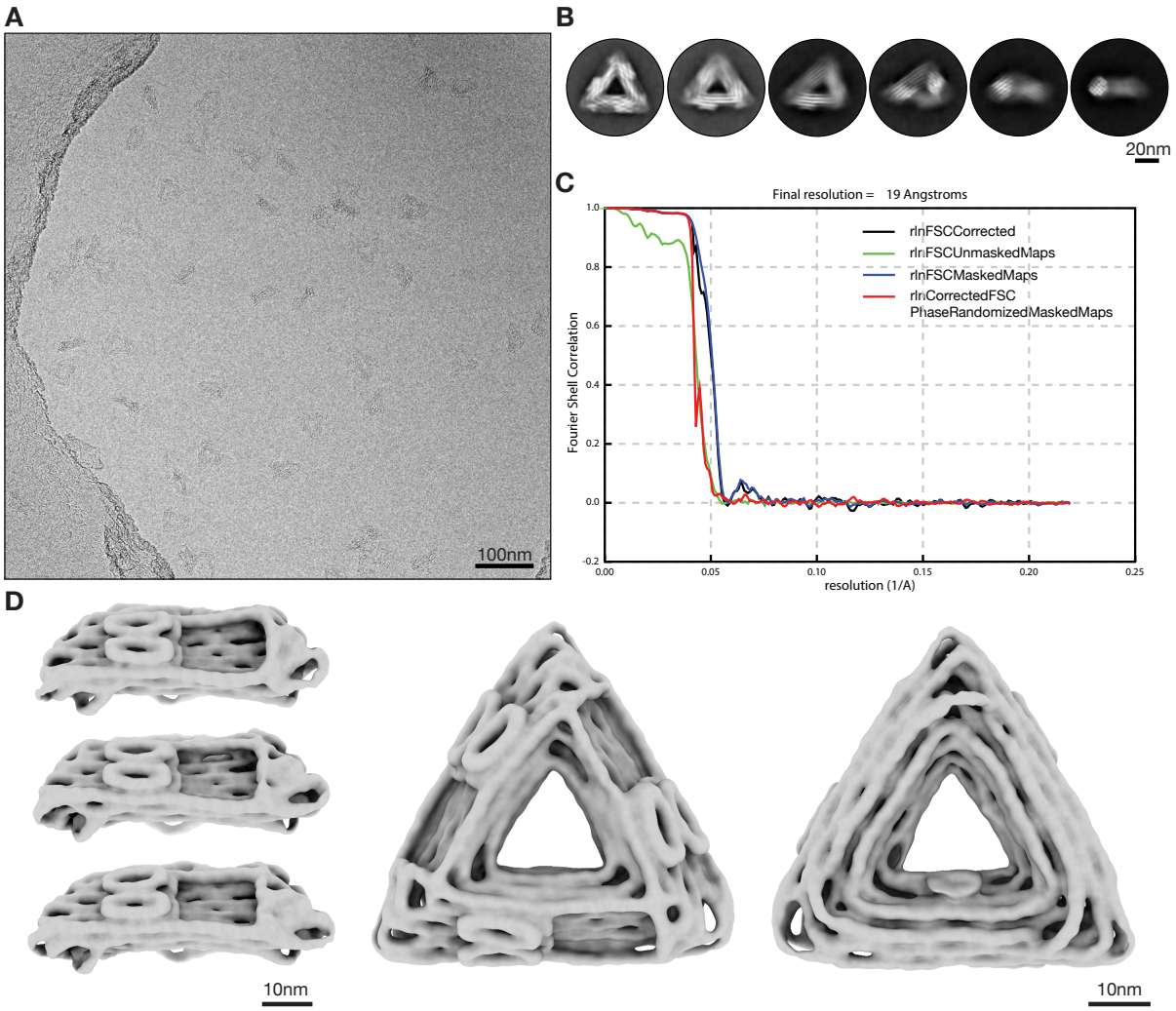

Supplementary Figure 3 | Cryo-EM reconstruction of the octahedron triangle. (**A**) Cryo-EM micrograph of the octahedron triangle in free-standing ice. (**B**) Two-dimensional class averages showing different orientations. (**C**) Graph showing different FSC curves which were used for resolution estimation. (**D**) Electron density map shown from different viewing angles.

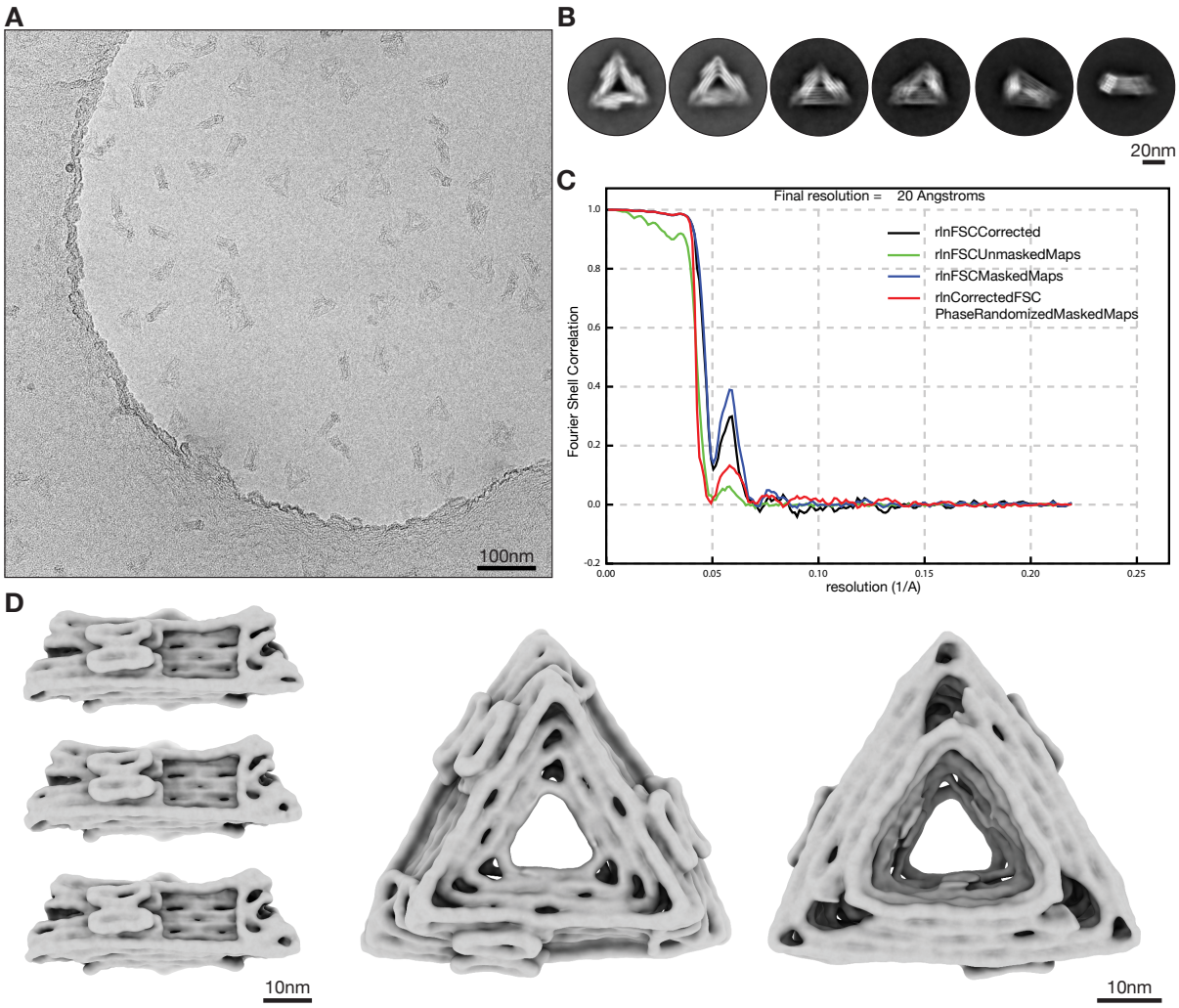

Supplementary Figure 4 | Cryo-EM reconstruction of the T=1 triangle. (**A**) Cryo-EM micrograph of the T=1 triangle in free-standing ice. (**B**) Two-dimensional class averages showing different orientations. (**C**) Graph showing different FSC curves which were used for resolution estimation. (**D**) Electron density map shown from different viewing angles.

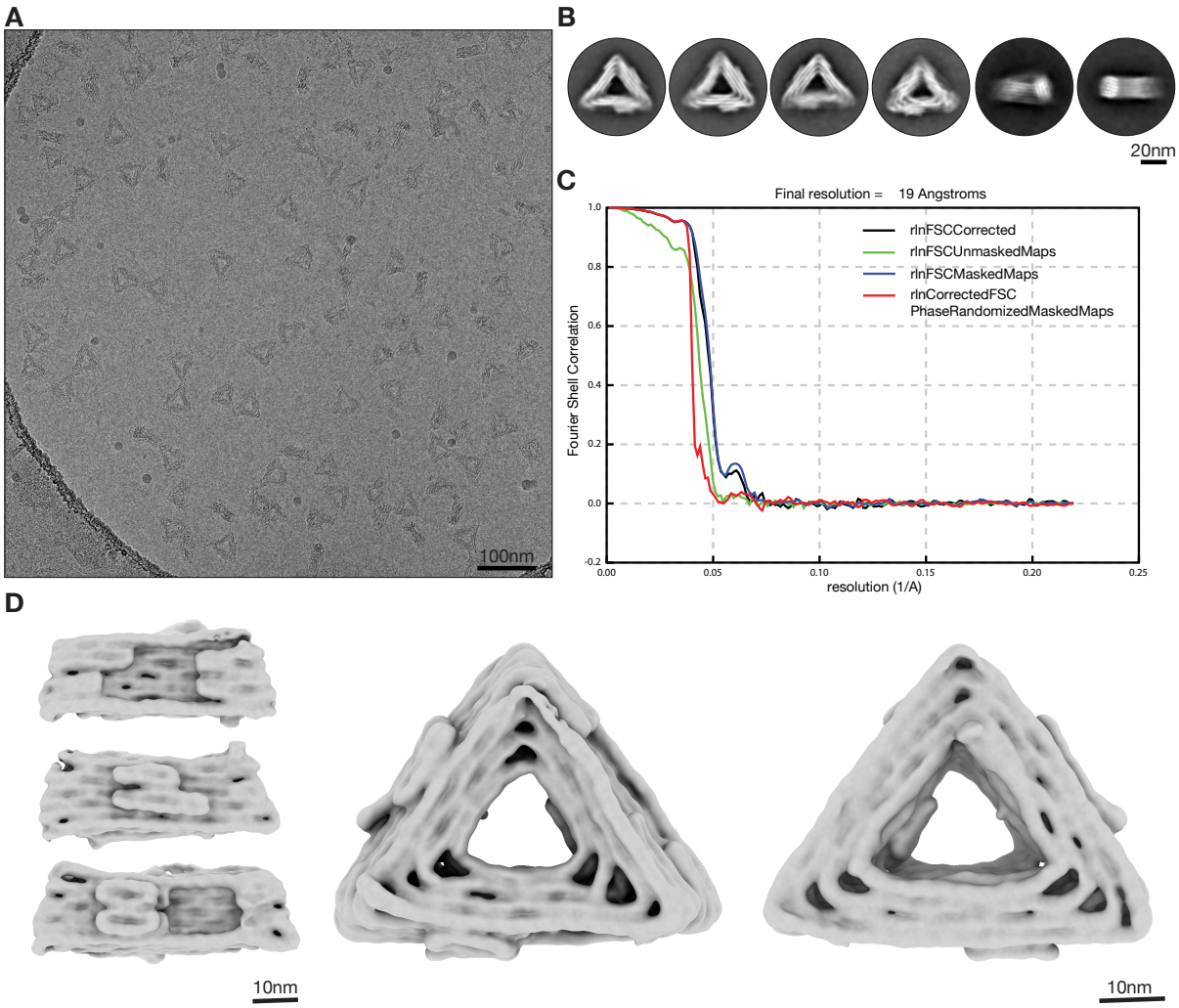

Supplementary Figure 5 | Cryo-EM reconstruction of the T=3 triangle. (**A**) Cryo-EM micrograph of the T=3 triangle in free-standing ice. (**B**) Two-dimensional class averages showing different orientations. (**C**) Graph showing different FSC curves which were used for resolution estimation. (**D**) Electron density map shown from different viewing angles.

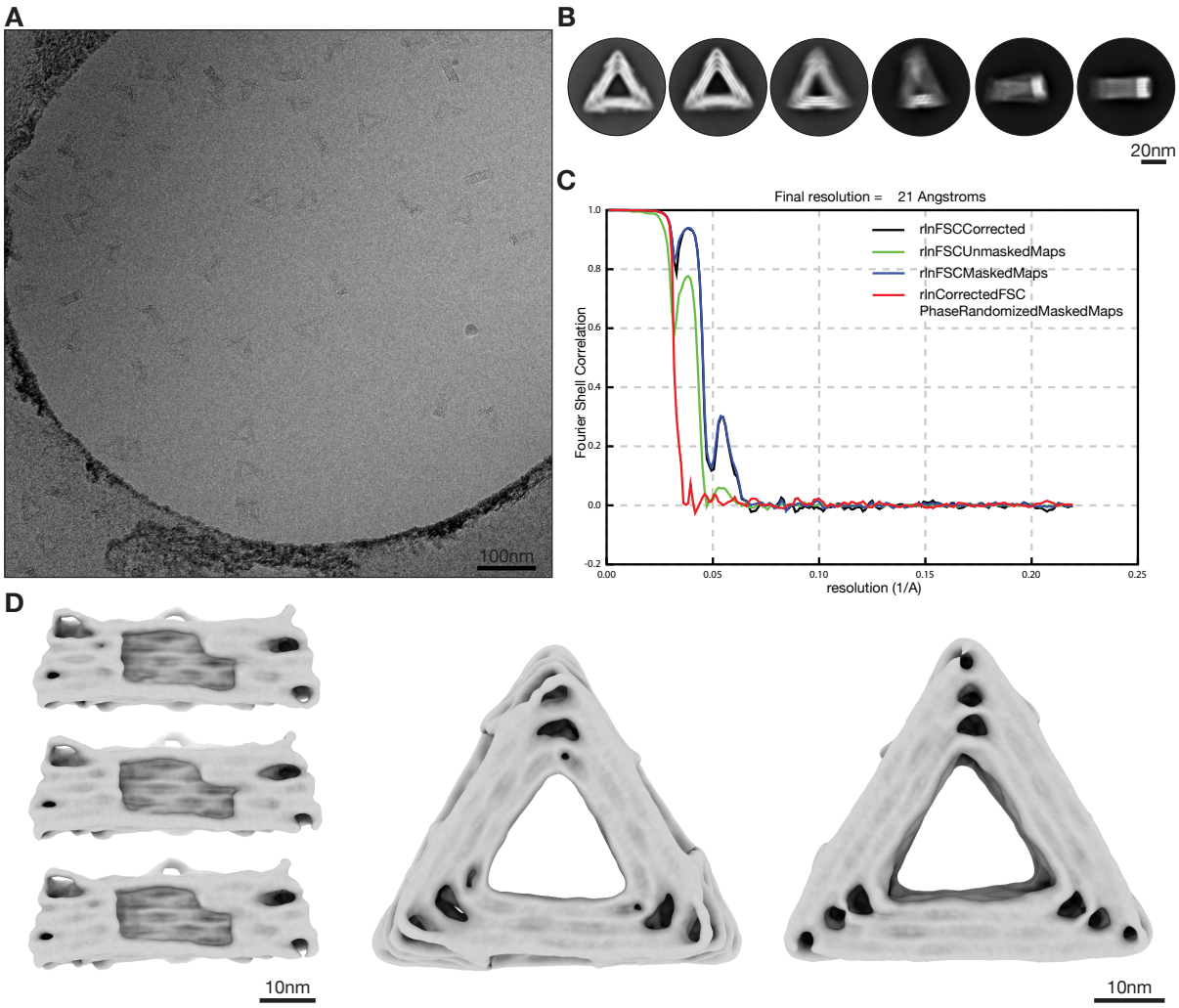

Supplementary Figure 6 | Cryo-EM reconstruction of the T=4 triangle T_{equi}. (**A**) Cryo-EM micrograph of the T_{equi} triangle in free-standing ice. (**B**) Two-dimensional class averages showing different orientations. (**C**) Graph showing different FSC curves which were used for resolution estimation. (**D**) Electron density map shown from different viewing angles.

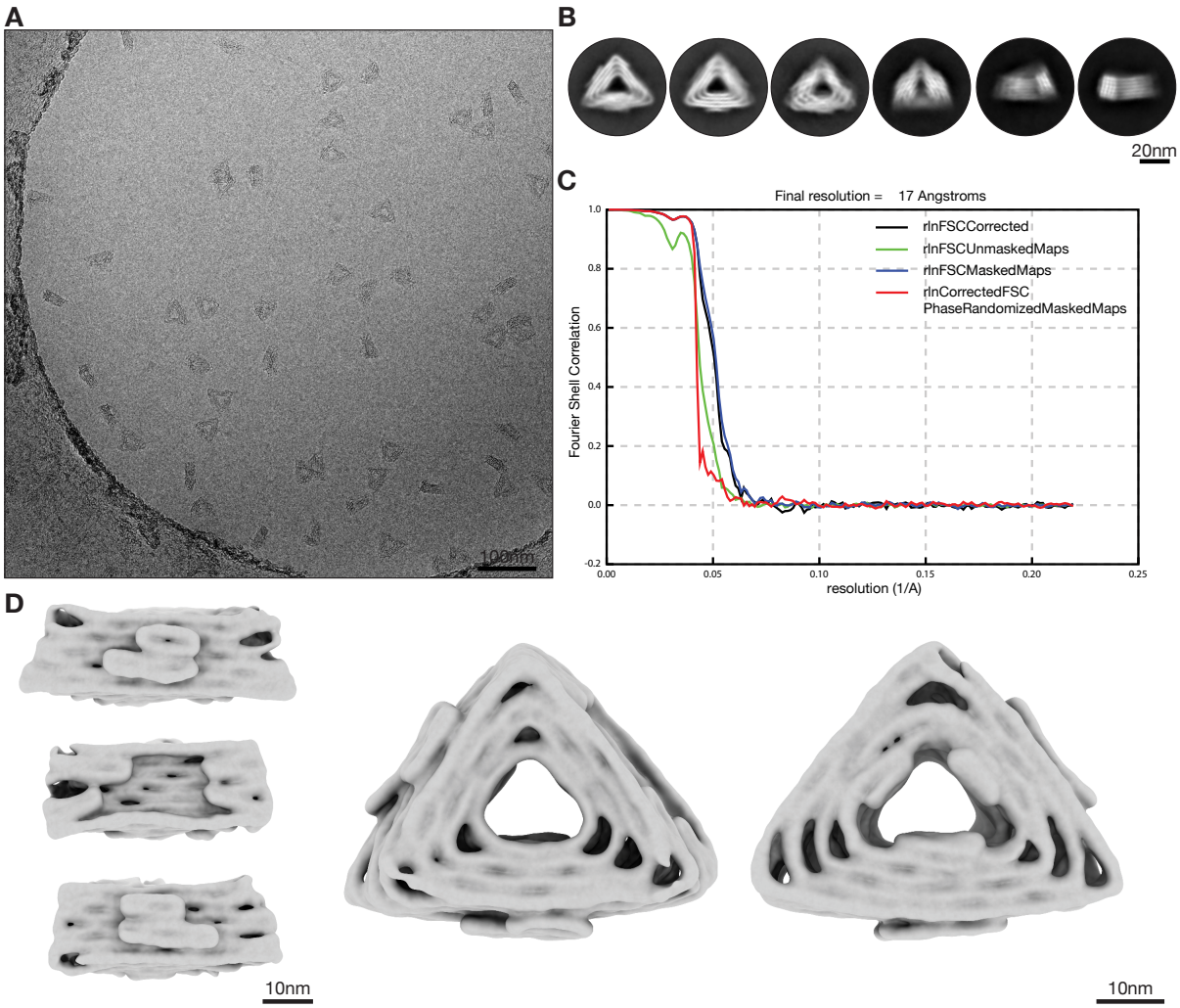

Supplementary Figure 7 | Cryo-EM reconstruction of the T=4 triangle T_{iso}. (**A**) Cryo-EM micrograph of the T_{iso} triangle in free-standing ice. (**B**) Two-dimensional class averages showing different orientations. (**C**) Graph showing different FSC curves which were used for resolution estimation. (**D**) Electron density map shown from different viewing angles.

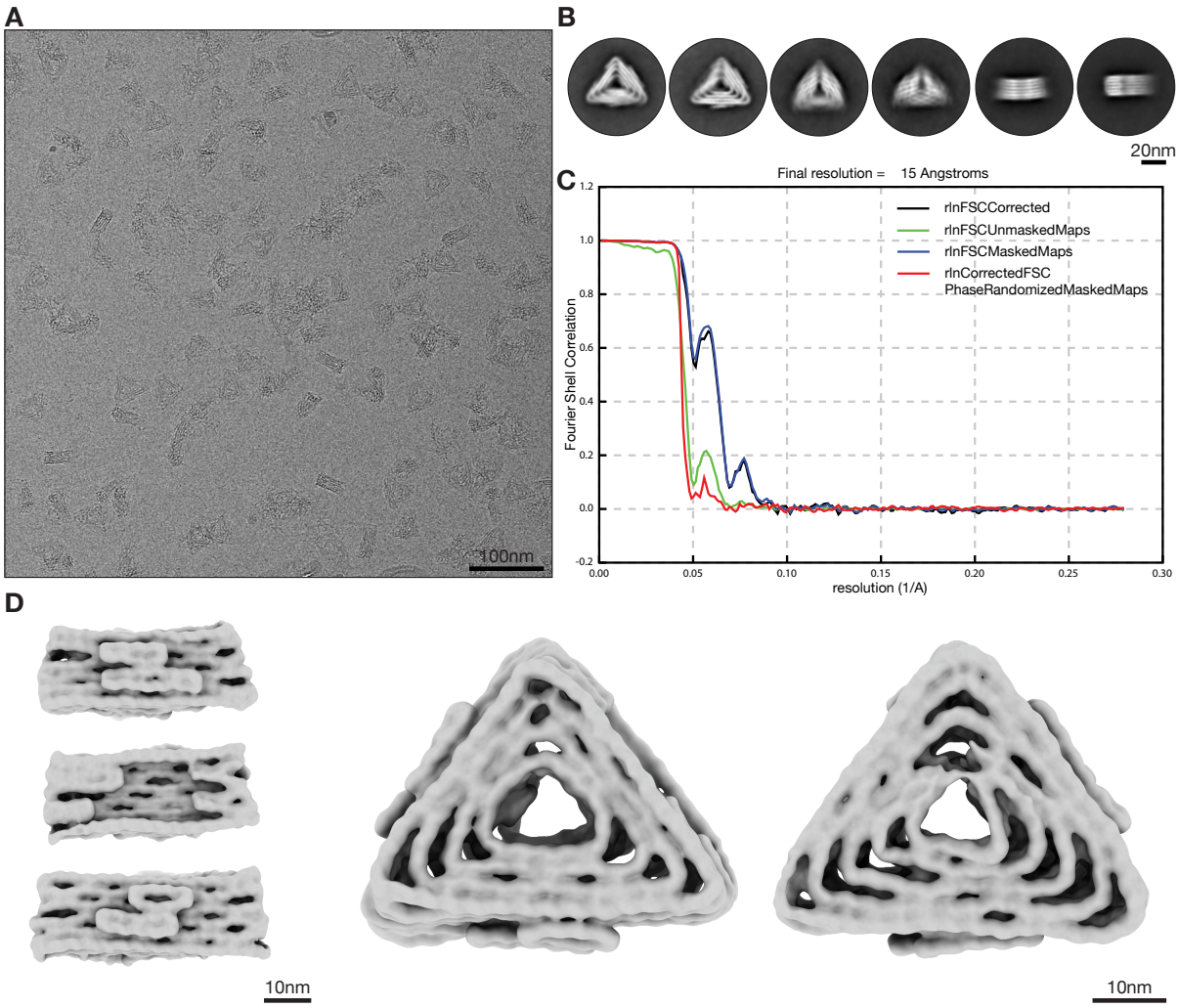

Supplementary Figure 8 | Cryo-EM reconstruction of the T=9 triangle T_{pent}. (**A**) Cryo-EM micrograph of the T_{pent} triangle in free-standing ice. (**B**) Two-dimensional class averages showing different orientations. (**C**) Graph showing different FSC curves which were used for resolution estimation. (**D**) Electron density map shown from different viewing angles.

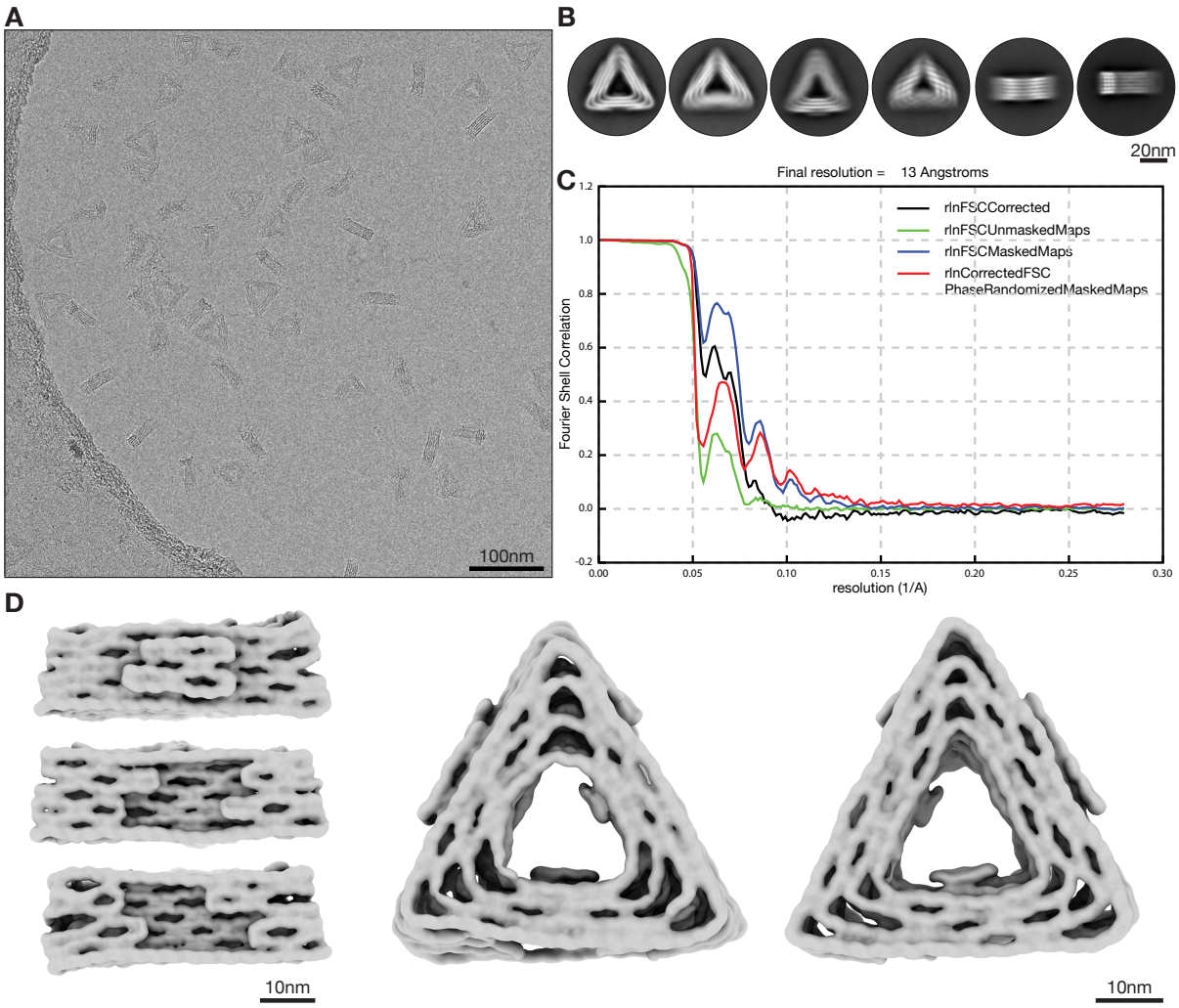

Supplementary Figure 9 | Cryo-EM reconstruction of the T=9 triangle T_{hex1}. (**A**) Cryo-EM micrograph of the T_{hex1} triangle in free-standing ice. (**B**) Two-dimensional class averages showing different orientations. (**C**) Graph showing different FSC curves which were used for resolution estimation. (**D**) Electron density map shown from different viewing angles.

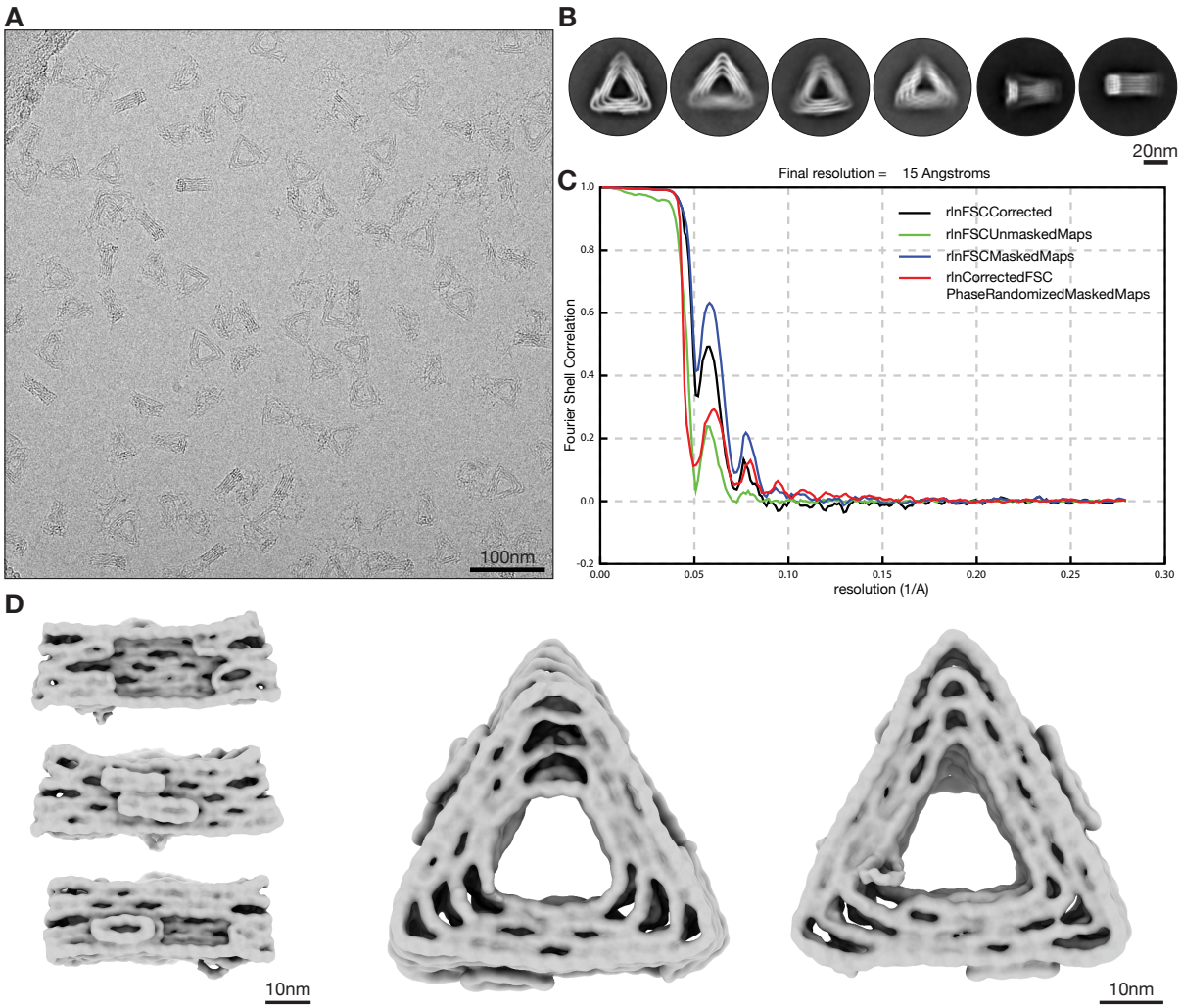

Supplementary Figure 10 | Cryo-EM reconstruction of the T=9 triangle T_{hex2}. (**A**) Cryo-EM micrograph of the T_{hex2} triangle in free-standing ice. (**B**) Two-dimensional class averages showing different orientations. (**C**) Graph showing different FSC curves which were used for resolution estimation. (**D**) Electron density map shown from different viewing angles.

	Octa	T=1	T=3	T=4 (equi)	T=4 (iso)	T=9 (pent)	T=9 (hex1)	T=9 (hex2)
measure angle	34.9°	23.8°	13.7°	6.2°	11.0°	7.1°	3.8°	5.1°
theoretical angle	35.3°	20.9°	11.6°	10.1°	10.1°	6.6°	6.6°	6.6°

Supplementary Table 1 | Measured bevel angles of cryo-EM reconstructions. Measured angle: bevel angle measured in chimera from the cryo-EM reconstructions of the single triangles. Theoretical angle: desired angle for shell assembly.

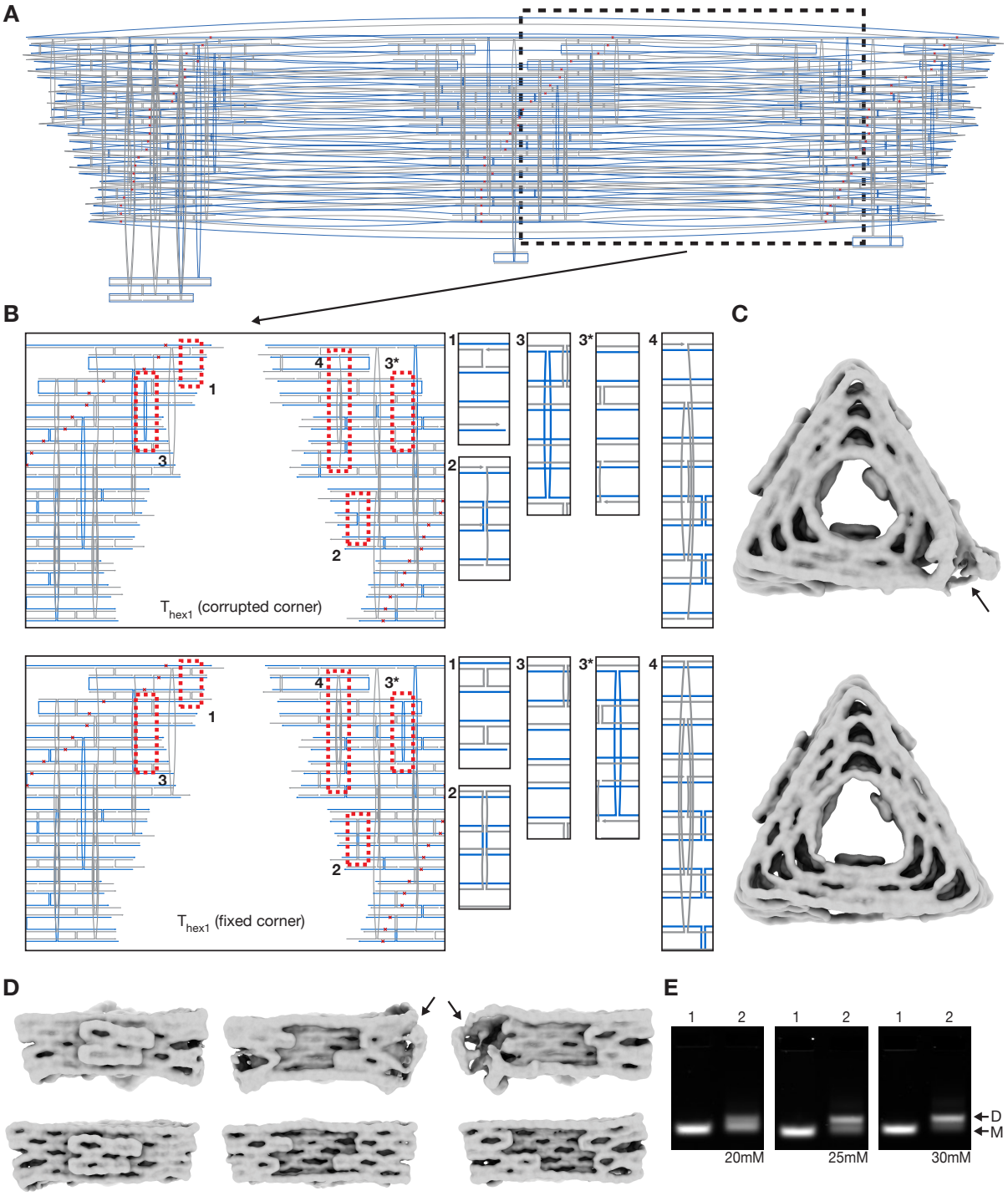

Supplementary Figure 11 | Correction for folding defects in T_{hex1}. (**A**) Design diagram of the T_{hex1} triangle with fixed corner. (**B**) Zoom-in on the location of the corrupted corner showing the differences between the two versions in the design diagram. (**C** and **D**) Cryo-EM map of the two T_{hex1} triangle versions. The arrows indicate the location of the corrupted corner. (**E**) 1.5% agarose gels with different $MgCl_2$ concentrations showing the dimerization of T_{pent} and T_{hex1} triangles. All sides not involved in the binding of the two triangles were passivated with polyT extensions at the stacking contacts. While the corrupted corner prevents the two triangles to bind to each other because of missing stacking contacts, the triangle with fixed corners binds to T_{pent} and assembles into dimers. Lane 1: T_{pent} + T_{hex1} (corrupted corner), Lane 2: T_{pent} + T_{hex1} (fixed corner). D: dimer, M: monomer.

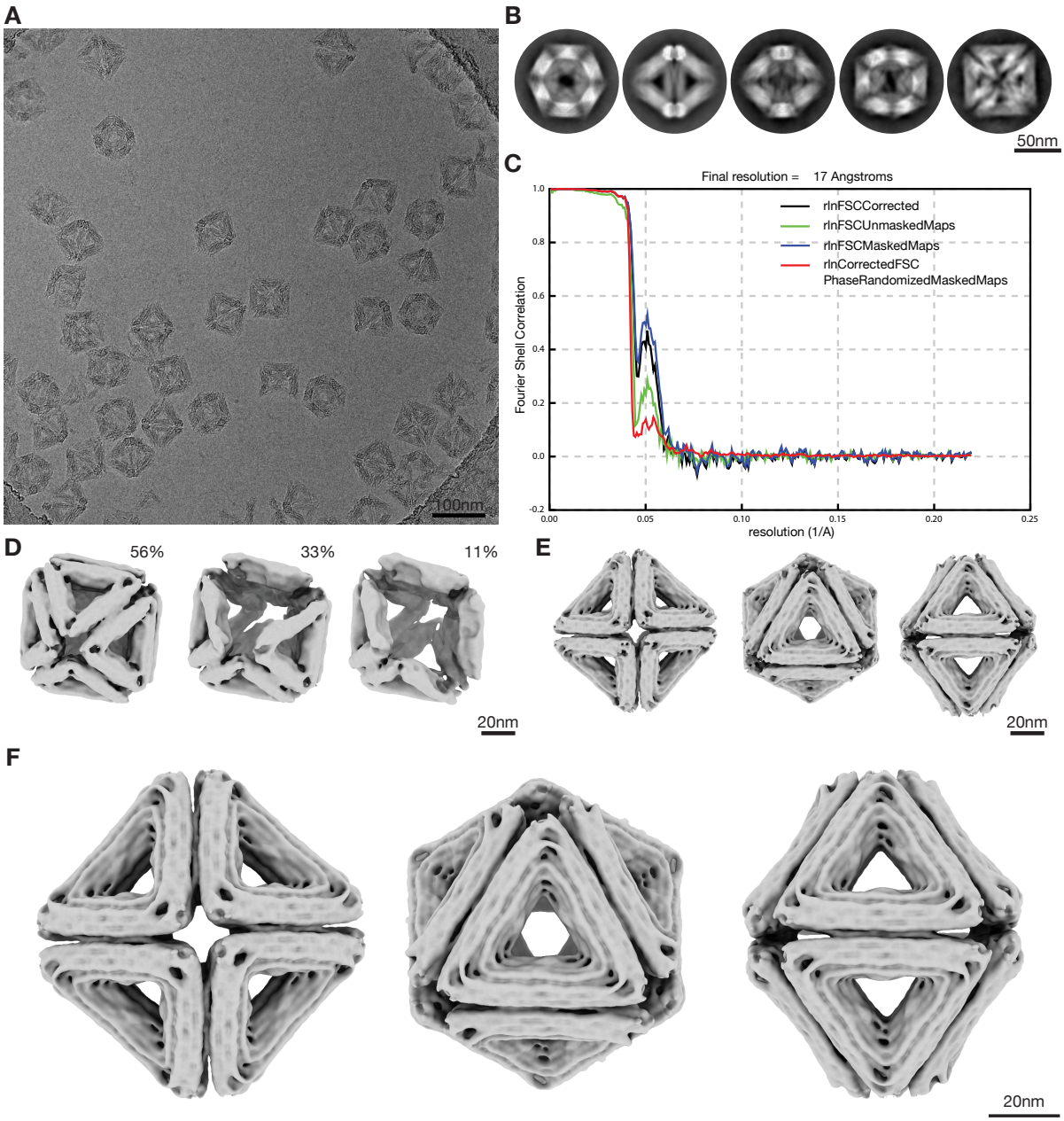

Supplementary Figure 12 | Cryo-EM reconstruction of the assembled octahedron at 17.5 mM $MgCl_2$. (**A**) Cryo-EM micrograph of the octahedron in free-standing ice at 17.5 mM $MgCl_2$. (**B**) Two-dimensional class averages showing different orientations. (**C**) Graph showing different FSC curves which were used for resolution estimation. (**D**) Classes after 3d classification in relion3. (**E**) Refinement without using any symmetry (C1). (**F**) Electron density map shown from the 4-fold, 3-fold and 2-fold symmetry axis (left to right).

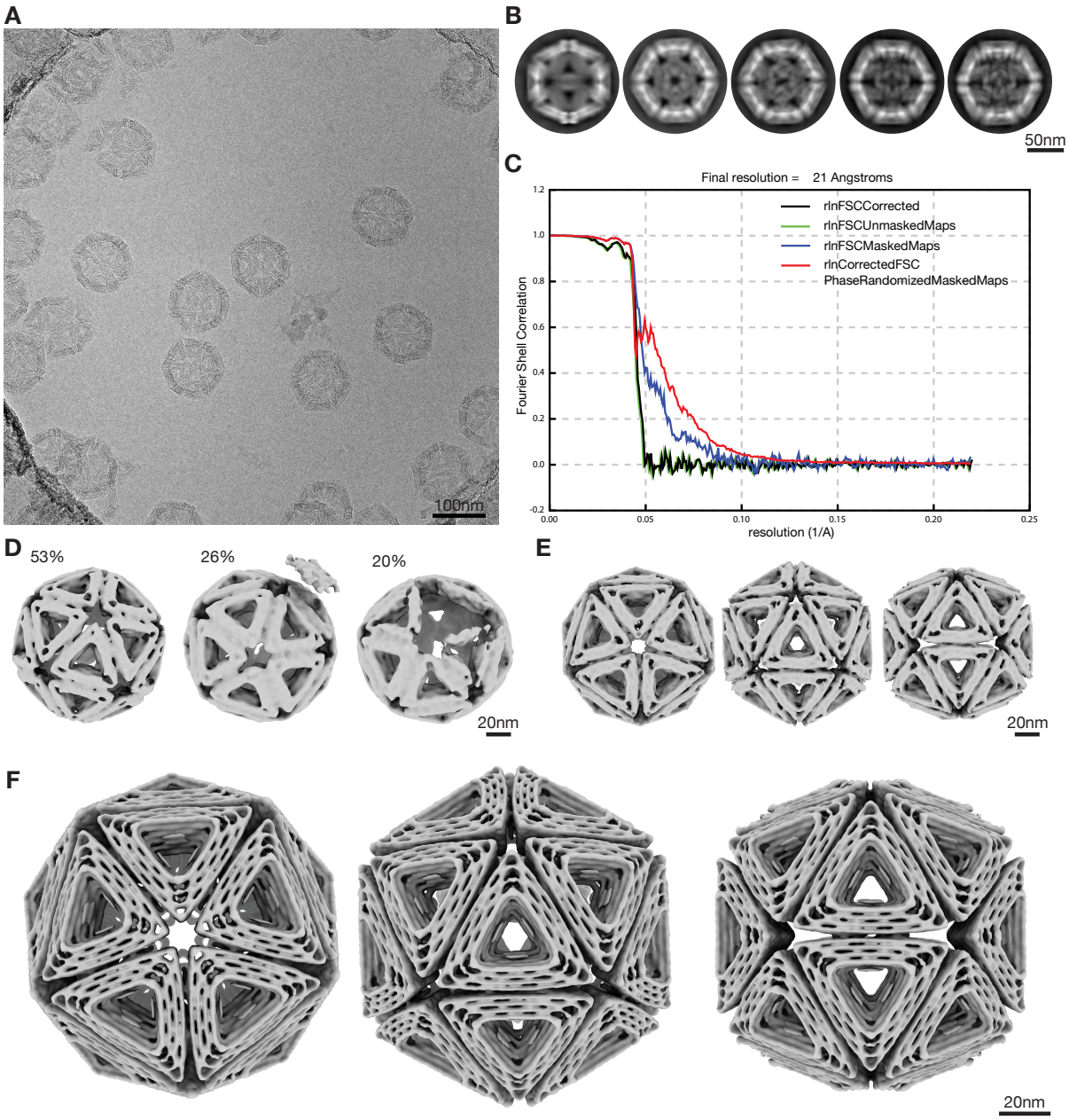

Supplementary Figure 13 | Cryo-EM reconstruction of the T=1 shell at 20 mM $MgCl_2$. (**A**) Cryo-EM micrograph of the T=1 shell in free-standing ice. (**B**) Two-dimensional class averages showing different orientations. (**C**) Graph showing different FSC curves which were used for resolution estimation. (**D**) Classes after 3d classification in relion3. (**E**) Refinement without using any symmetry (C1). (**F**) Electron density map shown from the 5-fold, 3-fold and 2-fold symmetry axis (left to right).

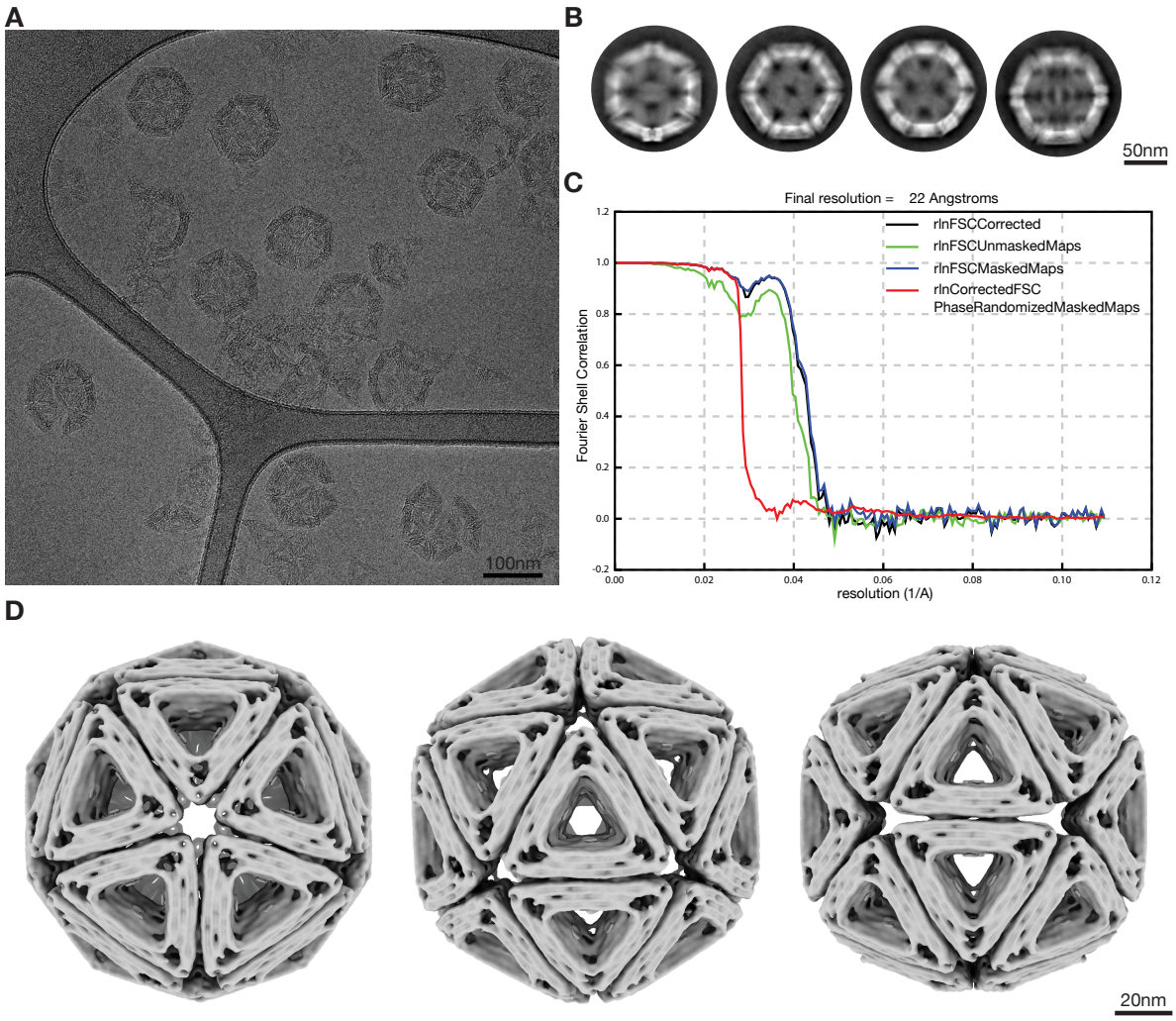

Supplementary Figure 14 | Cryo-EM reconstruction of the T=1 shell at 25 mM $MgCl_2$. (**A**) Cryo-EM micrograph of T=1 shells on a lacey carbon grid with carbon support. (**B**) Two-dimensional class averages showing different orientations. (**C**) Graph showing different FSC curves which were used for resolution estimation. (**D**) Electron density map shown from the 5-fold, 3-fold and 2-fold symmetry axis (left to right, respectively).

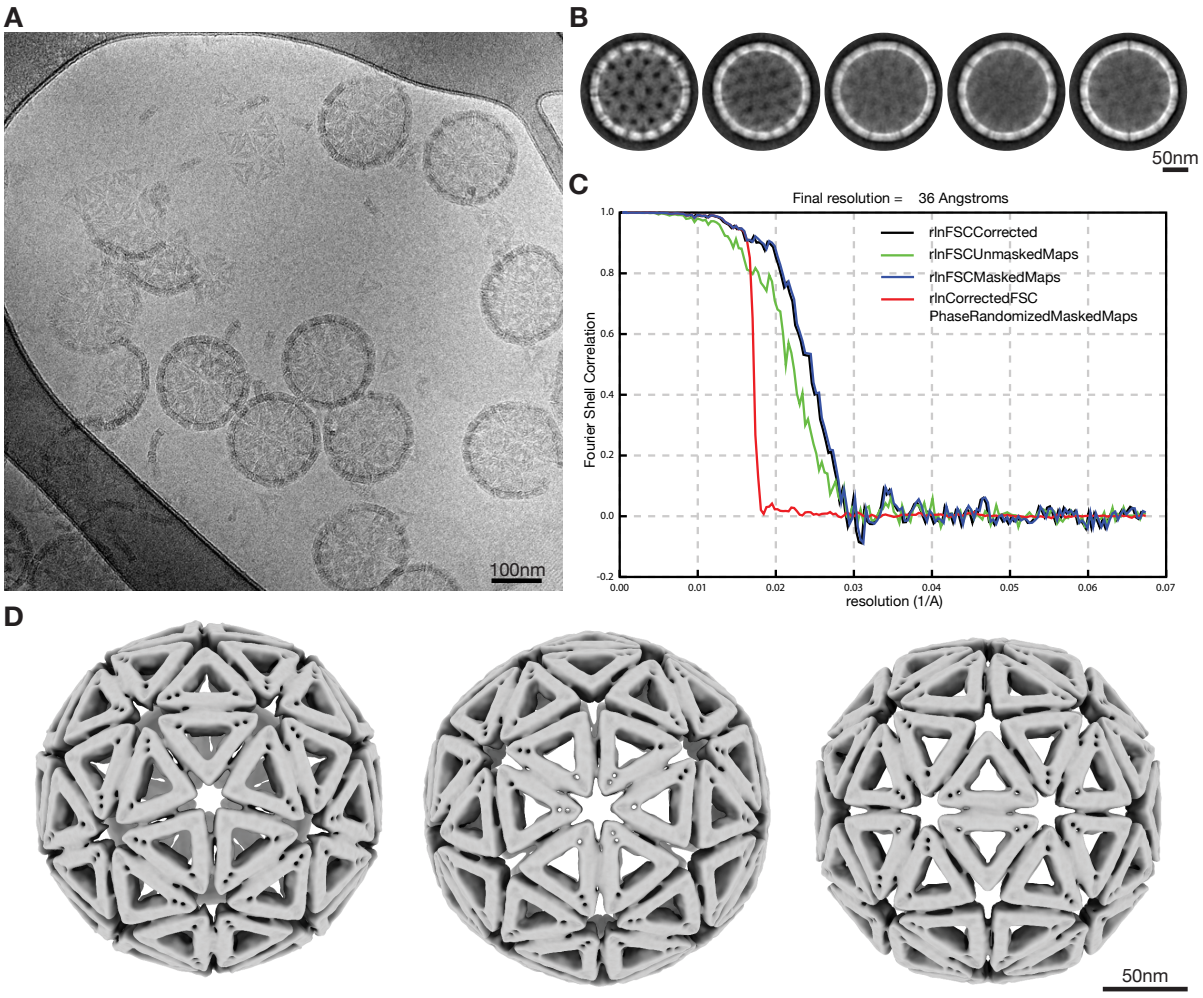

Supplementary Figure 15 | Cryo-EM reconstruction of the T=3 shell at 20 mM $MgCl_2$. (**A**) Cryo-EM micrograph of T=3 shells on a lacey carbon grid with carbon support. (**B**) Two-dimensional class averages showing different orientations. (**C**) Graph showing different FSC curves which were used for resolution estimation. (**D**) Electron density map shown from the 5-fold, 3-fold and 2-fold symmetry axis (left to right).

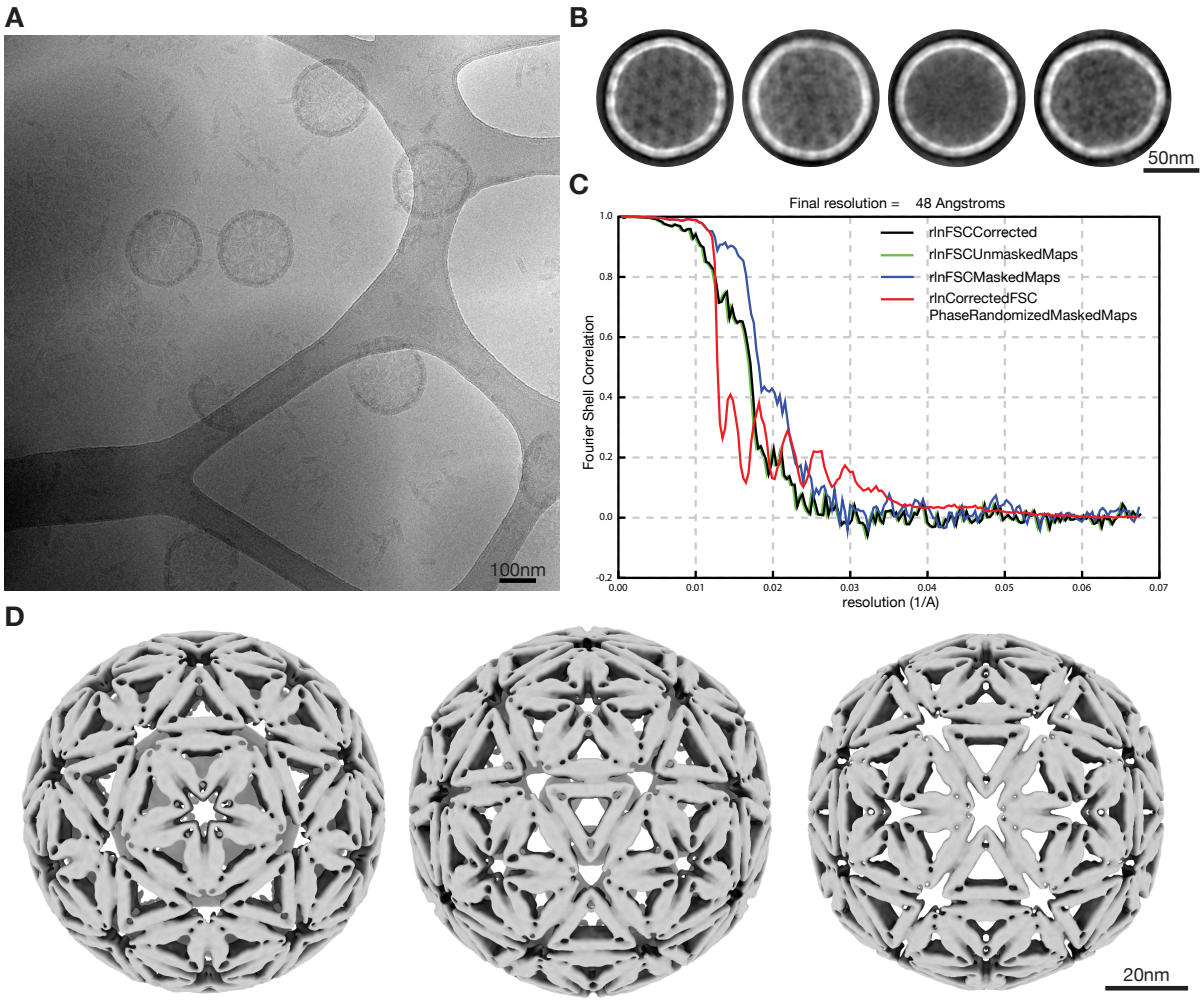

Supplementary Figure 16 | Cryo-EM reconstruction of the T=4 shell at 25 mM $MgCl_2$. (**A**) Cryo-EM micrograph of T=4 shells on a lacey carbon grid with carbon support. (**B**) Two-dimensional class averages showing different orientations. (**C**) Graph showing different FSC curves which were used for resolution estimation. (**D**) Electron density map shown from the 5-fold, 3-fold and 2-fold symmetry axis (left to right).

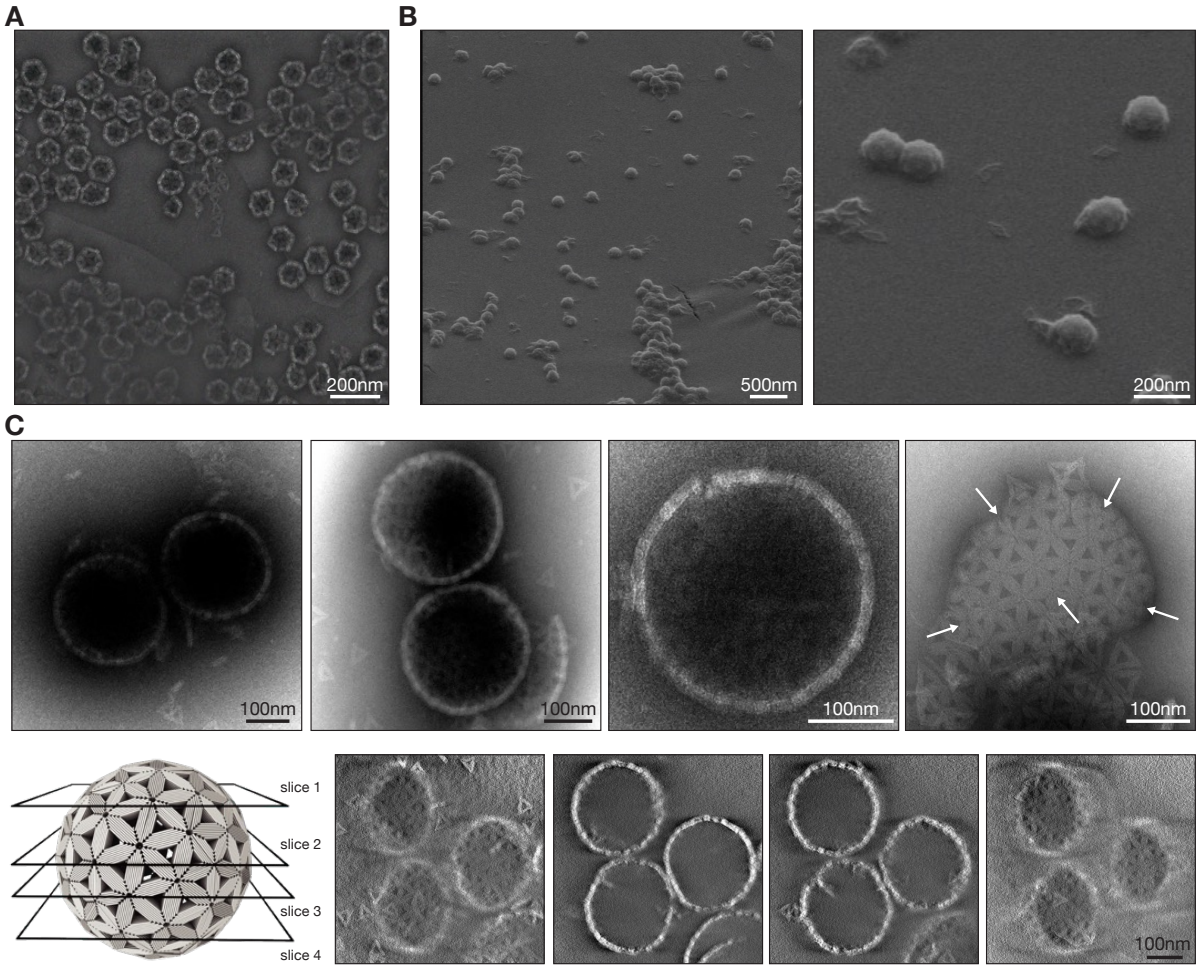

Supplementary Figure 17 | TEM and HIM data of T=1, T=3 and T=9 shells. (**A**) Negative stain TEM image of assembled T=1 triangles assembled at 25 mM $MgCl_2$. (**B**) HIM images of T=3 shells coated with a 5 nm layer of AuPd. (**C**) Negative stain TEM images of assembled T=9 shells. Top: exemplary images of fully or partially assembled shells. The white arrows indicate the right locations of pentamers within the assembly. Bottom: Four slices of a tomogram showing three fully assembled T=9 shells.

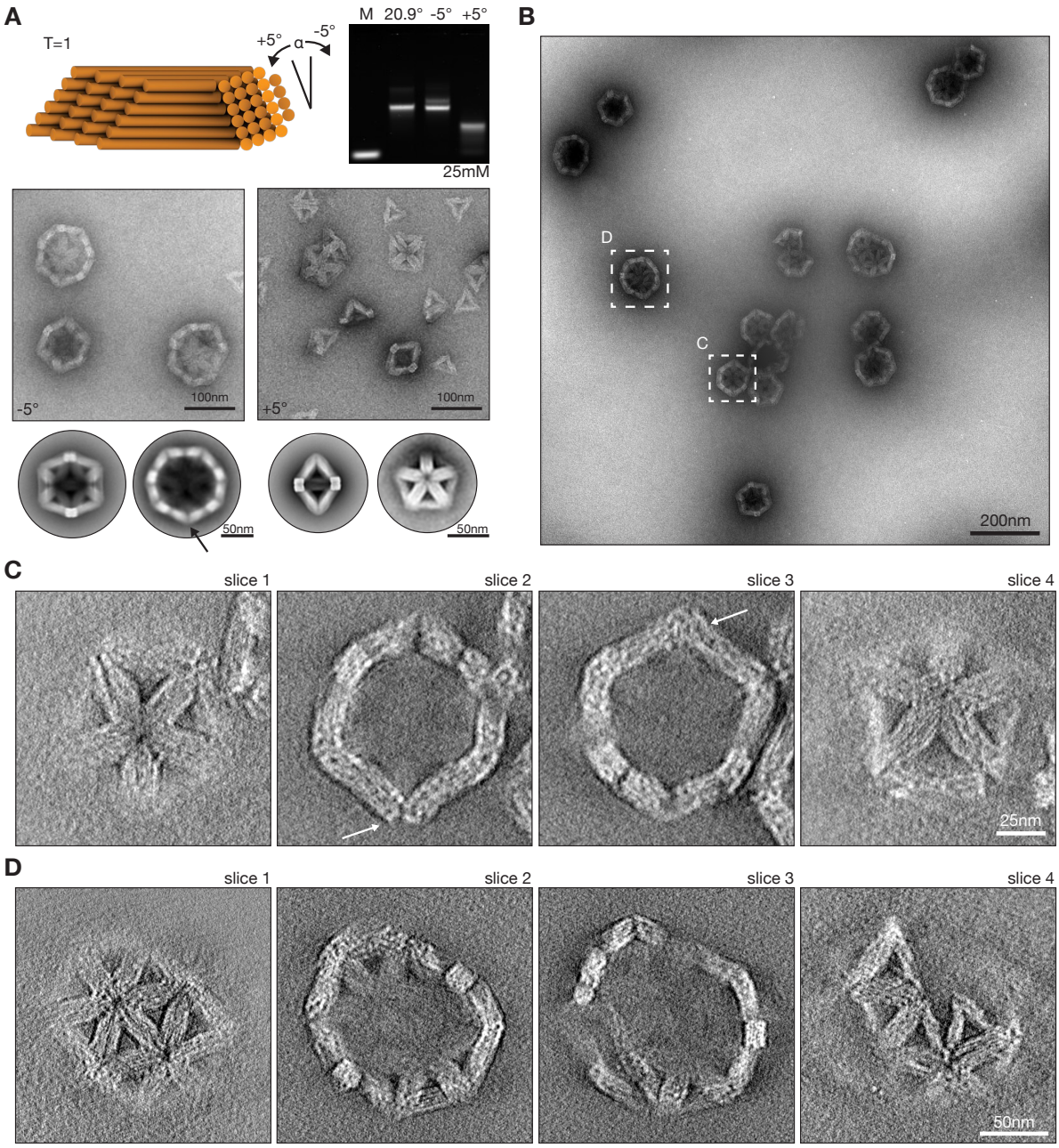

Supplementary Figure 18 | Negative stain EM tomograms of the T=1 triangle with +/-5° bevel angle. (**A**) Top left: Schematics of a T=1 triangle design with a modified bevel angle by 5° in both directions (original bevel angle 20.9°). Top right: Laser-scanned image of an agarose gel on which shell assembly reactions of all three design variants were electrophoresed. Bottom: exemplary negative-staining TEM micrographs and two-dimensional class averages of shell assembly products. (**B**) Negative stain TEM image of assembled T=1 triangles with a decreased bevel angle by -5° assembled at 35 mM $MgCl_2$. The dotted squares indicate the assemblies whose tomograms are shown in (C) and (D). (**C**) Four slices of a tomogram of an assembled T=1 shell. The white arrows indicate locations of stress release that accumulates because of the wrong bevel angle. (**D**) Four slices of a tomogram of a not fully closed assembly.

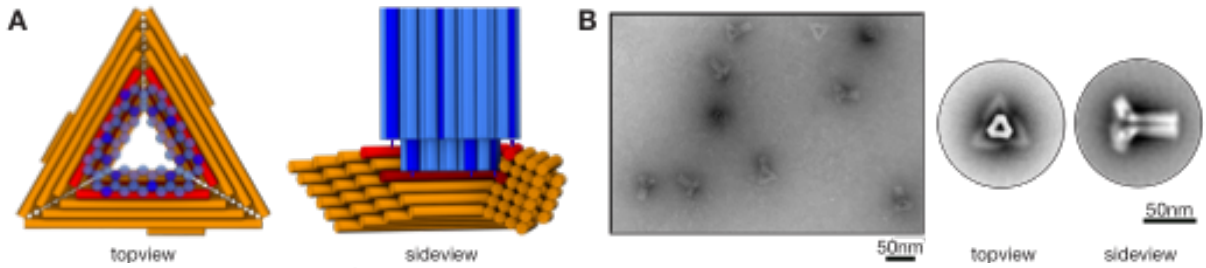

Supplementary Figure 19 | Design strategy T=1 triangle and a triangular brick structure. (**A**) Schematic representation of T=1 triangle dimerization (shown in orange) with the protruding brick (shown in blue) in top and side view. Each cylinder represents a double stranded DNA helix. The cylinders colored in red inside the triangle and in dark blue inside the tail mark those helices connecting the two objects. The thin lines between the two structures indicate single stranded DNA sticky ends extending from the triangle to the brick-like structure. (**B**) Field of view of a negative stain TEM image of the dimerized structures (left) and 2D class averages of the dimer in top and side view (right).

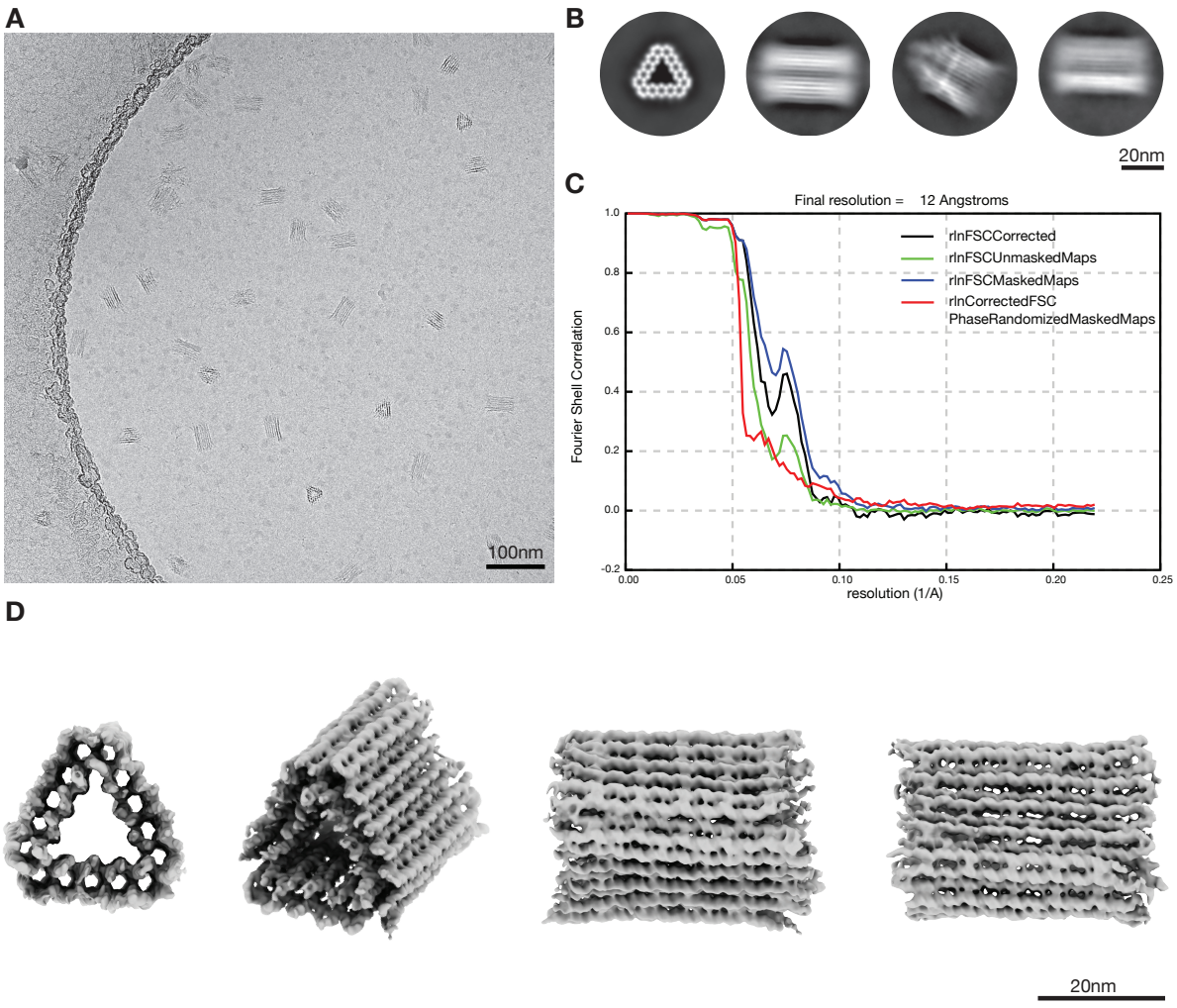

Supplementary Figure 20 | Cryo-EM reconstruction of the triangular brick. (**A**) Cryo-EM micrograph of the triangular brick in free-standing ice at 5 mM $MgCl_2$. (**B**) Two-dimensional class averages showing different orientations. (**C**) Graph showing different FSC curves which were used for resolution estimation. (**D**) Electron density map shown from different viewing angles.

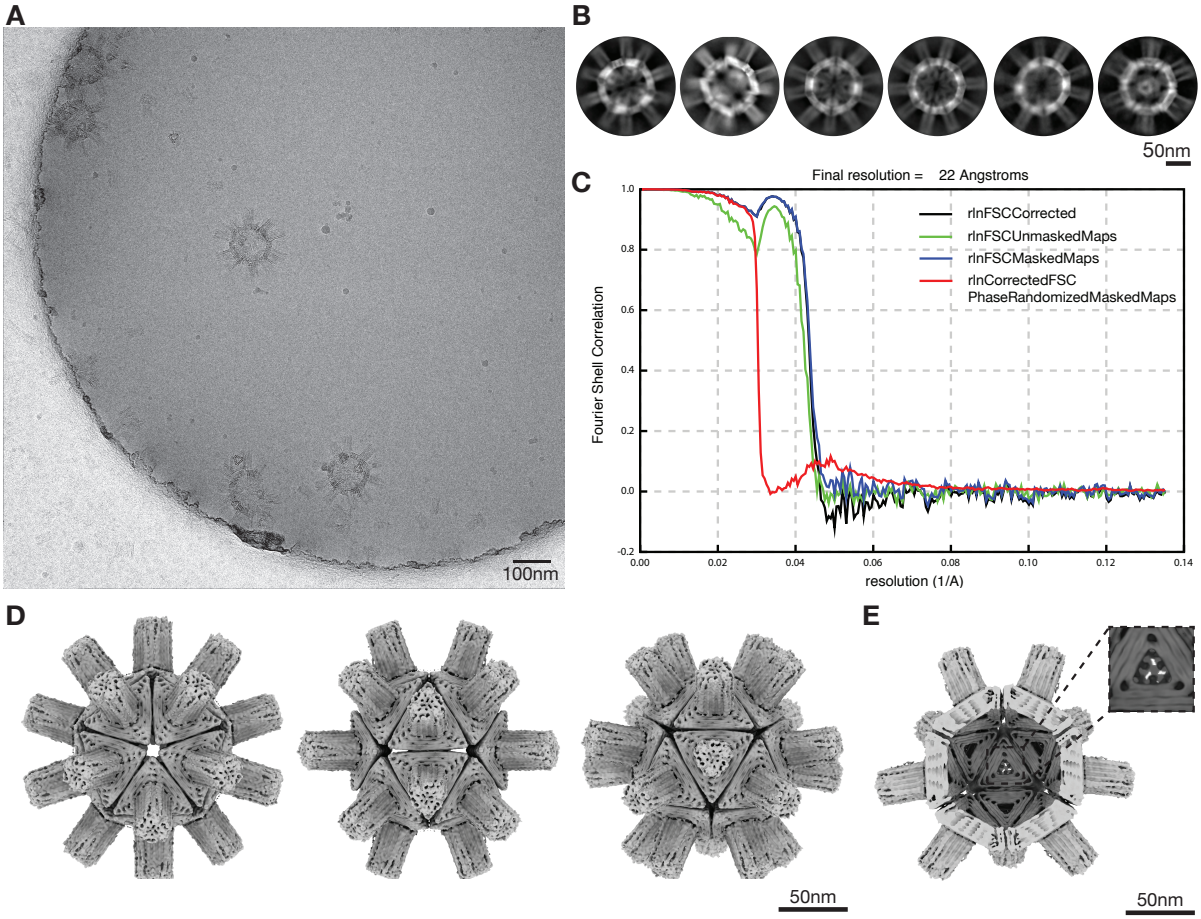

Supplementary Figure 21 | Cryo-EM reconstruction of the spiky shell at 22.5 mM $MgCl_2$. (**A**) Cryo-EM micrograph of the spiky shell in free-standing ice at 22.5 mM $MgCl_2$. (**B**) Two-dimensional class averages showing different orientations. (**C**) Graph showing different FSC curves which were used for resolution estimation. (**D**) Electron density map shown from the 5-fold, 2-fold and 3-fold symmetry axis (left to right, respectively). (**E**) Cut through the density map shown in (D).

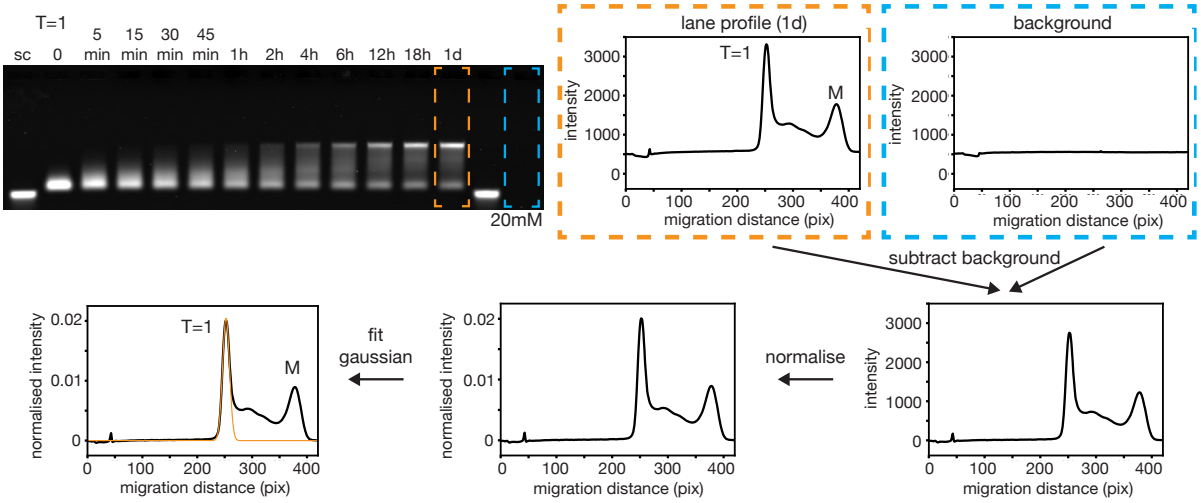

Supplementary Figure 22 | Exemplary procedure for extracting complete shell yield from agarose gels (done with Igor Pro 7). We extracted the lane profiles of the lanes containing the sample (orange) as well as of an empty lane (blue) to get the background signal. Subsequently, we subtracted the background, normalized the graph and fitted a Gaussian to the shell peak. The area underneath the Gaussian curve is the completed shell yield. sc: M13-8064 scaffold strand as reference.

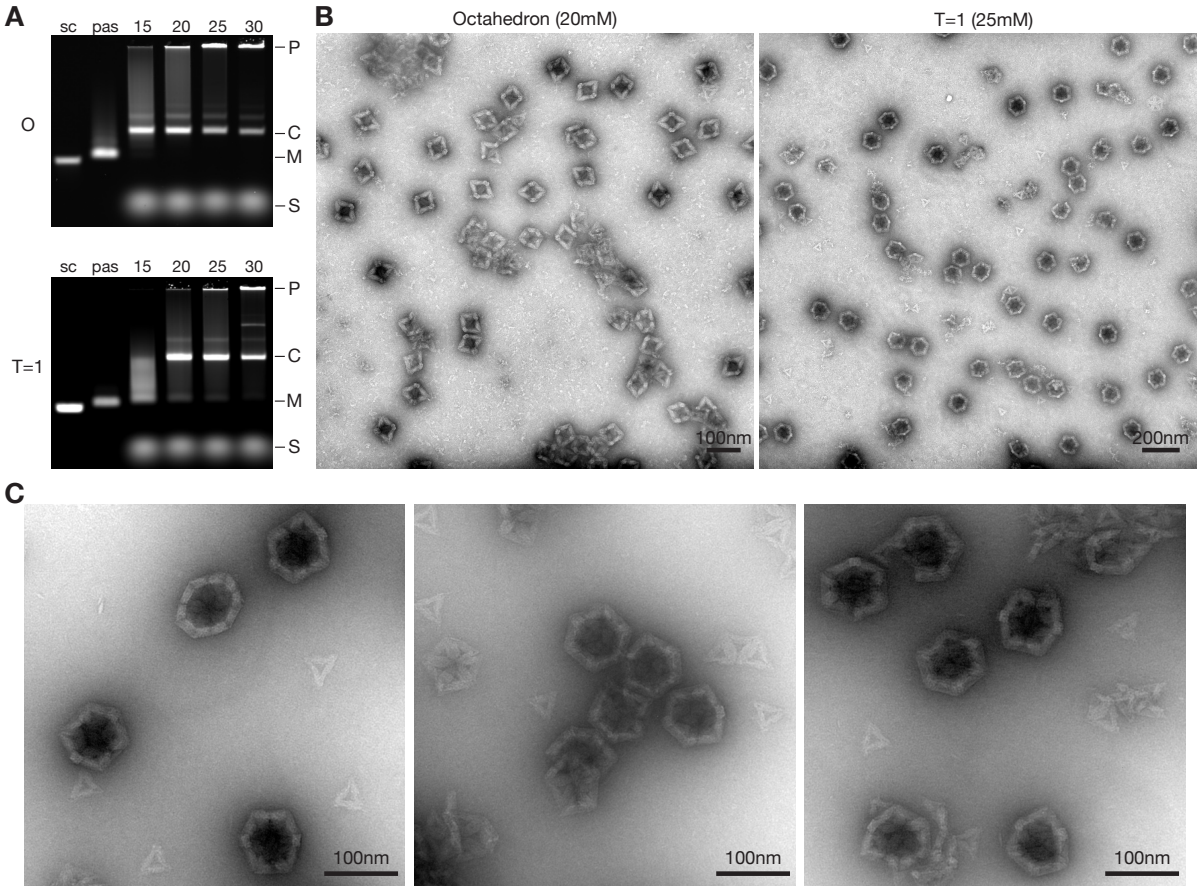

Supplementary Figure 23 | One-pot assembly during the triangle folding reaction of octahedral and T=1 shells. (A) 0.5% agarose gels containing 0.5x TBE buffer and 20 mM $MgCl_2$. The gels ran for 1.5 h at 90 V bias voltage. The buffer was exchanged after 45min. While the octahedron triangles assemble at all tested $MgCl_2$ concentrations into shells during the triangle folding reaction, the T=1 triangles only assemble at 20mM $MgCl_2$ or higher into closed shells. There are staple strands in solution because the triangles are folded with four times excess of staple over scaffold strands and not purified before loading them to the agarose gel. The folding reaction mixtures contained different amounts of $MgCl_2$ (15-30 mM) and were subjected to a thermal annealing ramp from 60°C to 45°C decreasing the temperature by 1°C per hour. sc: M13-8064 scaffold reference, pas: passivated triangle, 15-30: $MgCl_2$ concentration in mM present in the folding reaction. P: pocket, C: shell, M: monomer, S: excess staples. (**B**) Negative stain TEM images of octahedra and T=1 shells assembled during the folding reaction of the triangles at 20 and 25 mM $MgCl_2$, respectively. Single stranded excess staple strands are still visible. (**C**) Negative stain TEM images of T=1 shells assembled from PEG purified triangles at 20 mM $MgCl_2$ for 2 days at 40°C. Instead of using gel purification to purify the DNA-origami triangles, PEG purification was used as previously described (*1*).

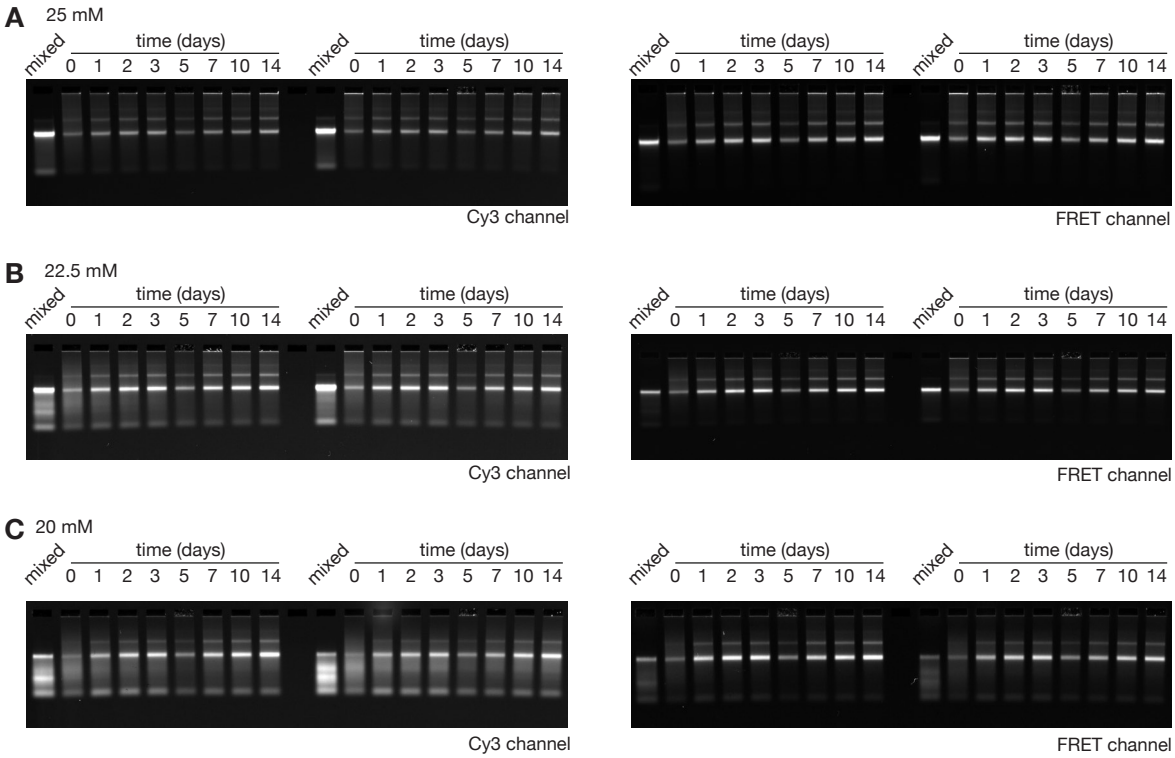

Supplementary Figure 24 | Subunit exchange experiments. Agarose gels used for extracting the FRET ratio of the subunit exchange experiments. The gels were run at 25 mM (**A**), 22.5 mM (**B**) and 20 mM $MgCl_2$ (**C**). All gels are 0.5% agarose gels containing 0.5x TBE buffer with different $MgCl_2$ concentrations and ran for 1.5 h at 90 V bias voltage. The buffer was exchanged after 45 min. The same gel was scanned in a Cy3 (left) and FRET (right) channel. Triangles with Cy3 and Cy5 labeled oligonucleotides at appropriate locations and unlabeled triangles were assembled separately at 25 mM $MgCl_2$ before mixing the assembled shells and adjusting the $MgCl_2$ concentration. The mixtures were incubated up to 14 days at 40°C. At indicated timepoints aliquots were taken, frozen in liquid nitrogen and stored at -20°C. As reference for fully exchanged subunits, labeled and unlabeled triangles were assembled in a 1:1 ratio at 25 mM $MgCl_2$ (mixed).

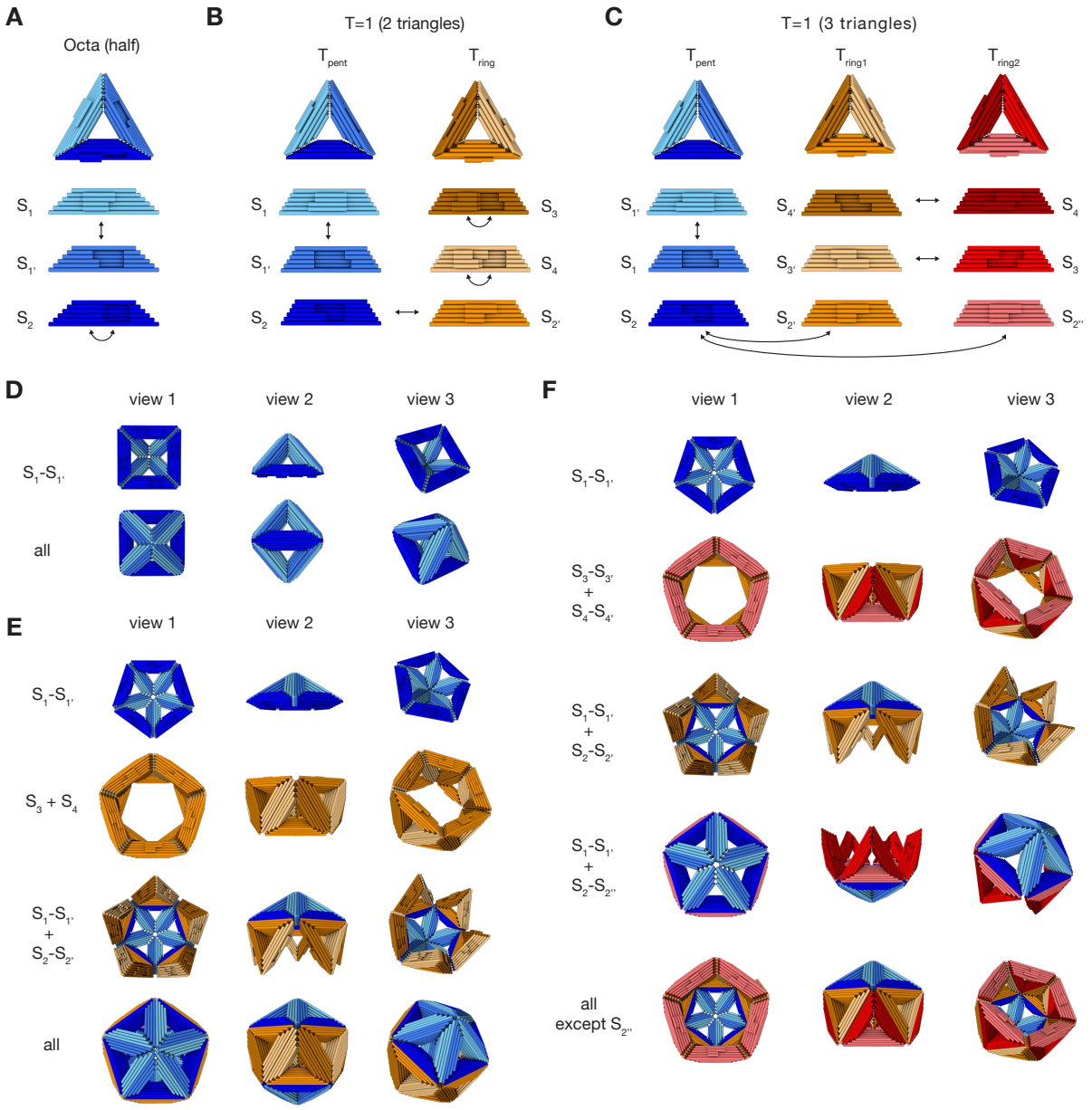

Supplementary Figure 25 | Designing triangular subunits for partial shell objects. Cylindrical model of DNA-origami triangles assembling into half octahedra (**A+D**), half T=1 shells (**B+E**) or a T=1 shells with a missing pentagonal vertex (**C+F**). The sides of the triangles are modified with protrusions (light) and recesses (dark). The arrows indicate shape-complementary sides. Depending on the activation of certain sided the triangles form different kind of assemblies. All sides not involved in the binding of the triangles were passivated with poly-T extensions at the stacking contacts.

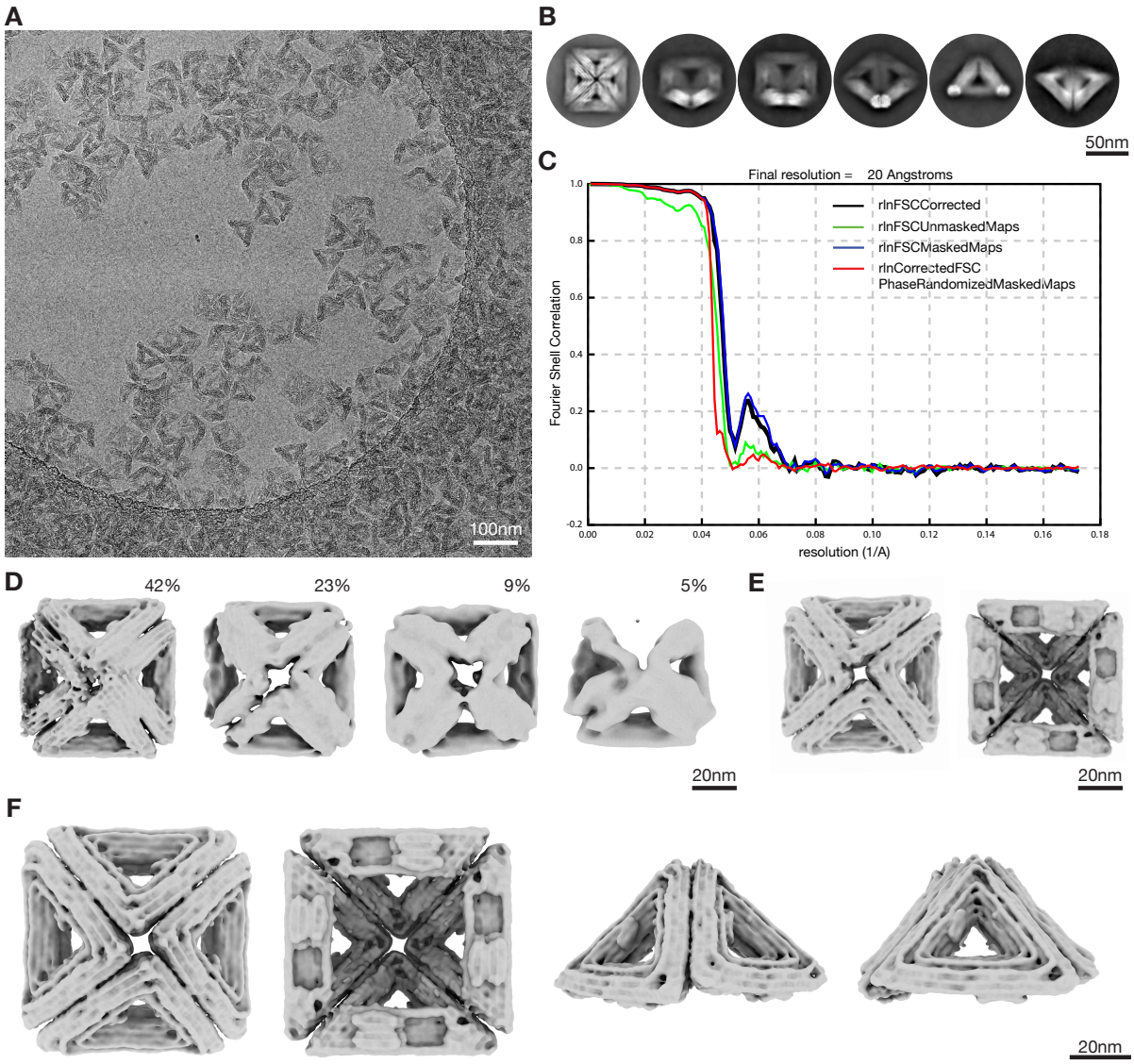

Supplementary Figure 26 | Cryo-EM reconstruction of the half octahedron shell. (**A**) Cryo-EM micrograph of the half octahedron shell in free-standing ice. (**B**) Two-dimensional class averages showing different orientations. (**C**) Graph showing different FSC curves which were used for resolution estimation. (**D**) Classes after 3d classification in relion3. (**E**) Refinement without using any symmetry (C1). (**F**) Electron density map of the half octahedron shell reconstructed with C4 symmetry.

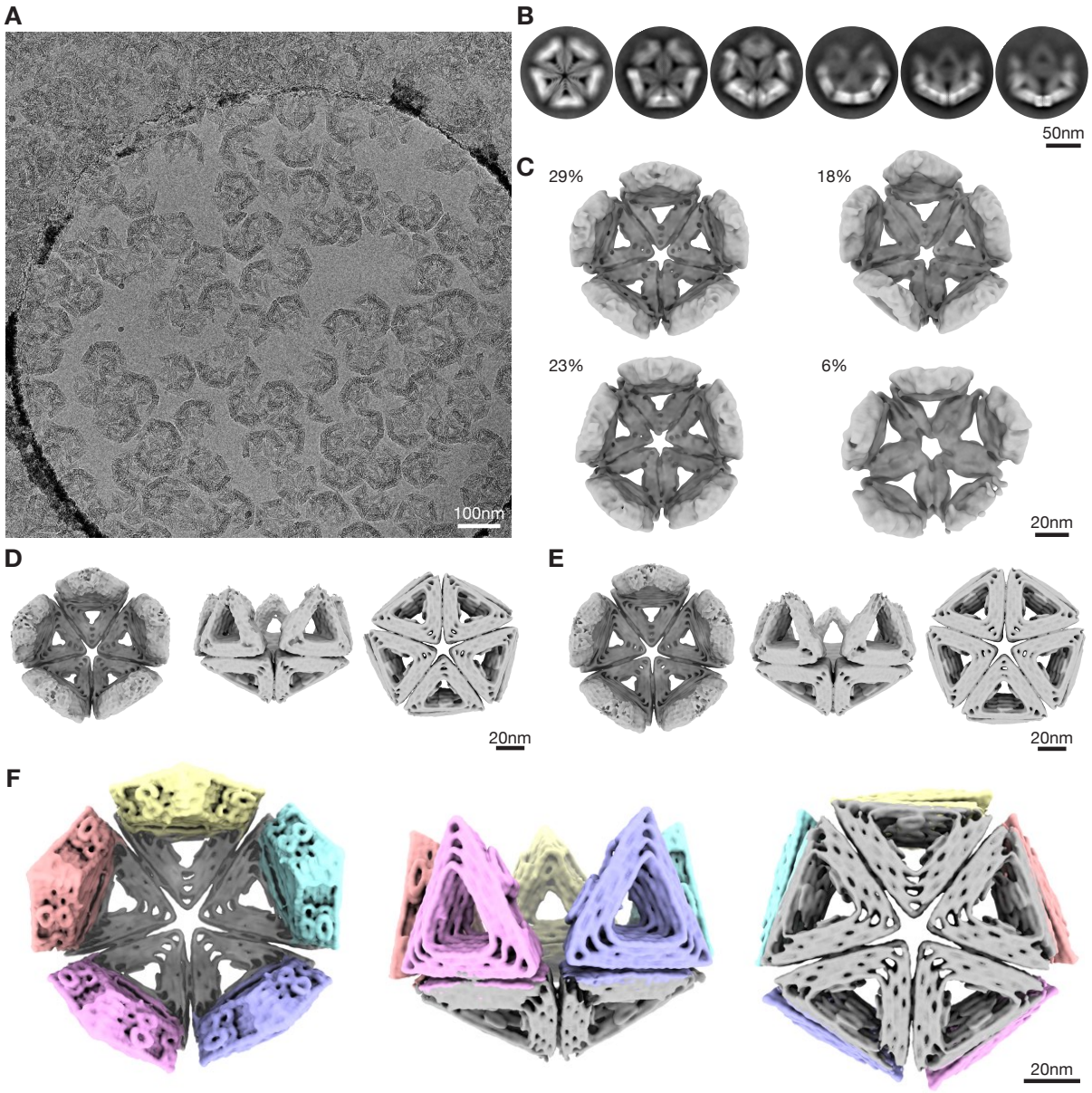

Supplementary Figure 27 | Cryo-EM reconstruction of the half T=1 shell. (**A**) Cryo-EM micrograph of the half T=1 shell in free-standing ice. (**B**) Two-dimensional class averages showing different orientations. (**C**) Classes after 3d classification in relion3. (**D**) Refinement without using any symmetry (C1). (**E**) Refinement with using C5 symmetry. (**F**) Multibody refinement using six bodies indicated by the colors in relion3.

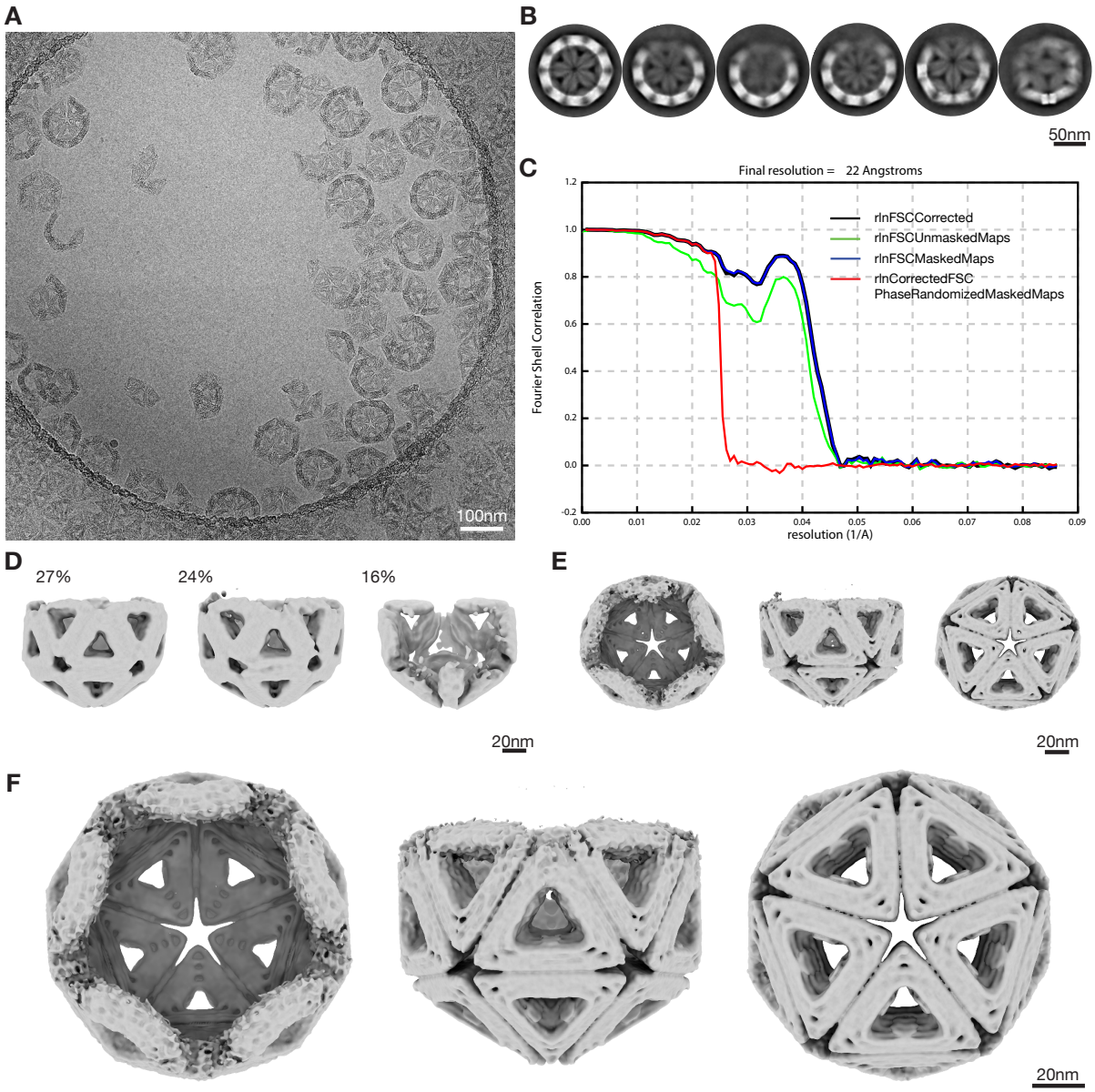

Supplementary Figure 28 | Cryo-EM reconstruction of the T=1 shell with a missing pentagon vertex. (**A**) Cryo-EM micrograph of T=1 shell with a missing pentagon vertex in free-standing ice. (**B**) Two-dimensional class averages showing different orientations. (**C**) Graph showing different FSC curves which were used for resolution estimation. (**D**) Classes after 3d classification in relion3. (**E**) Refinement without using any symmetry (C1). (**F**) Electron density map of the T=1 shell missing one pentagon vertex reconstructed with C5 symmetry.

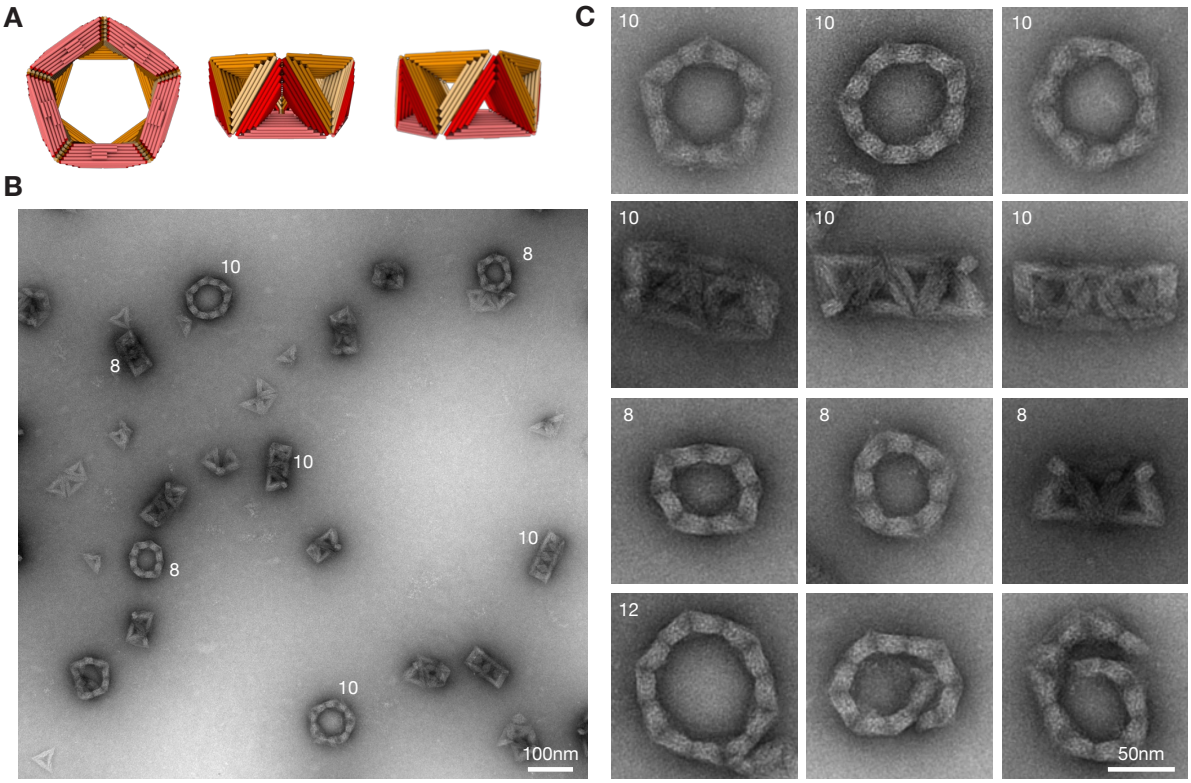

Supplementary Figure 29 | Negative stain TEM images of T_{ring1} and T_{ring2}. (**A**) Cylindrical model of the DNA-origami ring containing 10 triangles. (**B**) Negative stain images of rings formed by T_{ring1} and T_{ring2} assembled for 1d at 40°C ($c_{triangle}$=10nM, c_{MgCl2}=25mM). The white numbers show the number of triangles within a ring. (**C**) Exemplary particles showing rings with 8, 10 or 12 triangles as well as not fully closed rings.

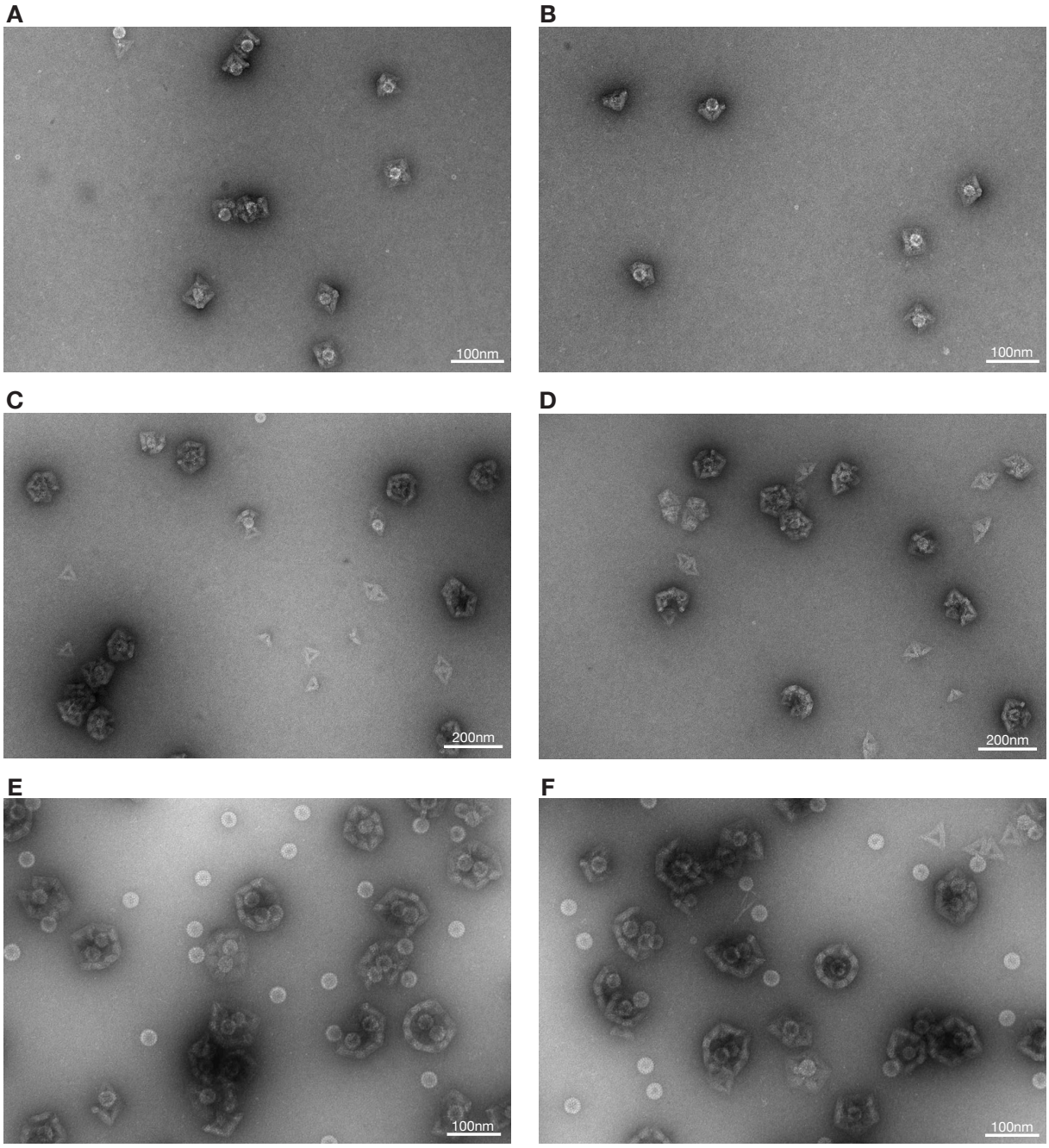

Supplementary Figure 30 | Negative stain EM images of encapsulated HBV core particles using a half octahedron (**A**)+(**B**), a half T`=1 shell (**C**)+(**D**) and a T=1 shell with a missing pentagonal vertex (**E**)+(**F**). All shells were assembled at 30 mM $MgCl_2$, incubated with the DNA modified 17H7 antibody overnight and subsequently incubated with the HBV particles for 1-4h or overnight. (A)-(D) DNA-origami half shells were added in excess over HBV particles. Therefore, all HBV particles are bound. (E)+(F) HBV particles were added in excess. All shells are occupied by at least one HBV particle.

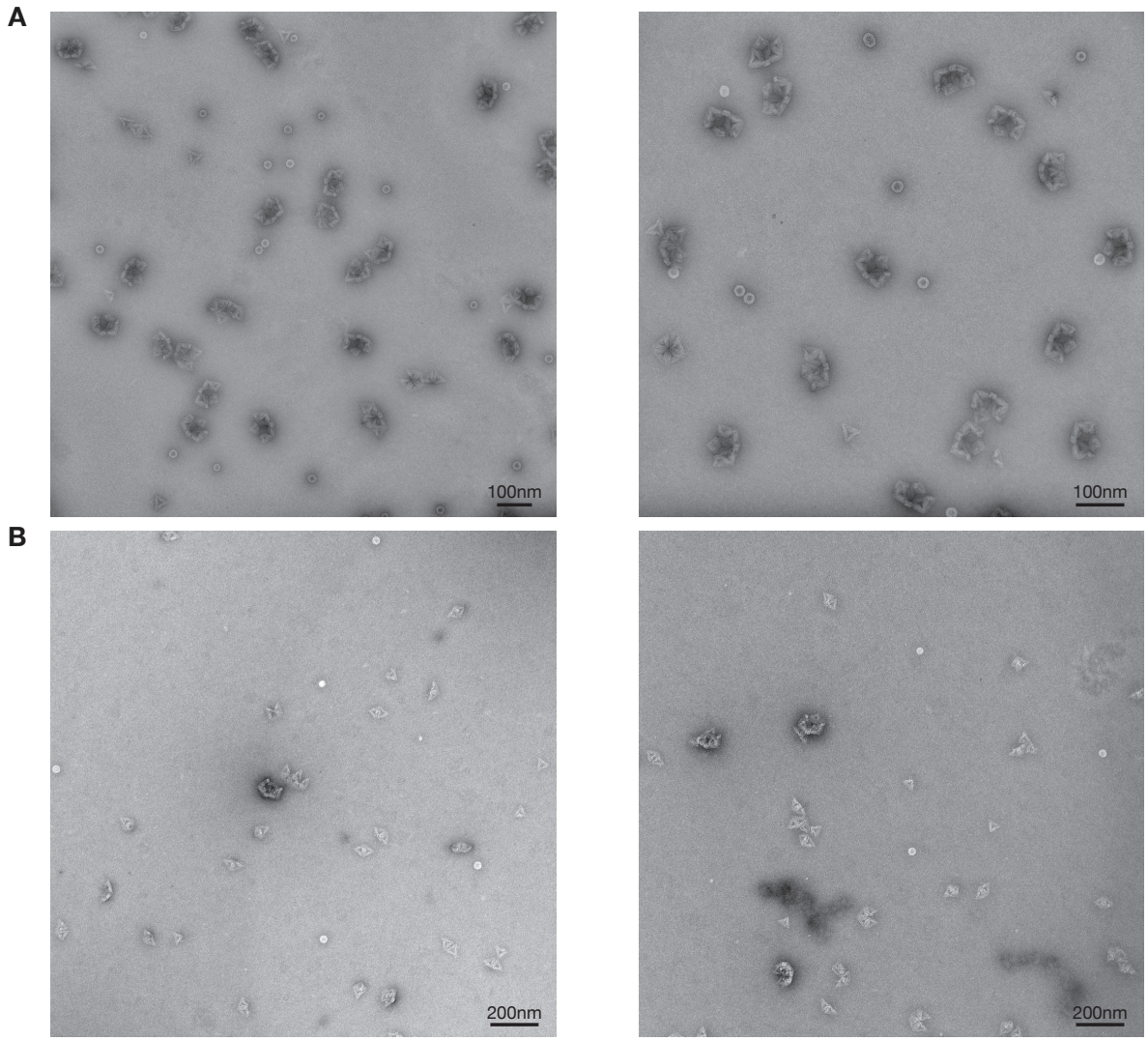

Supplementary Figure 31 | Negative control of HBV binding. (**A**) Negative stain images of HBV core particles and half T=1 shells without 17H7 antibodies. (**B**) Negative stain images of half T=1 shells equipped with 4D06 HBsAg antibodies and HBV core particles.

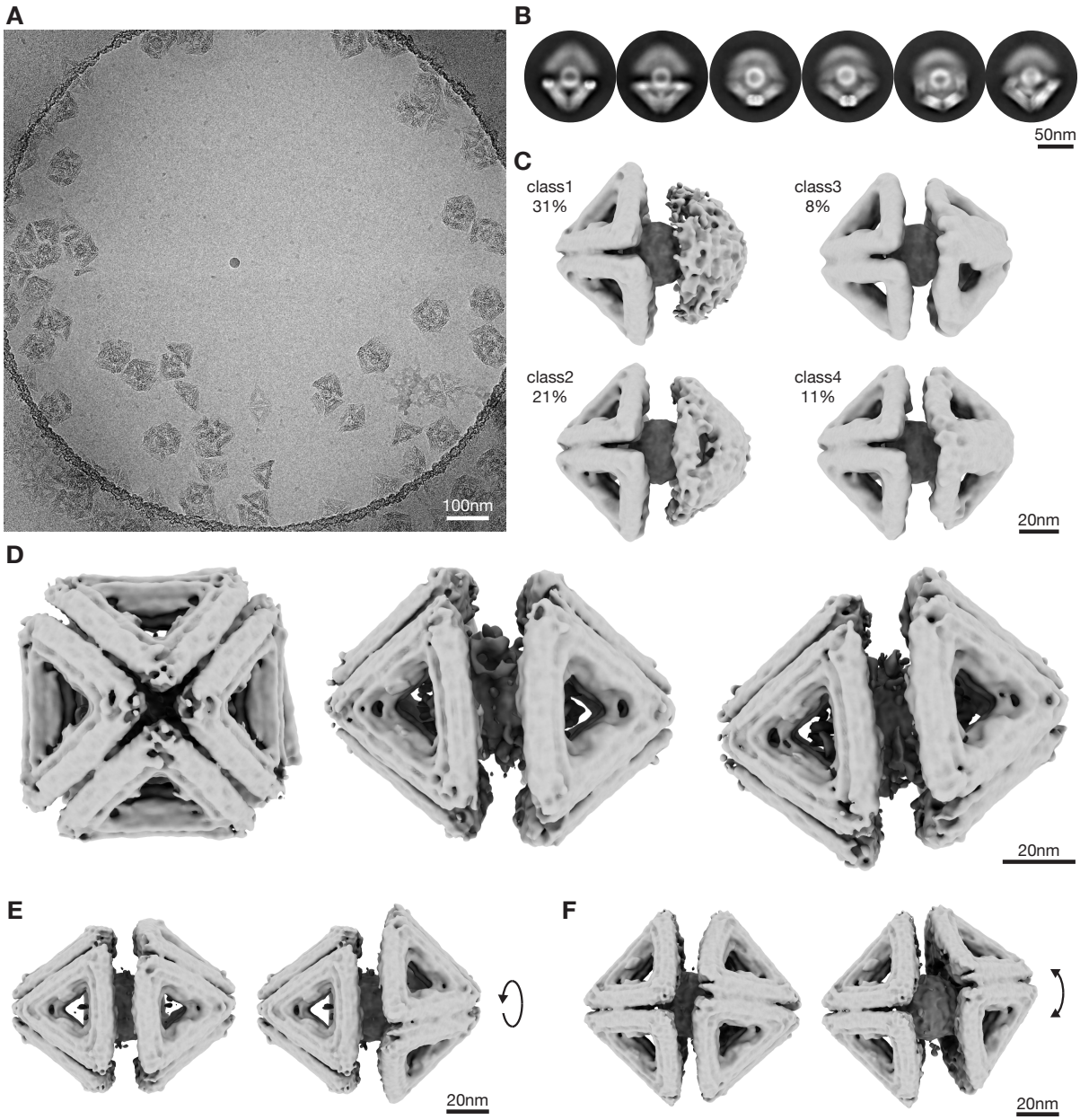

Supplementary Figure 32 | Cryo-EM reconstruction of the half octahedron shell with a trapped HBV core particle. (**A**) Cryo-EM micrograph of the half octahedron shell with HBV core particles in free-standing ice. (**B**) Two-dimensional class averages showing different orientations. (**C**) Classes after 3d classification in relion3. One half of class1 and class2 is not well defined because of the averaging of multiple conformation of the second half shell. (**D**) Multibody refinement with three bodies (the two half shells and the HBV core particle) using the particles in class3 and class4 in (C). (**E**) First eigenvector of the multibody refinement showing a rotational movement of the second half shell. (**F**) Second eigenvector of the multibody refinement showing a sliding movement of the second half shell.

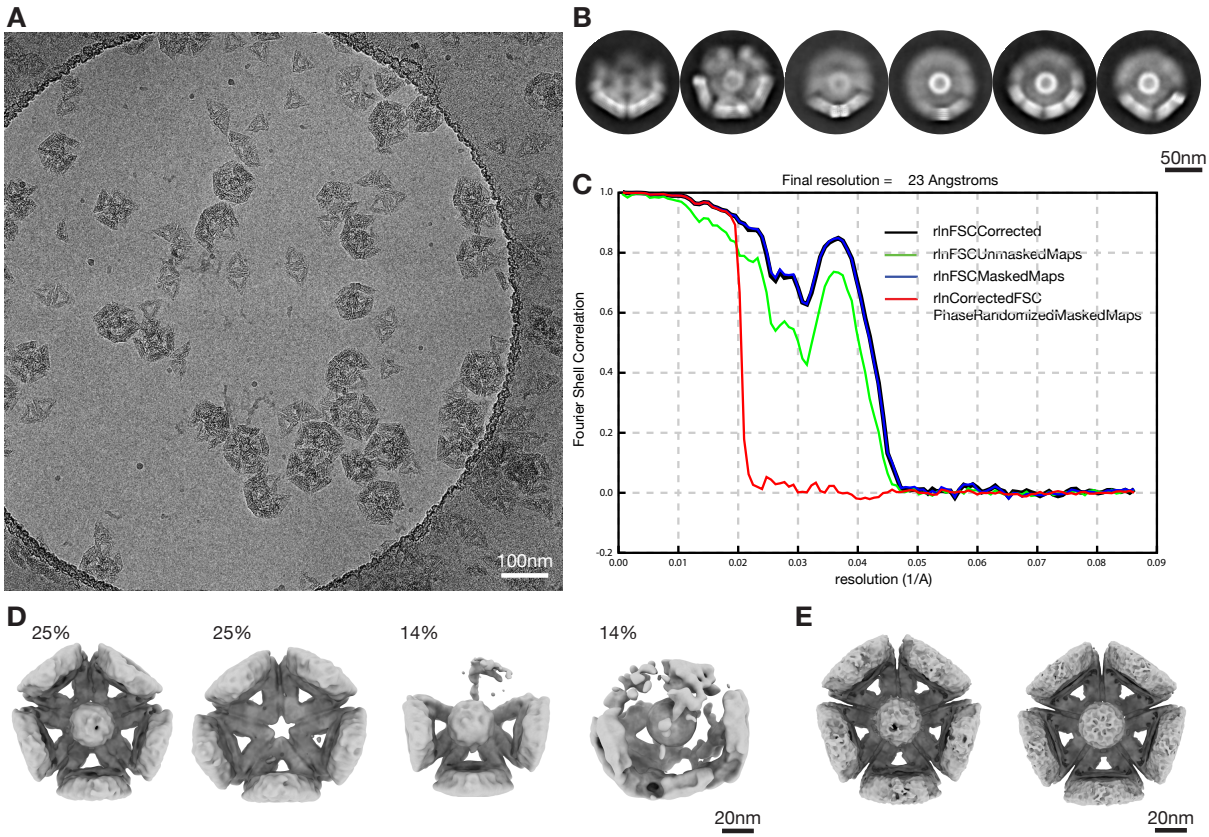

Supplementary Figure 33 | Cryo-EM reconstruction of the half T=1 shell with a trapped HBV core particle. (**A**) Cryo-EM micrograph of the half T=1 shell with a trapped HBV core particle in free-standing ice. (**B**) Two-dimensional class averages showing different orientations. (**C**) Graph showing different FSC curves which were used for resolution estimation. (**D**) Classes after 3d classification in relion3. (**E**) Refinement without (left) and with (right) using C5 symmetry.

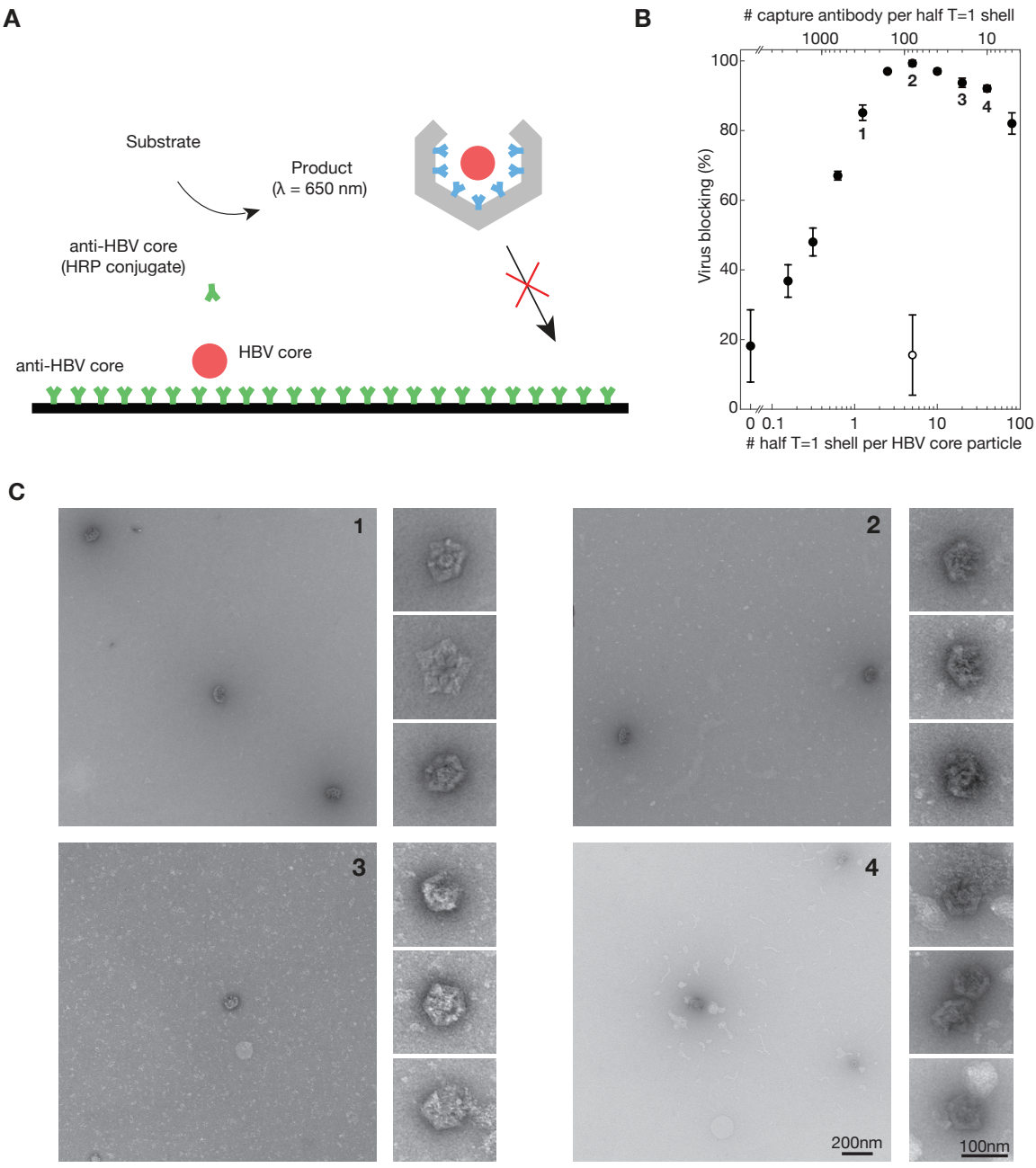

Supplementary Figure 34 | In vitro virus blocking ELISA. (**A**) Schematics of the in vitro blocking ELISA. The HBV core particle by itself can bind to the immobilized CAgHB antibodies and can be visualized by a subsequent flushing of an anti-CAgHB conjugated with a horseradish peroxidase (HRP). When the HBV core particle is engulfed by a half T=1 particle, the shell sterically occludes the core particle from binding to the surface and the signal of the HRP is reduced. **(B)** In vitro virus blocking ELISA experiments of 2.5 pM HBV core particle incubated with pre-assembled mixtures of 1 nM oligonucleotide-conjugated capture antibody and various concentrations of half T=1 shells. Data is presented as mean ± s.d., n = 3 independent measurements. **(C)** Negative stain TEM images of selected samples from the in vitro blocking ELISA indicated by numbers in (B). The half T=1 shell concentration were: (1) 3.1 pM, (2) 12.5 pM, (3) 50 pM, (4) 100 pM.

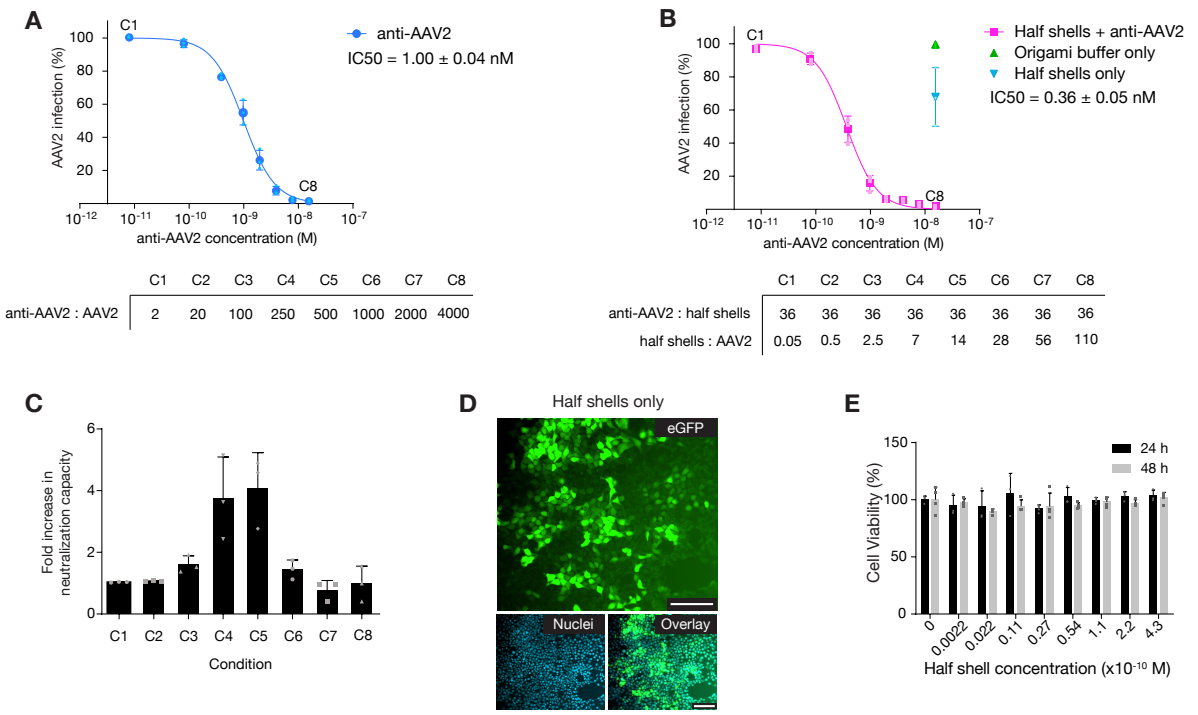

	C1	C2	C3	C4	C5	C6	C7	C8
anti-AAV2 : AAV2	2	20	100	250	500	1000	2000	4000

	C1	C2	C3	C4	C5	C6	C7	C8
anti-AAV2 : half shells	36	36	36	36	36	36	36	36
half shells : AAV2	0.05	0.5	2.5	7	14	28	56	110

Supplementary Figure 35 | Dose-response characterization of neutralization capacity and cell viability. Complete IC_{50} curves for both free antibody (anti-AAV2, **A**) and origami half shells + anti-AAV2 (**B**). Concentration of half shells + anti-AAV2 in (B) is normalized to the concentration of anti-AAV2. Origami buffer only and half shell only conditions do not contain anti-AAV2, but the respective data points are positioned for easy visualization. Concentration of the half shells only is identical to that used in the highest half shell + anti-AAV2 condition. Below each graph is the approximate number of anti-AAV2 antibodies, and number of half shells, per AAV2 virus particle. All ratios are based on the total number of virus particles. Data in (A) and (B) is presented as mean ± s.d., n = 3 biologically independent experiments. Individual data points are overlayed. (**C**) Fold-increase in neutralization capacity that is achieved by conjugation of the anti-AAV2 antibody to the origami half shells, for each of the concentrations in the IC_{50} curves (A) and (B), denoted as C1–C8. Data is presented as mean ± s.d., n = 3 biologically independent experiments. Individual data points are overlayed. (**D**) Representative epifluorescent images demonstrating expression of eGFP by infected cells for origami half shells without conjugated anti-AAV2. Images are representative from one of n = 3 biologically independent experiments, with similar results each time, scale bars represent 100 μm. (**E**) Viability of HEK293T cells exposed to half shell origami structures for 24 h and 48 h. Half shell concentrations are identical to those used in the IC_{50} characterization (B). Exposure of HEK293T cells to the DNA origami half shells did not result in dose-dependent toxicity. Data is presented as mean ± s.d., n = 3 and 4 biologically independent experiments, for 24 h and 48 h respectively. Individual data points are overlayed.

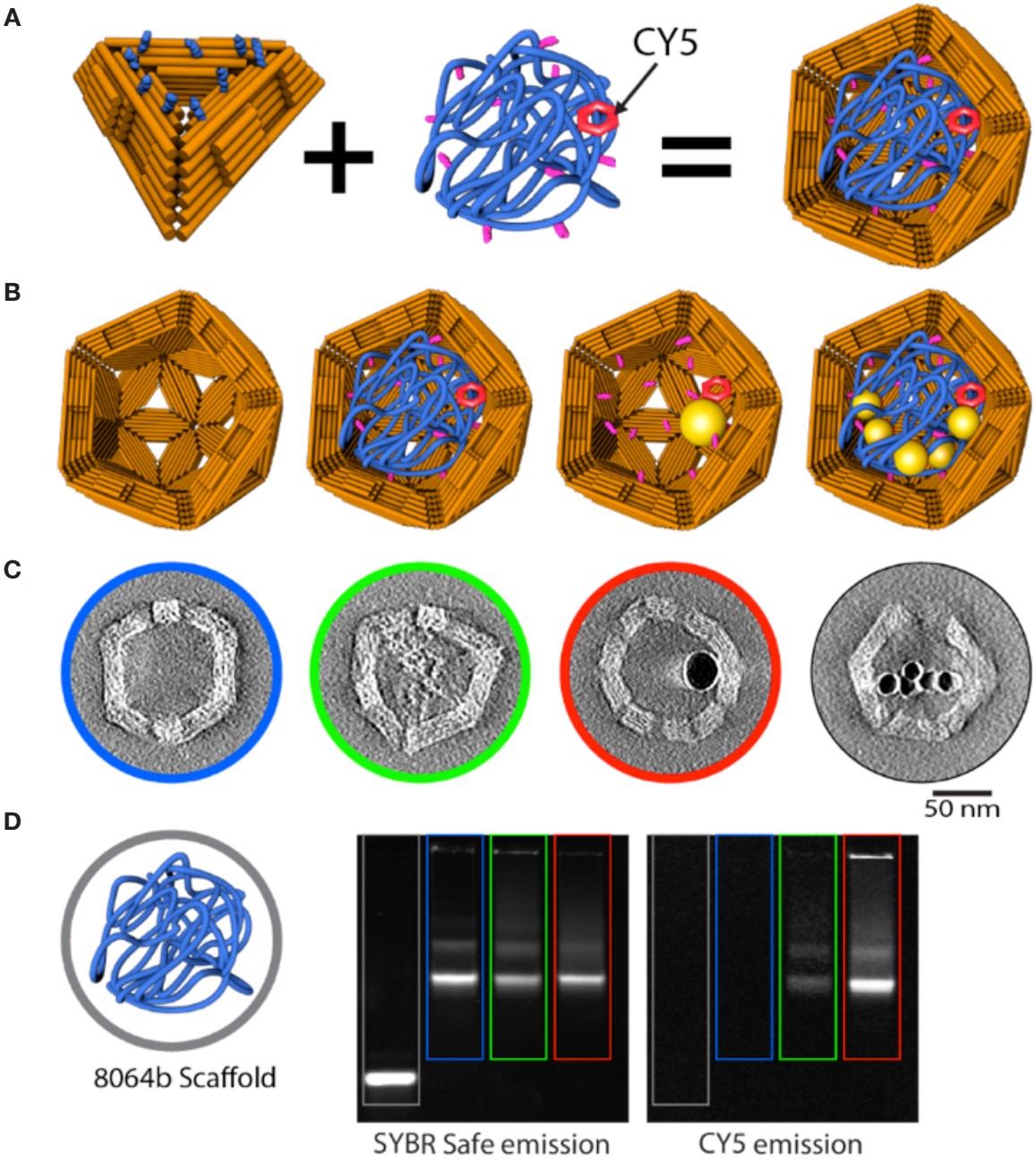

Supplementary Figure 36 | Encapsulation of circular ssDNA and gold Nanoparticles in T=1 shell. (**A**) From left, schematic of modified T=1 monomers with ssDNA handles. Middle, a circular ssDNA with attached complimentary handles and tagged with CY5. Right, encapsulated ssDNA in T=1 shell. Illustration shows half shell, but a complete shell is meant. (**B**) From left, schematics of an empty shell, encapsulated circular ssDNA, an encapsulated single gold nanoparticle, and encapsulated gold-labeled circular ssDNA. (**C**) Slices of negative stain TEM tomograms of each shell in (B). (**D**) Laser scanned fluorescent gels of T=1 shells, with and without cargo. Both gel images are taken from the same gel but with different wavelengths. Each column of the gel is color coded with the corresponding particle in sections (C) and (D). The left gel image shows the SYBR safe emission where we see the bands for the scaffold and for assembled shells. On the right gel, emission from CY5 indicates the cargo is in the same position as the assembled shell.

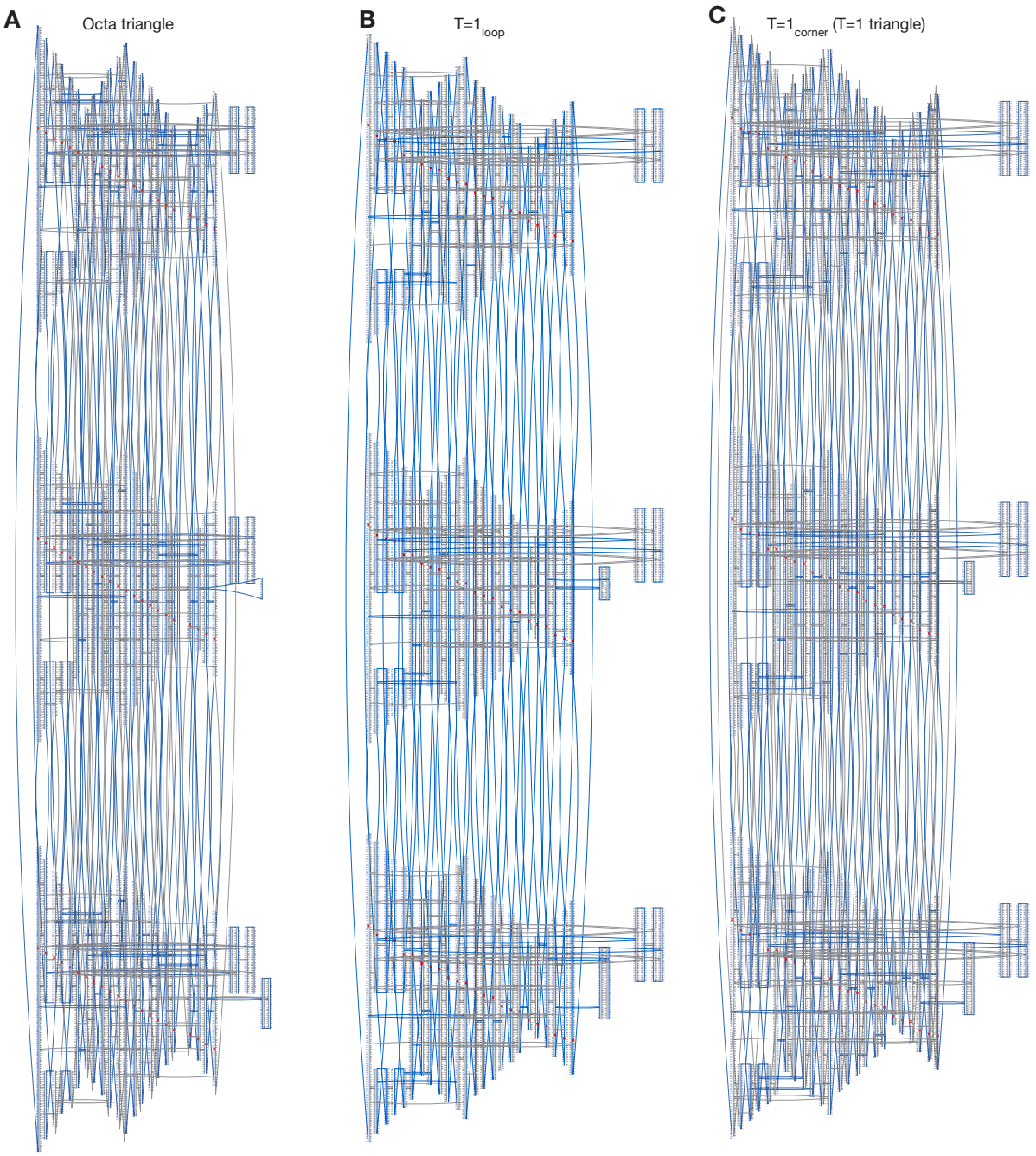

Supplementary Figure 37 | Design diagram of Octa and T=1 triangles prepared with caDNAno v0.1. Oligonucleotides that connect two different sides have five additional single-stranded thymidines at the corner.

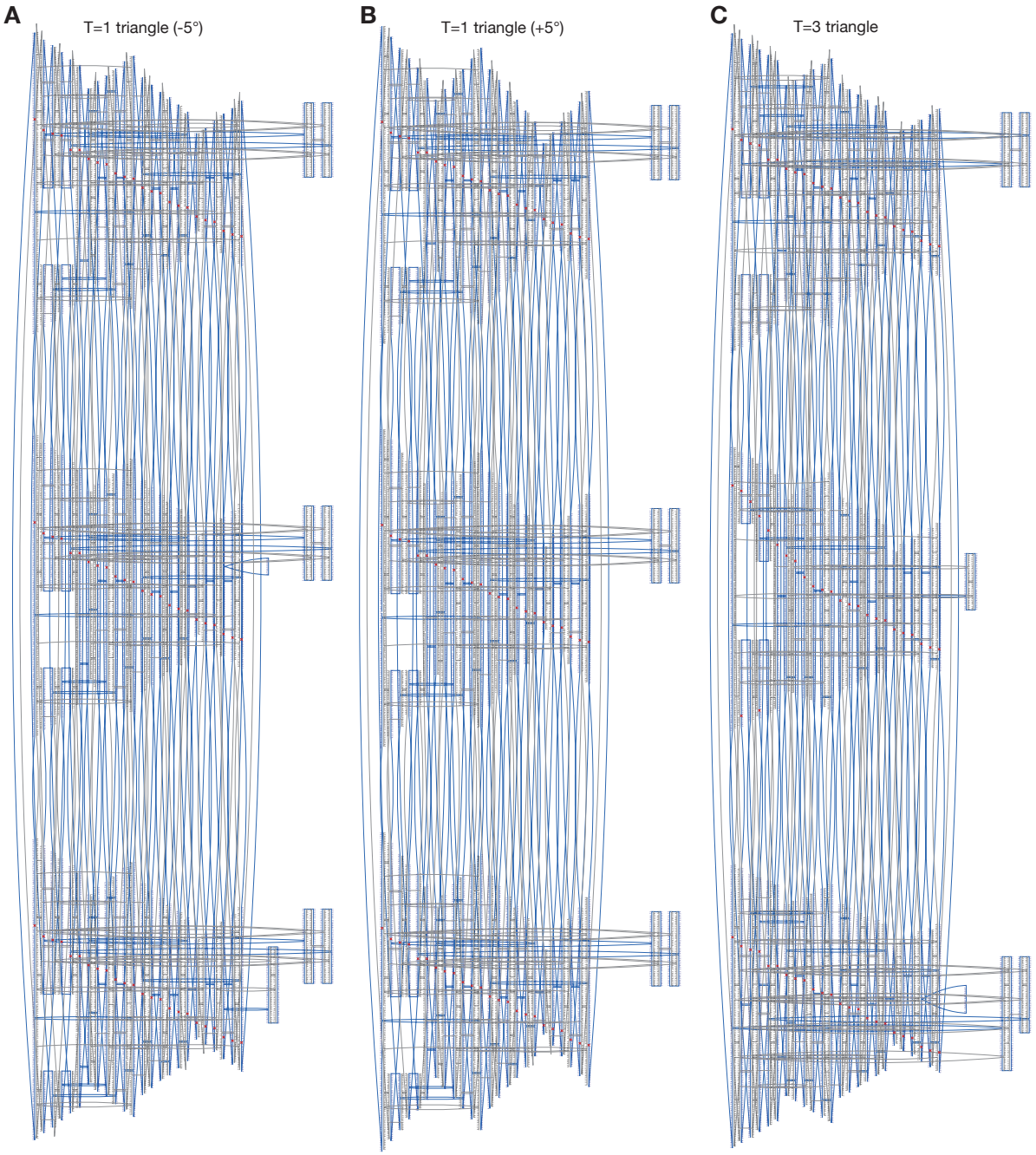

Supplementary Figure 38 | Design diagram of T=1 triangles with altered bevel angle and T=3 triangle prepared with caDNAno v0.1. Oligonucleotides that connect two different sides have five additional single-stranded thymidines at the corner.

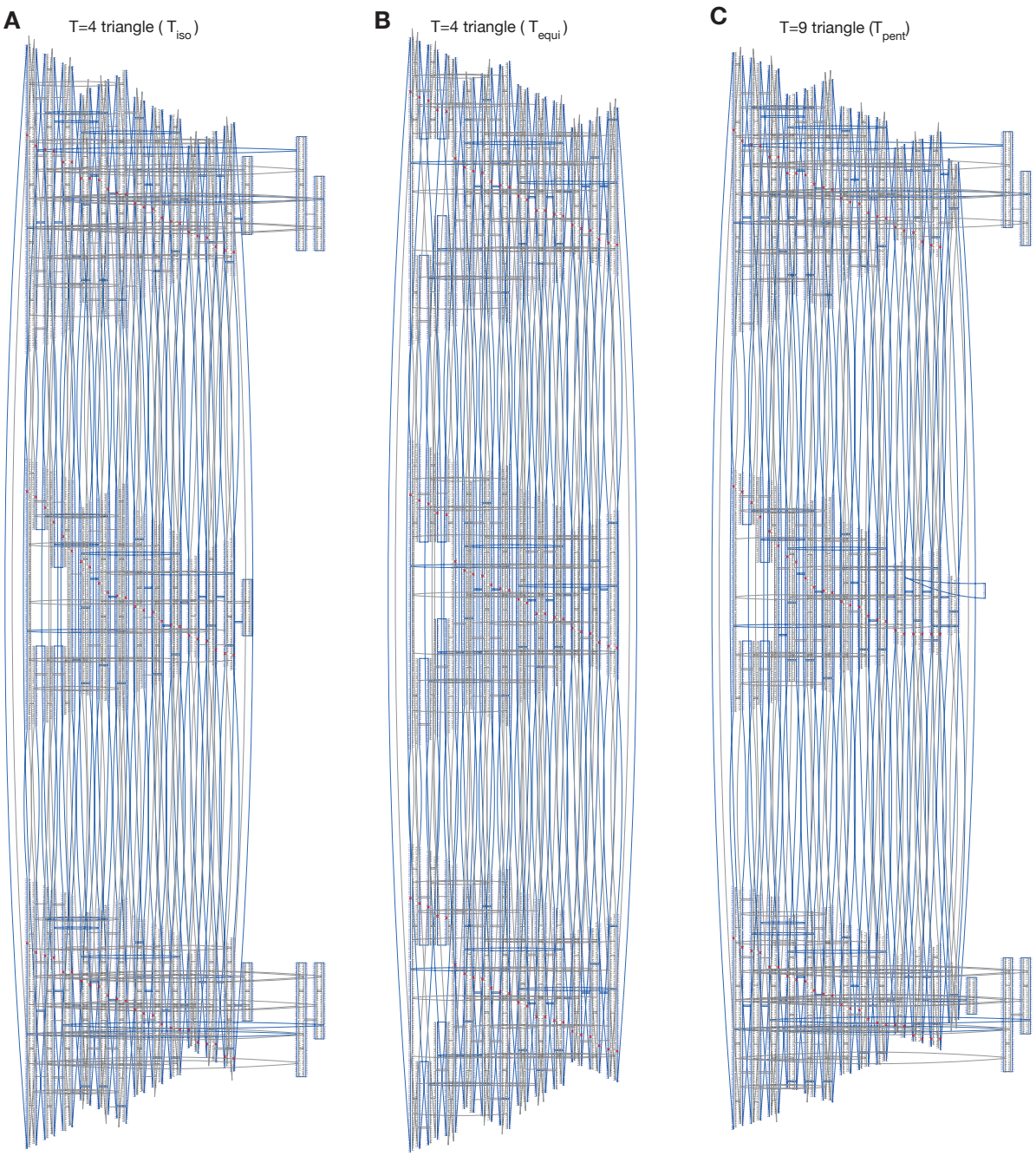

Supplementary Figure 39 | Design diagram of T=4 triangles and T_{pent} prepared with caDNAno v0.1. Oligonucleotides that connect two different sides have five additional single-stranded thymidines at the corner.

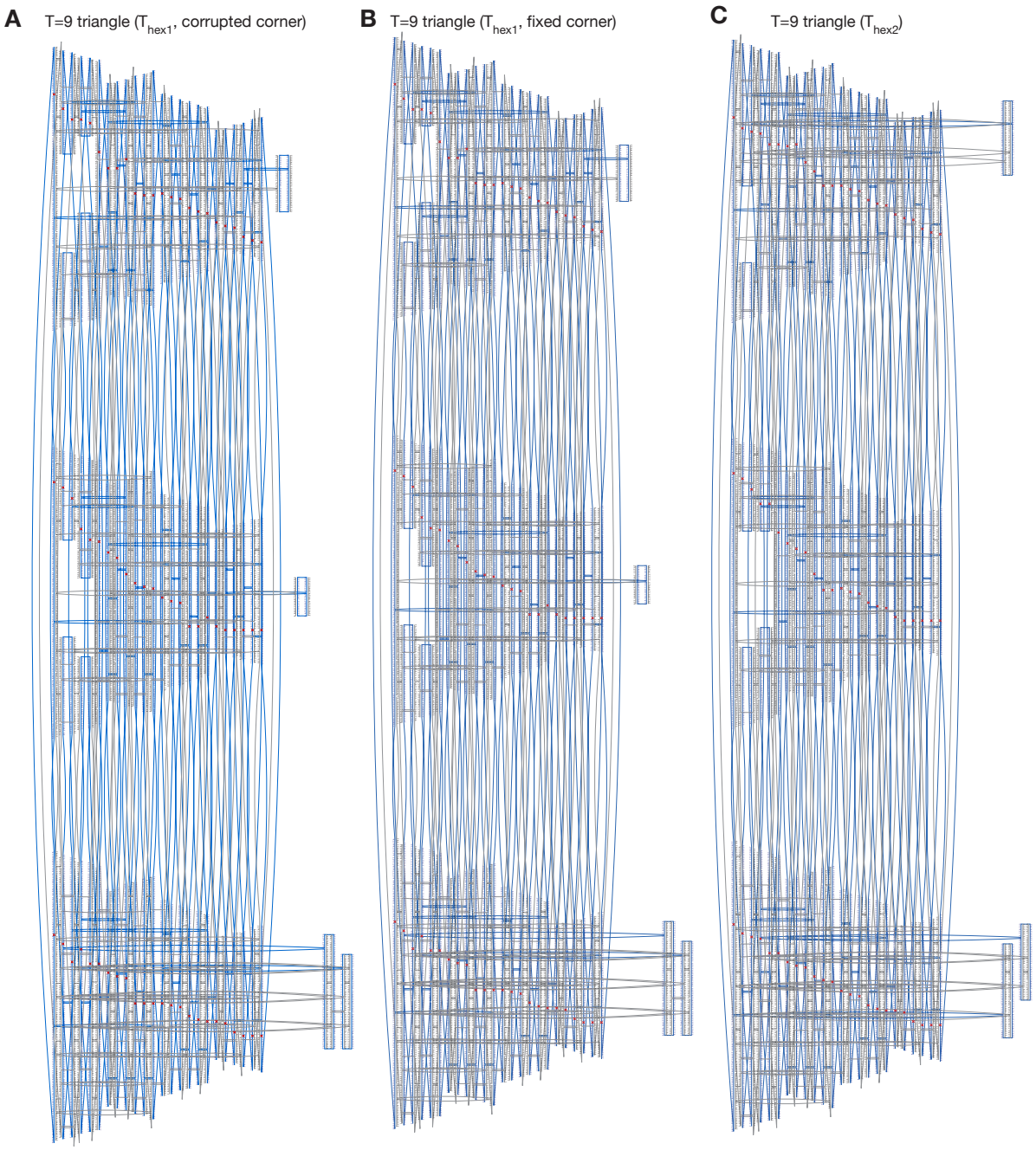

Supplementary Figure 40 | Design diagram of T=9 triangles T_{hex1} and T_{hex2} prepared with caDNAno v0.1. Oligonucleotides that connect two different sides have five additional single-stranded thymidines at the corner.

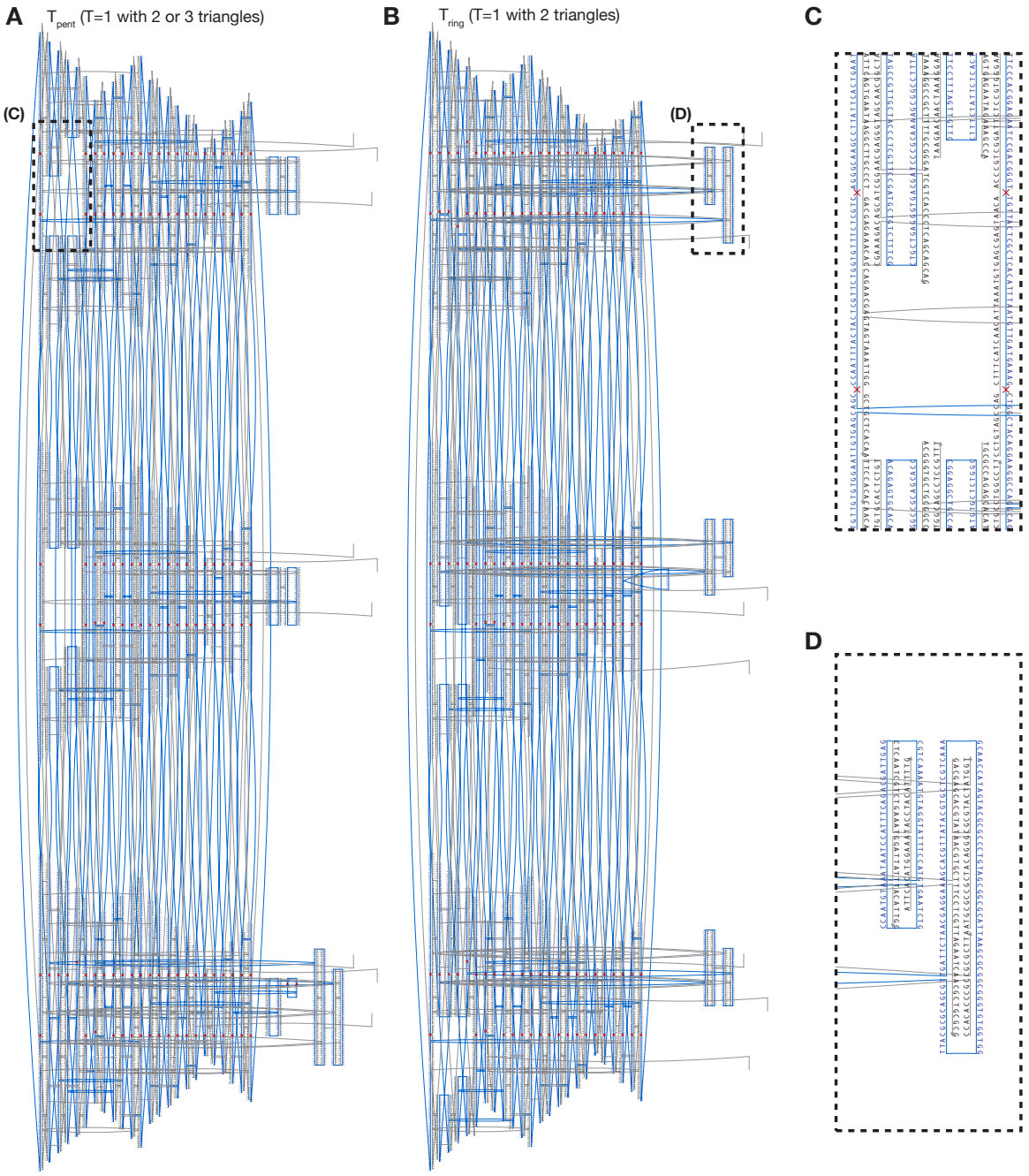

Supplementary Figure 41 | Design diagram of half-shell T=1 triangles prepared with caDNAno v0.1. (**A**)+(**B**) The T_{pent} triangle can be used to assemble half T=1 shells together with the T_{ring} triangle or to assemble T=1 shells missing a pentagon vertex together with T_{ring1} and T_{ring2} triangles (see Supplementary Fig. 25B,C). Oligonucleotides that connect two different sides have five additional single-stranded thymidines at the corner. Every side is equipped with three handles for attaching the antibodies (seq.: GCAGTAGAGTAGGTAGAGATTAGGCA-oligonucleotide). (**C**)+(**D**) Zoom on the recess and protrusion of the T_{pent} and T_{ring} triangle in (A) and (B). Six oligos building the recess were modified with overhangs complementary to parts of the scaffold in the protrusion to increase the binding strength for assembling half T=1 shells. In order to assemble T=1 shells with a missing pentagonal vertex (T_{pent} + T_{ring1} + T_{ring2}, Supplementary Fig. 25C), the overhangs of three bases were removed in (C).

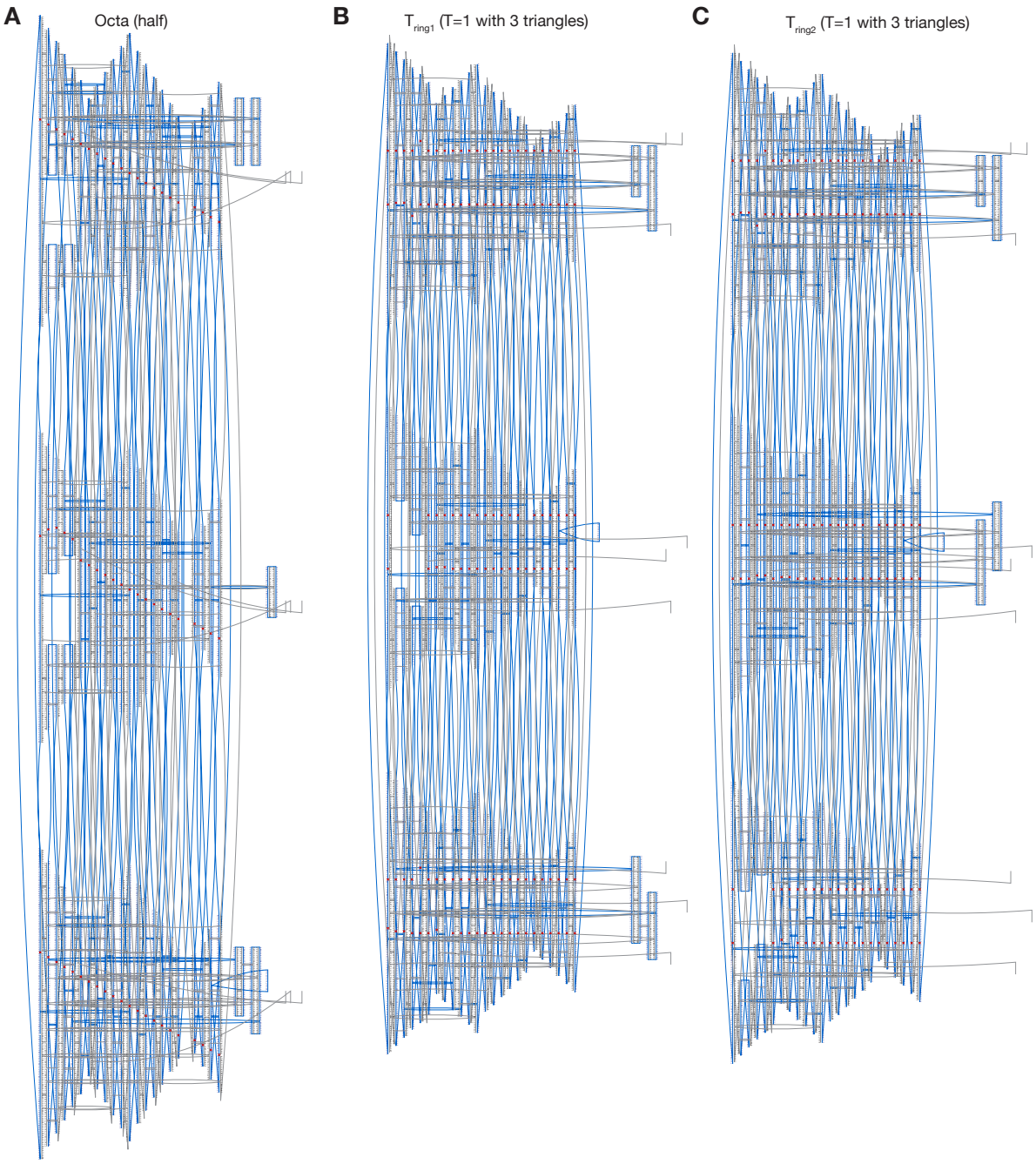

Supplementary Figure 42 | Design diagram of Octa and T=1 half-shell triangles prepared with caDNAno v0.1. Oligonucleotides that connect two different sides have five additional single-stranded thymidines at the corner. Every side is equipped with three handles for attaching the antibodies (seq.: GCAGTAGAGTAGGTAGAGATTAGGCA-oligo). The T_{ring1} and T_{ring2} triangles can assemble T=1 shells missing a pentagon vertex together with T_{pent} triangles (Supplementary Fig. 25C, Supplementary Fig. 41A).

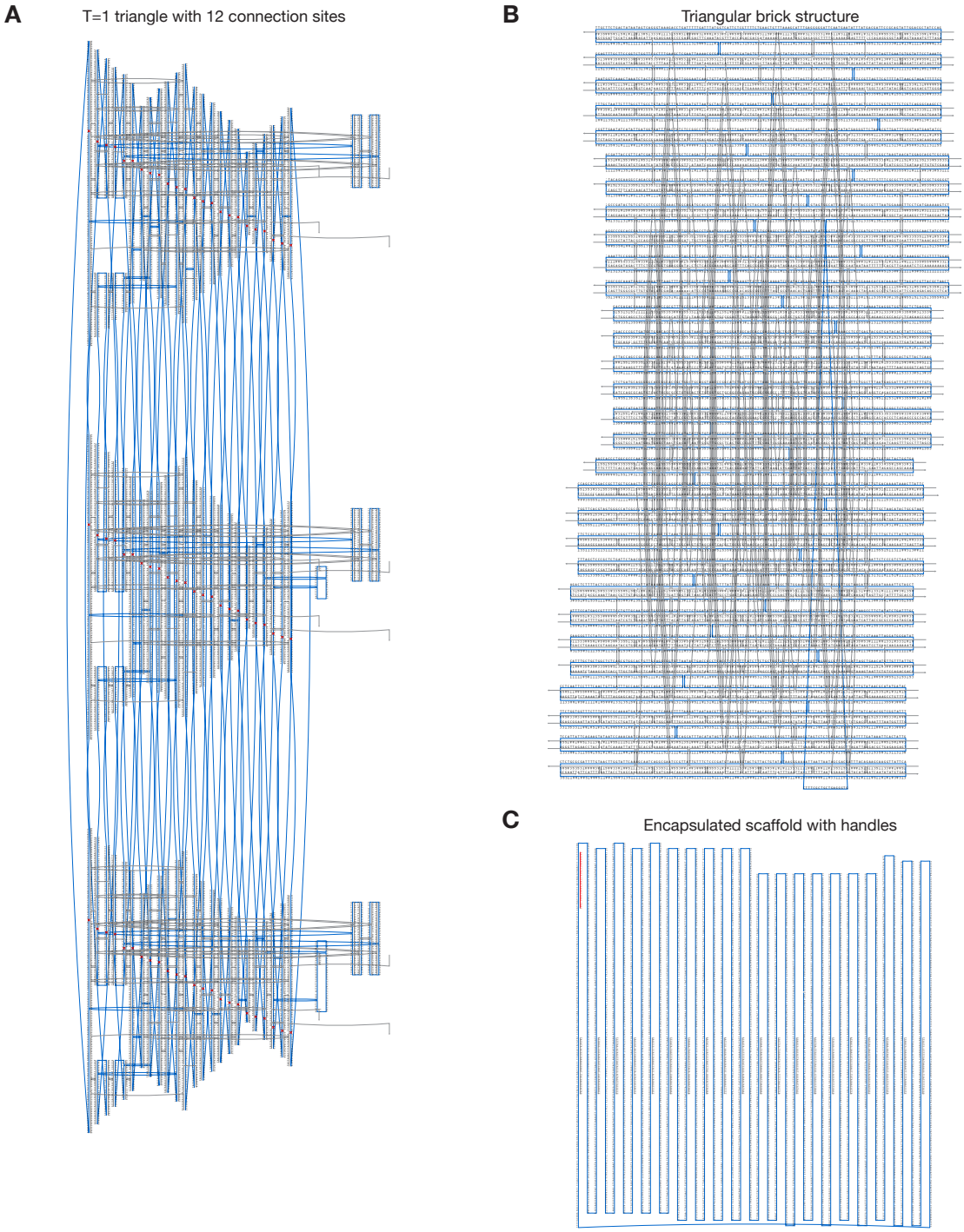

Supplementary Figure 43 | Design diagrams for modified T=1 shells prepared with caDNAno v0.1**.** (**A**) T=1 triangle with protruding oligonucleotides. (**B**) Triangular brick structure with connections sites. (**C**) Single-stranded scaffold with 20 handles for triangle (grey) and one handle for Cy5 (red) attachment.

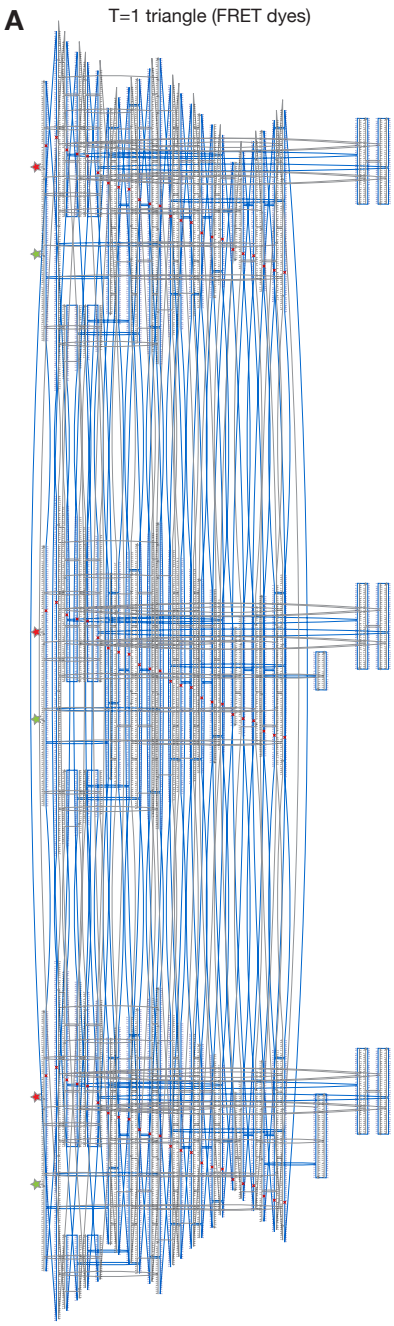

Supplementary Figure 44 | Design diagrams for T=1 triangles with modifications prepared with caDNAno v0.1**.** (**A**) T=1 triangle with Cy3 (green star) and Cy5 (red star) modifications on the 5’ end.

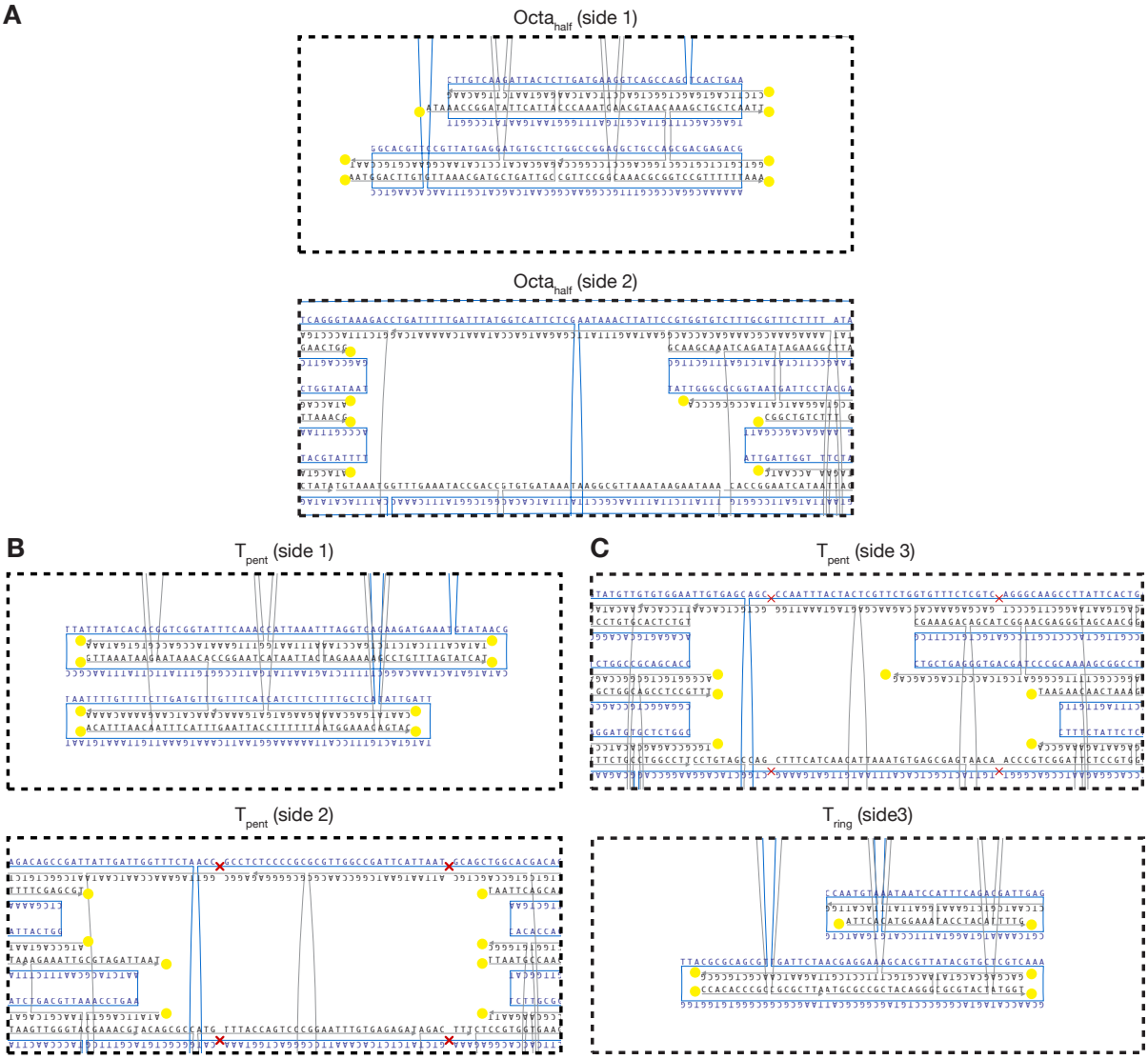

Supplementary Figure 45 | Design diagrams UV-welding at stacking contacts prepared with caDNAno v0.1**.** Protrusions and recesses have sticky overhangs and one optional, additional thymine base (yellow circle) for UV-welding in order to stabilize the partial shells in cell medium. (**A**) Protrusion and recess of the half octahedron (see Supplementary Fig. 42A). (**B**)+(**C**) Protrusion and recess of the half T=1 shell triangles T_{pent} and T_{ring} (see Supplementary Fig. 41C,D). Side 1 binds to side 2 (B) and side 3 of T_{pent} to side 3 of T_{ring} (C).

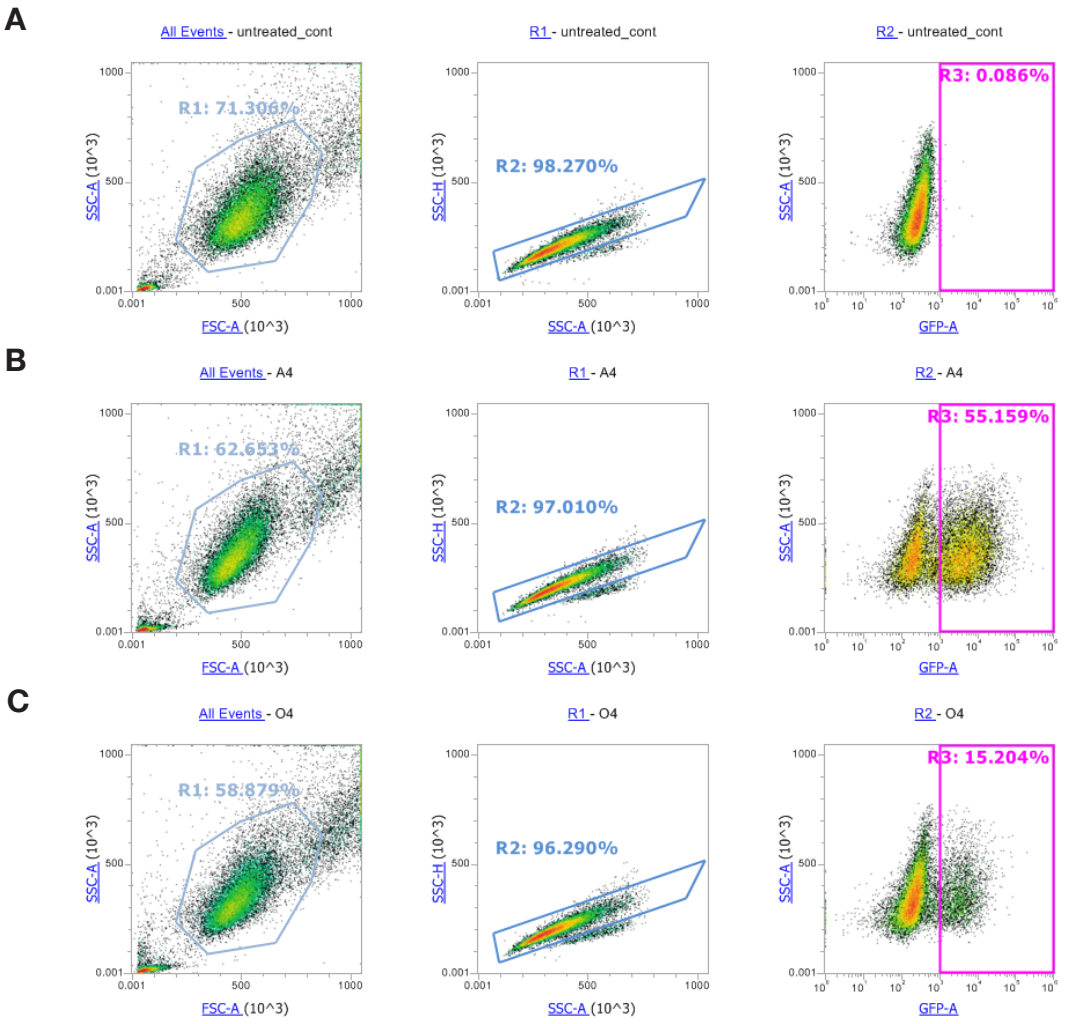

Supplementary Figure 46 | Representative gates for flow cytometry sample processing. From left to right: cell populations were first gated on forward scatter-area (FCS-A) versus side scatter-area (SSC-A) (gate 'R1'), single cells were selected by gating SSC-A versus side scatter height (SSC-H) (gate 'R2'), and then assessed for eGFP expression (gate 'R3'). (**A**) Untreated cells were used as a negative control. (**B**) and (**C**) give representative gates for samples treated with anti-AAV2 only and origami half shells + anti-AAV2 respectively, at concentrations corresponding to C4 in Supplementary Fig. 35.

Object	Denaturation phase temperature (15 min) (°C)	Temperature ramp (1°C/1h)	Storage temperature (°C)	Scaffold
T_octa	65	60-56°C	20	M13 8064
T=1	65	58-54°C	20	M13 8064
T=1 -5°	65	58-54°C	20	M13 8064
T=1 +5°	65	58-54°C	20	M13 8064
T=3	65	54-52°C	20	M13 8064
T=4_iso	65	56-54°C	20	M13 8064
T=4_equi	65	58-54°C	20	M13 8064
T=9_pent	65	56-52°C	20	M13 7249
T=9_hex1	65	56-52°C	20	M13 8064
T=9_hex2	65	58-54°C	20	M13 8064
T_octa_half	65	58-54°C	20	M13 8064
T_pent T=1 (2/3 triangles)	65	58-54°C	20	M13 8064
T_ ring T=1 (2 triangles)	65	56-52°C	20	M13 8064
T_ring1 T=1 (3 triangles)	65	56-52°C	20	M13 8064
T_ring2 T=1 (3 triangles)	65	56-52°C	20	M13 8064
triangular brick	65	60-44°C	20	M13 8064

Supplementary Table 2 | Temperature ramps and scaffold molecules used for self-assembly of shell building blocks. For scaffold sequences see section *Scaffold sequences* in the supplementary information. For staple sequences see design_sequnces.xlsx.

Object	Concentration (nM)	# of particles for re-finement	# of fractions	Dose (e/A^2)	Pixel size (A/pix)	Resolution of resulting 3D map (A)	Symmetry
Octa monomer (EMD-12009)	700	16524	5	42.57	2.28	18.69	C1
T=1 monomer (EMD-12010)	500	9496	7	51.16	2.28	20.27	C1
T=3 monomer (EMD-12011)	500	11080	7	53.17	2.28	19.09	C1
T=4_iso (EMD-12012)	500	16904	7	48.53	2.28	17.22	C1
T=4_equi (EMD-12013)	500	34288	7	48.26	2.28	21.21	C1
T=9_pent (EMD-12008)	800	25053	8	47.9	1.79	14.92	C1
T=9_hex1 (EMD-12014)	800	38498	13	36.85	1.79	12.92	C1
T=9_hex2 (EMD-12015)	800	11481	8	48	1.79	15.04	C1
Octa shell (17.5mM) (EMD-12016)	130	3384	11	42.71	2.28	19.64	O
T=1 shell (20 mM) (EMD-12021)	110	2578	10	51.11	2.28	21	I1
T=1 shell (25 mM) (EMD-12024)	50 (lacey carbon grid)	720	7	31.26	2.28	22.21	I1
T=3 shell (20 mM) (EMD-12019)	20	612	-	22.96	3.71	36.15	I1

T=4 shell (25 mM) (EMD-12020)	21 (T_iso) 7 (T_equi)	255	-	25	3.71	47.87	I1
spiky shell (22.5mM) (EMD-12049)	150	3847	8 (dataset1) 11 (dataset2)	25.76 (dataset1) 30.00 (dataset 2)	3.76	22	I1
triangular brick (EMD-12046)	1000	38132	7	78.6	2.28	11.9	C1
Octa_half Shell (30mM) (EMD-12007)	180	6801	10	40.44	2.9	20.41	C4
Octa_half shell (30mM) + HBV core (EMD-12044)	40	2707	7	44.38	2.9	23	C1
T=1_half shell (2 triangles, 30mM) (EMD-12045)	180	8725	10	40.44	2.9	15.16	C1
T=1_half shell + HBV core (2 triangles, 30mM) (EMD-12022)	50	1770	7	44.79	2.9	23	C5
T=1_15mer shell (3 triangles, 30mM) (EMD-12023)	210	3194	10	29.17	2.9	22.3	C5

Supplementary Table 3 | Cryo-EM imaging conditions.

Supplementary Note 1

See also Engelhardt et al (*2*). For staple sequences see Supplementary Sequences.

M13 8064:

GGCAATGACCTGATAGCCTTTGTAGATCTCTCAAAAATAGCTACCCTCTCCGGCATTAATTTATCAGCTAGAACGGTTGAATATCATATTGATGGTGATTTGACTGTCTCCGG
CCTTTCTCACCCTTTTGAATCTTTACCTACACATTACTCAGGCATTGCATTTAAAATATATGAGGGTTCTAAAAATTTTTATCCTTGCGTTGAAATAAAGGCTTCTCCCGCAAAA
GTATTACAGGGTCATAATGTTTTTGGTACAACCGATTTAGCTTTATGCTCTGAGGCTTTATTGCTTAATTTTGCTAATTCTTTGCCTTGCCTGTATGATTTATTGGATGTTAATGC
TACTACTATTAGTAGAATTGATGCCACCTTTTCAGCTCGCGCCCCAAATGAAAATATAGCTAAACAGGTTATTGACCATTTGCGAAATGTATCTAATGGTCAAACTAAATCTAC
TCGTTCGCAGAATTGGGAATCAACTGTTATATGGAATGAAACTTCCAGACACCGTACTTTAGTTGCATATTTAAAACATGTTGAGCTACAGCATTATATTCAGCAATTAAGCTC
TAAGCCATCCGCAAAAATGACCTCTTATCAAAAGGAGCAATTAAAGGTACTCTCTAATCCTGACCTGTTGGAGTTTGCTTCCGGTCTGGTTCGCTTTGAAGCTCGAATTAAAA
CGCGATATTTGAAGTCTTTCGGGGCTTCCTCTTAATCTTTTTGATGCAATCCGCTTTGCTTCTGACTATAATAGTCAGGGTAAAGACCTGATTTTTGATTTATGGTCATTCTCGTT
TTCTGAACTGTTTAAAGCATTTGAGGGGGATTCAATGAATATTTATGACGATTCCGCAGTATTGGACGCTATCCAGTCTAAACATTTTACTATTACCCCCTCTGGCAAAACTTC
TTTTGCAAAAGCCTCTCGCTATTTTGGTTTTTATCGTCGTCTGGTAAACGAGGGTTATGATAGTGTTGCTCTTACTATGCCTCGTAATTCCTTTTGGCGTTATGTATCTGCATTA
GTTGAATGTGGTATTCCTAAATCTCAACTGATGAATCTTTCTACCTGTAATAATGTTGTTCCGTTAGTTCGTTTTATTAACGTAGATTTTTCTTCCCAACGTCCTGACTGGTATAA
TGAGCCAGTTCTTAAAATCGCATAAGGTAATTCACAATGATTAAAGTTGAAATTAAACCATCTCAAGCCCAATTTACTACTCGTTCTGGTGTTTCTCGTCAGGGCAAGCCTTAT
TCACTGAATGAGCAGCTTTGTTACGTTGATTTGGGTAATGAATATCCGGTTCTTGTCAAGATTACTCTTGATGAAGGTCAGCCAGCCTATGCGCCTGGTCTGTACACCGTTCA
TCTGTCCTCTTTCAAAGTTGGTCAGTTCGGTTCCCTTATGATTGACCGTCTGCGCCTCGTTCCGGCTAAGTAACATGGAGCAGGTCGCGGATTTCGACACAATTTATCAGGC
GATGATACAAATCTCCGTTGTACTTTGTTTCGCGCTTGGTATAATCGCTGGGGGTCAAAGATGAGTGTTTTAGTGTATTCTTTTGCCTCTTTCGTTTTAGGTTGGTGCCTTCGT
AGTGGCATTACGTATTTTACCCGTTTAATGGAAACTTCCTCATGAAAAAGTCTTTAGTCCTCAAAGCCTCTGTAGCCGTTGCTACCCTCGTTCCGATGCTGTCTTTCGCTGCT
GAGGGTGACGATCCCGCAAAAGCGGCCTTTAACTCCCTGCAAGCCTCAGCGACCGAATATATCGGTTATGCGTGGGCGATGGTTGTTGTCATTGTCGGCGCAACTATCGGG
TATCAAGCTGTTTAAGAAATTCACCTCGAAAGCAAGCTGATAAACCGATACAATTAAAGGCTCCTTTTGGAGCCTTTTTTTTGGAGATTTTCAACGTGAAAAAATTATTATTCGC
AATTCCTTTAGTTGTTCCTTTCTATTCTCACTCCGCTGAAACTGTTGAAAGTTGTTTAGCAAAATCCCATACAGAAAATTCATTTACTAACGTCTGGAAAGACGACAAAACTTTA
GATCGTTACGCTAACTATGAGGGCTGTCTGTGGAATGCTACAGGCGTTGTAGTTTGTACTGGTGACGAAACTCAGTGTTACGGTACATGGGTTCCTATTGGGCTTGCTATCCC
CTGAAAATGAGGGTGGTGGCTCTGAGGGTGGCGGTTCTGAGGGTGGCGGTTCTGAGGGTGGCGGTACTAAACCTCCTGAGTACGGTGATACACCTATTCCGGGCTATACT
TATATCAACCCTCTCGACGGCACTTATCCGCCTGGTACTGAGCAAAACCCCGCTAATCCTAATCCTTCTCTTGAGGAGTCTCAGCCTCTTAATACTTTCATGTTTCAGAATAA
TAGGTTCCGAAATAGGCAGGGGGCATTAACTGTTTATACGGGCACTGTTACTCAAGGCACTGACCCCGTTAAAACTTATTACCAGTACACTCCTGTATCATCAAAAGCCATG
TATGACGCTTACTGGAACGGTAAATTCAGAGACTGCGCTTTCCATTCTGGCTTTAATGAGGATTTATTTGTTTGTGAATATCAAGGCCAATCGTCTGACCTGCCTCAACCTCCT
GTCAATGCTGGCGGCGGCTCTGGTGGTGGTTCTGGTGGCGGCTCTGAGGGTGGTGGCTCTGAGGGTGGCGGTTCTGAGGGTGGCGGCTCTGAGGGAGGCGGTTCCGGT
GGTGGCTCTGGTTCCGGTGATTTTGATTATGAAAAGATGGCAAACGCTAATAAGGGGGCTATGACCGAAAATGCCGATGAAAACGCGCTACAGTCTGACGCTAAAGGCAAA
CTTGATTCTGTCGCTACTGATTACGGTGCTGCTATCGATGGTTTCATTGGTGACGTTTCCGGCCTTGCTAATGGTAATGGTGCTACTGGTGATTTTGCTGGCTCTAATTCCCA
AATGGCTCAAGTCGGTGACGGTGATAATTCACCTTTAATGAATAATTTCCGTCAATATTTACCTTCCCTCCCTCAATCGGTTGAATGTCGCCCTTTTGTCTTTGGCGCTGGTAA
ACCATATGAATTTTCTATTGATTGTGACAAAATAAACTTATTCCGTGGTGTCTTTGCGTTTCTTTTATATGTTGCCACCTTTATGTATGTATTTTCTACGTTTGCTAACATACTGCG
TAATAAGGAGTCTTAATCATGCCAGTTCTTTTGGGTATTCCGTTATTATTGCGTTTCCTCGGTTTCCTTCTGGTAACTTTGTTCGGCTATCTGCTTACTTTTCTTAAAAAGGGCTT
CGGTAAGATAGCTATTGCTATTTCATTGTTTCTTGCTCTTATTATTGGGCTTAACTCAATTCTTGTGGGTTATCTCTCTGATATTAGCGCTCAATTACCCTCTGACTTTGTTCAGG
GTGTTCAGTTAATTCTCCCGTCTAATGCGCTTCCCTGTTTTTATGTTATTCTCTCTGTAAAGGCTGCTATTTTCATTTTTGACGTTAAACAAAAAATCGTTTCTTATTTGGATTGG
GATAAATAATATGGCTGTTTATTTTGTAACTGGCAAATTAGGCTCTGGAAAGACGCTCGTTAGCGTTGGTAAGATTCAGGATAAAATTGTAGCTGGGTGCAAAATAGCAACTAA

TCTTGATTTAAGGCTTCAAAACCTCCCGCAAGTCGGGAGGTTCGCTAAAACGCCTCGCGTTCTTAGAATACCGGATAAGCCTTCTATATCTGATTTGCTTGCTATTGGGCGC
GGTAATGATTCCTACGATGAAAATAAAAACGGCTTGCTTGTTCTCGATGAGTGCGGTACTTGGTTTAATACCCGTTCTTGGAATGATAAGGAAAGACAGCCGATTATTGATTG
GTTTCTACATGCTCGTAAATTAGGATGGGATATTATTTTTCTTGTTCAGGACTTATCTATTGTTGATAAACAGGCGCGTTCTGCATTAGCTGAACATGTTGTTTATTGTCGTCGT
CTGGACAGAATTACTTTACCTTTTGTCGGTACTTTATATTCTCTTATTACTGGCTCGAAAATGCCTCTGCCTAAATTACATGTTGGCGTTGTTAAATATGGCGATTCTCAATTAA
GCCCTACTGTTGAGCGTTGGCTTTATACTGGTAAGAATTTGTATAACGCATATGATACTAAACAGGCTTTTTCTAGTAATTATGATTCCGGTGTTTATTCTTATTTAACGCCTTAT
TTATCACACGGTCGGTATTTCAAACCATTAAATTTAGGTCAGAAGATGAAATTAACTAAAATATATTTGAAAAAGTTTTCTCGCGTTCTTTGTCTTGCGATTGGATTTGCATCAG
CATTTACATATAGTTATATAACCCAACCTAAGCCGGAGGTTAAAAAGGTAGTCTCTCAGACCTATGATTTTGATAAATTCACTATTGACTCTTCTCAGCGTCTTAATCTAAGCTA
TCGCTATGTTTTCAAGGATTCTAAGGGAAAATTAATTAATAGCGACGATTTACAGAAGCAAGGTTATTCACTCACATATATTGATTTATGTACTGTTTCCATTAAAAAAGGTAATT
CAAATGAAATTGTTAAATGTAATTAATTTTGTTTTCTTGATGTTTGTTTCATCATCTTCTTTTGCTCAGGTAATTGAAATGAATAATTCGCCTCTGCGCGATTTTGTAACTTGGTAT
TCAAAGCAATCAGGCGAATCCGTTATTGTTTCTCCCGATGTAAAAGGTACTGTTACTGTATATTCATCTGACGTTAAACCTGAAAATCTACGCAATTTCTTTATTTCTGTTTTAC
GTGCAAATAATTTTGATATGGTAGGTTCTAACCCTTCCATTATTCAGAAGTATAATCCAAACAATCAGGATTATATTGATGAATTGCCATCATCTGATAATCAGGAATATGATGA
TAATTCCGCTCCTTCTGGTGGTTTCTTTGTTCCGCAAAATGATAATGTTACTCAAACTTTTAAAATTAATAACGTTCGGGCAAAGGATTTAATACGAGTTGTCGAATTGTTTGTA
AAGTCTAATACTTCTAAATCCTCAAATGTATTATCTATTGACGGCTCTAATCTATTAGTTGTTAGTGCTCCTAAAGATATTTTAGATAACCTTCCTCAATTCCTTTCAACTGTTGAT
TTGCCAACTGACCAGATATTGATTGAGGGTTTGATATTTGAGGTTCAGCAAGGTGATGCTTTAGATTTTTCATTTGCTGCTGGCTCTCAGCGTGGCACTGTTGCAGGCGGTGT
TAATACTGACCGCCTCACCTCTGTTTTATCTTCTGCTGGTGGTTCGTTCGGTATTTTTAATGGCGATGTTTTAGGGCTATCAGTTCGCGCATTAAAGACTAATAGCCATTCAAA
AATATTGTCTGTGCCACGTATTCTTACGCTTTCAGGTCAGAAGGGTTCTATCTCTGTTGGCCAGAATGTCCCTTTTATTACTGGTCGTGTGACTGGTGAATCTGCCAATGTAAA
TAATCCATTTCAGACGATTGAGCGTCAAAATGTAGGTATTTCCATGAGCGTTTTTCCTGTTGCAATGGCTGGCGGTAATATTGTTCTGGATATTACCAGCAAGGCCGATAGTTT
GAGTTCTTCTACTCAGGCAAGTGATGTTATTACTAATCAAAGAAGTATTGCTACAACGGTTAATTTGCGTGATGGACAGACTCTTTTACTCGGTGGCCTCACTGATTATAAAAA
CACTTCTCAGGATTCTGGCGTACCGTTCCTGTCTAAAATCCCTTTAATCGGCCTCCTGTTTAGCTCCCGCTCTGATTCTAACGAGGAAAGCACGTTATACGTGCTCGTCAAA
GCAACCATAGTACGCGCCCTGTAGCGGCGCATTAAGCGCGGCGGGTGTGGTGGTTACGCGCAGCGTGACCGCTACACTTGCCAGCGCCCTAGCGCCCGCTCCTTTCGC
TTTCTTCCCTTCCTTTCTCGCCACGTTCGCCGGCTTTCCCCGTCAAGCTCTAAATCGGGGGCTCCCTTTAGGGTTCCGATTTAGTGCTTTACGGCACCTCGACCCCAAAAAA
CTTGATTTGGGTGATGGTTCACGTAGTGGGCCATCGCCCTGATAGACGGTTTTTCGCCCTTTGACGTTGGAGTCCACGTTCTTTAATAGTGGACTCTTGTTCCAAACTGGAA
CAACACTCAACCCTATCTCGGGCTATTCTTTTGATTTATAAGGGATTTTGCCGATTTCGGAACCACCATCAAACAGGATTTTCGCCTGCTGGGGCAAACCAGCGTGGACCGC
TTGCTGCAACTCTCTCAGGGCCAGGCGGTGAAGGGCAATCAGCTGTTGCCCGTCTCACTGGTGAAAAGAAAAACCACCCTGGCGCCCAATACGCAAACCGCCTCTCCCC
GCGCGTTGGCCGATTCATTAATGCAGCTGGCACGACAGGTTTCCCGACTGGAAAGCGGGCAGTGAGCGCAACGCAATTAATGTGAGTTAGCTCACTCATTAGGCACCCCA
GGCTTTACACTTTATGCTTCCGGCTCGTATGTTGTGTGGAATTGTGAGCGGATAACAATTTCACACAGGAAACAGCTATGACCATGATTACGAATTCGAGCTCGGTACCCGG
GGATCCTCAACTGTGAGGAGGCTCACGGACGCGAAGAACAGGCACGCGTGCTGGCAGAAACCCCCGGTATGACCGTGAAAACGGCCCGCCGCATTCTGGCCGCAGCAC
CACAGAGTGCACAGGCGCGCAGTGACACTGCGCTGGATCGTCTGATGCAGGGGGCACCGGCACCGCTGGCTGCAGGTAACCCGGCATCTGATGCCGTTAACGATTTGCT
GAACACACCAGTGTAAGGGATGTTTATGACGAGCAAAGAAACCTTTACCCATTACCAGCCGCAGGGCAACAGTGACCCGGCTCATACCGCAACCGCGCCCGGCGGATTG
AGTGCGAAAGCGCCTGCAATGACCCCGCTGATGCTGGACACCTCCAGCCGTAAGCTGGTTGCGTGGGATGGCACCACCGACGGTGCTGCCGTTGGCATTCTTGCGGTTG
CTGCTGACCAGACCAGCACCACGCTGACGTTCTACAAGTCCGGCACGTTCCGTTATGAGGATGTGCTCTGGCCGGAGGCTGCCAGCGACGAGACGAAAAAACGGACCGC
GTTTGCCGGAACGGCAATCAGCATCGTTTAACTTTACCCTTCATCACTAAAGGCCGCCTGTGCGGCTTTTTTTACGGGATTTTTTTATGTCGATGTACACAACCGCCCAACTG
CTGGCGGCAAATGAGCAGAAATTTAAGTTTGATCCGCTGTTTCTGCGTCTCTTTTTCCGTGAGAGCTATCCCTTCACCACGGAGAAAGTCTATCTCTCACAAATTCCGGGACT
GGTAAACATGGCGCTGTACGTTTCGCCGATTGTTTCCGGTGAGGTTATCCGTTCCCGTGGCGGCTCCACCTCTGAAAGCTTGGCACTGGCCGTCGTTTTACAACGTCGTGA
CTGGGAAAACCCTGGCGTTACCCAACTTAATCGCCTTGCAGCACATCCCCCTTTCGCCAGCTGGCGTAATAGCGAAGAGGCCCGCACCGATCGCCCTTCCCAACAGTTGC
GCAGCCTGAATGGCGAATGGCGCTTTGCCTGGTTTCCGGCACCAGAAGCGGTGCCGGAAAGCTGGCTGGAGTGCGATCTTCCTGAGGCCGATACTGTCGTCGTCCCCTC
AAACTGGCAGATGCACGGTTACGATGCGCCCATCTACACCAACGTGACCTATCCCATTACGGTCAATCCGCCGTTTGTTCCCACGGAGAATCCGACGGGTTGTTACTCGCT
CACATTTAATGTTGATGAAAGCTGGCTACAGGAAGGCCAGACGCGAATTATTTTTGATGGCGTTCCTATTGGTTAAAAAATGAGCTGATTTAACAAAAATTTAATGCGAATTTT
AACAAAATATTAACGTTTACAATTTAAATATTTGCTTATACAATCTTCCTGTTTTTGGGGCTTTTCTGATTATCAACCGGGGTACATATGATTGACATGCTAGTTTTACGATTACC
GTTCATCGATTCTCTTGTTTGCTCCAGACTCTCA

M13 7249:

TGATAGACGGTTTTTCGCCCTTTGACGTTGGAGTCCACGTTCTTTAATAGTGGACTCTTGTTCCAAACTGGAACAACACTCAACCCTATCTCGGGCTATTCTTTTGATTTATAA
GGGATTTTGCCGATTTCGGAACCACCATCAAACAGGATTTTCGCCTGCTGGGGCAAACCAGCGTGGACCGCTTGCTGCAACTCTCTCAGGGCCAGGCGGTGAAGGGCAAT
CAGCTGTTGCCCGTCTCACTGGTGAAAAGAAAAACCACCCTGGCGCCCAATACGCAAACCGCCTCTCCCCGCGCGTTGGCCGATTCATTAATGCAGCTGGCACGACAGGT
TTCCCGACTGGAAAGCGGGCAGTGAGCGCAACGCAATTAATGTGAGTTAGCTCACTCATTAGGCACCCCAGGCTTTACACTTTATGCTTCCGGCTCGTATGTTGTGTGGAAT
TGTGAGCGGATAACAATTTCACACAGGAAACAGCTATGACCATGATTACGAATTCGAGCTCGGTACCCGGGGATCCTCTAGAGTCGACCTGCAGGCATGCAAGCTTGGCAC
TGGCCGTCGTTTTACAACGTCGTGACTGGGAAAACCCTGGCGTTACCCAACTTAATCGCCTTGCAGCACATCCCCCTTTCGCCAGCTGGCGTAATAGCGAAGAGGCCCGC
ACCGATCGCCCTTCCCAACAGTTGCGCAGCCTGAATGGCGAATGGCGCTTTGCCTGGTTTCCGGCACCAGAAGCGGTGCCGGAAAGCTGGCTGGAGTGCGATCTTCCTG
AGGCCGATACTGTCGTCGTCCCCTCAAACTGGCAGATGCACGGTTACGATGCGCCCATCTACACCAACGTGACCTATCCCATTACGGTCAATCCGCCGTTTGTTCCCACG
GAGAATCCGACGGGTTGTTACTCGCTCACATTTAATGTTGATGAAAGCTGGCTACAGGAAGGCCAGACGCGAATTATTTTTGATGGCGTTCCTATTGGTTAAAAAATGAGCTG
ATTTAACAAAAATTTAATGCGAATTTTAACAAAATATTAACGTTTACAATTTAAATATTTGCTTATACAATCTTCCTGTTTTTGGGGCTTTTCTGATTATCAACCGGGGTACATATG
ATTGACATGCTAGTTTTACGATTACCGTTCATCGATTCTCTTGTTTGCTCCAGACTCTCAGGCAATGACCTGATAGCCTTTGTAGATCTCTCAAAAATAGCTACCCTCTCCGGC
ATTAATTTATCAGCTAGAACGGTTGAATATCATATTGATGGTGATTTGACTGTCTCCGGCCTTTCTCACCCTTTTGAATCTTTACCTACACATTACTCAGGCATTGCATTTAAAA
TATATGAGGGTTCTAAAAATTTTTATCCTTGCGTTGAAATAAAGGCTTCTCCCGCAAAAGTATTACAGGGTCATAATGTTTTTGGTACAACCGATTTAGCTTTATGCTCTGAGGC
TTTATTGCTTAATTTTGCTAATTCTTTGCCTTGCCTGTATGATTTATTGGATGTTAATGCTACTACTATTAGTAGAATTGATGCCAACCTTTTCAGCTCGCGCCCCAAATGAAAATA
TAGCTAAACAGGTTATTGACCATTTGCGAAATGTATCTAATGGTCAAACTAAATCTACTCGTTCGCAGAATTGGGAATCAACTGTTATATGGAATGAAACTTCCAGACACCGTA
CTTTAGTTGCATATTTAAAACATGTTGAGCTACAGCATTATATTCAGCAATTAAGCTCTAAGCCATCCGCAAAAATGACCTCTTATCAAAAGGAGCAATTAAAGGTACTCTCTAA
TCCTGACCTGTTGGAGTTTGCTTCCGGTCTGGTTCGCTTTGAAGCTCGAATTAAAACGCGATATTTGAAGTCTTTCGGGCTTCCTCTTAATCTTTTTGATGCAATCCGCTTTGC
TTCTGACTATAATAGTCAGGGTAAAGACCTGATTTTTGATTTATGGTCATTCTCGTTTTCTGAACTGTTTAAAGCATTTGAGGGGGATTCAATGAATATTTATGACGATTCCGCA
GTATTGGACGCTATCCAGTCTAAACATTTTACTATTACCCCCTCTGGCAAAACTTCTTTTGCAAAAGCCTCTCGCTATTTTGGTTTTTATCGTCGTCTGGTAAACGAGGGTTAT
GATAGTGTTGCTCTTACTATGCCTCGTAATTCCTTTTGGCGTTATGTATCTGCATTAGTTGAATGTGGTATTCCTAAATCTCAACTGATGAATCTTTCTACCTGTAATAATGTTGT
TCCGTTTAGTTCGTTTTATTAACGTAGATTTTTCTTCCCAACGTCCTGACTGGTATAATGAGCCAGTTCTTAAAATCGCATAAGGTAATTCACAATGATTAAAGTTGAAATTAAAC
CATCTCAAGCCCAATTTACTACTCGTTCTGGTGTTTCTCGTCAGGGCAAGCCTTATTCACTGAATGAGCAGCTTTGTTACGTTGATTTGGGTAATGAATATCCGGTTCTTGTCA
AGATTACTCTTGATGAAGGTCAGCCAGCCTATGCGCCTGGTCTGTACACCGTTCATCTGTCCTCTTTCAAAGTTGGTCAGTTCGGTTCCCTTATGATTGACCGTCTGCGCCT
CGTTCCGGCTAAGTAACATGGAGCAGGTCGCGGATTTCGACACAATTTATCAGGCGATGATACAAATCTCCGTTGTACTTTGTTTCGCGCTTGGTATAATCGCTGGGGGTCA
AAGATGAGTGTTTTAGTGTATTCTTTTGCCTCTTTCGTTTTAGGTTGGTGCCTTCGTAGTGGCATTACGTATTTTACCCGTTTAATGGAAACTTCCTCATGAAAAAGTCTTTAGT
CCTCAAAGCCTCTGTAGCCGTTGCTACCCTCGTTCCGATGCTGTCTTTCGCTGCTGAGGGTGACGATCCCGCAAAAGCGGCCTTTAACTCCCTGCAAGCCTCAGCGACCG
AATATATCGGTTATGCGTGGGCGATGGTTGTTGTCATTGTCGGCGCAACTATCGGTATCAAGCTGTTTAAGAAATTCACCTCGAAAGCAAGCTGATAAACCGATACAATTAAA
GGCTCCTTTTGGAGCCTTTTTTTTGGAGATTTTCAACGTGAAAAAATTATTATTCGCAATTCCTTTAGTTGTTCCTTTCTATTCTCACTCCGCTGAAACTGTTGAAAGTTGTTTAG
CAAAATCCCATACAGAAAATTCATTTACTAACGTCTGGAAAGACGACAAAACTTTAGATCGTTACGCTAACTATGAGGGCTGTCTGTGGAATGCTACAGGCGTTGTAGTTTGT
ACTGGTGACGAAACTCAGTGTTACGGTACATGGGTTCCTATTGGGCTTGCTATCCCTGAAAATGAGGGTGGTGGCTCTGAGGGTGGCGGTTCTGAGGGTGGCGGTTCTGA
GGGTGGCGGTACTAAACCTCCTGAGTACGGTGATACACCTATTCCGGGCTATACTTATATCAACCCTCTCGACGGCACTTATCCGCCTGGTACTGAGCAAAACCCCGCTAA
TCCTAATCCTTCTCTTGAGGAGTCTCAGCCTCTTAATACTTTCATGTTTCAGAATAATAGGTTCCGAAATAGGCAGGGGGCATTAACTGTTTATACGGGCACTGTTACTCAAG
GCACTGACCCCGTTAAAACTTATTACCAGTACACTCCTGTATCATCAAAAGCCATGTATGACGCTTACTGGAACGGTAAATTCAGAGACTGCGCTTTCCATTCTGGCTTTAAT
GAGGATTTATTTGTTTGTGAATATCAAGGCCAATCGTCTGACCTGCCTCAACCTCCTGTCAATGCTGGCGGCGGCTCTGGTGGTGGTTCTGGTGGCGGCTCTGAGGGTGGT
GGCTCTGAGGGTGGCGGTTCTGAGGGTGGCGGCTCTGAGGGAGGCGGTTCCGGTGGTGGCTCTGGTTCCGGTGATTTTGATTATGAAAAGATGGCAAACGCTAATAAGG
GGGCTATGACCGAAAATGCCGATGAAAACGCGCTACAGTCTGACGCTAAAGGCAAACTTGATTCTGTCGCTACTGATTACGGTGCTGCTATCGATGGTTTCATTGGTGACGT
TTCCGGCCTTGCTAATGGTAATGGTGCTACTGGTGATTTTGCTGGCTCTAATTCCCAAATGGCTCAAGTCGGTGACGGTGATAATTCACCTTTAATGAATAATTTCCGTCAATA
TTTACCTTCCCTCCCTCAATCGGTTGAATGTCGCCCTTTTGTCTTTGGCGCTGGTAAACCATATGAATTTTCTATTGATTGTGACAAAATAAACTTATTCCGTGGTGTCTTTGCG
TTTCTTTTATATGTTGCCACCTTTATGTATGTATTTTCTACGTTTGCTAACATACTGCGTAATAAGGAGTCTTAATCATGCCAGTTCTTTTGGGTATTCCGTTATTATTGCGTTTCC
TCGGTTTCCTTCTGGTAACTTTGTTCGGCTATCTGCTTACTTTTCTTAAAAAGGGCTTCGGTAAGATAGCTATTGCTATTTCATTGTTTCTTGCTCTTATTATTGGGCTTAACTCA
ATTCTTGTGGGTTATCTCTCTGATATTAGCGCTCAATTACCCTCTGACTTTGTTCAGGGTGTTCAGTTAATTCTCCCGTCTAATGCGCTTCCCTGTTTTTATGTTATTCTCTCTGT
AAAGGCTGCTATTTTCATTTTTGACGTTAAACAAAAAATCGTTTCTTATTTGGATTGGGATAAATAATATGGCTGTTTATTTTGTAACTGGCAAATTAGGCTCTGGAAAGACGCT
CGTTAGCGTTGGTAAGATTCAGGATAAAATTGTAGCTGGGTGCAAAATAGCAACTAATCTTGATTTAAGGCTTCAAAACCTCCCGCAAGTCGGGAGGTTCGCTAAAACGCCT
CGCGTTCTTAGAATACCGGATAAGCCTTCTATATCTGATTTGCTTGCTATTGGGCGCGGTAATGATTCCTACGATGAAAATAAAAACGGCTTGCTTGTTCTCGATGAGTGCGG
TACTTGGTTTAATACCCGTTCTTGGAATGATAAGGAAAGACAGCCGATTATTGATTGGTTTCTACATGCTCGTAAATTAGGATGGGATATTATTTTTCTTGTTCAGGACTTATCT
ATTGTTGATAAACAGGCGCGTTCTGCATTAGCTGAACATGTTGTTTATTGTCGTCGTCTGGACAGAATTACTTTACCTTTTGTCGGTACTTTATATTCTCTTATTACTGGCTCGA
AAATGCCTCTGCCTAAATTACATGTTGGCGTTGTTAAATATGGCGATTCTCAATTAAGCCCTACTGTTGAGCGTTGGCTTTATACTGGTAAGAATTTGTATAACGCATATGATA
CTAAACAGGCTTTTTCTAGTAATTATGATTCCGGTGTTTATTCTTATTTAACGCCTTATTTATCACACGGTCGGTATTTCAAACCATTAAATTTAGGTCAGAAGATGAAATTAACT
AAAATATATTTGAAAAAGTTTTCTCGCGTTCTTTGTCTTGCGATTGGATTTGCATCAGCATTTACATATAGTTATATAACCCAACCTAAGCCGGAGGTTAAAAAGGTAGTCTCTC
AGACCTATGATTTTGATAAATTCACTATTGACTCTTCTCAGCGTCTTAATCTAAGCTATCGCTATGTTTTCAAGGATTCTAAGGGAAAATTAATTAATAGCGACGATTTACAGAA
GCAAGGTTATTCACTCACATATATTGATTTATGTACTGTTTCCATTAAAAAAGGTAATTCAAATGAAATTGTTAAATGTAATTAATTTTGTTTTCTTGATGTTTGTTTCATCATCTTC
TTTTGCTCAGGTAATTGAAATGAATAATTCGCCTCTGCGCGATTTTGTAACTTGGTATTCAAAGCAATCAGGCGAATCCGTTATTGTTTCTCCCGATGTAAAAGGTACTGTTAC
TGTATATTCATCTGACGTTAAACCTGAAAATCTACGCAATTTCTTTATTTCTGTTTTACGTGCAAATAATTTTGATATGGTAGGTTCTAACCCTTCCATTATTCAGAAGTATAATC
CAAACAATCAGGATTATATTGATGAATTGCCATCATCTGATAATCAGGAATATGATGATAATTCCGCTCCTTCTGGTGGTTTCTTTGTTCCGCAAAATGATAATGTTACTCAAAC
TTTTAAAATTAATAACGTTCGGGCAAAGGATTTAATACGAGTTGTCGAATTGTTTGTAAAGTCTAATACTTCTAAATCCTCAAATGTATTATCTATTGACGGCTCTAATCTATTAG
TTGTTAGTGCTCCTAAAGATATTTTAGATAACCTTCCTCAATTCCTTTCAACTGTTGATTTGCCAACTGACCAGATATTGATTGAGGGTTTGATATTTGAGGTTCAGCAAGGTGA
TGCTTTAGATTTTTCATTTGCTGCTGGCTCTCAGCGTGGCACTGTTGCAGGCGGTGTTAATACTGACCGCCTCACCTCTGTTTTATCTTCTGCTGGTGGTTCGTTCGGTATTTT
TAATGGCGATGTTTTAGGGCTATCAGTTCGCGCATTAAAGACTAATAGCCATTCAAAAATATTGTCTGTGCCACGTATTCTTACGCTTTCAGGTCAGAAGGGTTCTATCTCTGT
TGGCCAGAATGTCCCTTTTATTACTGGTCGTGTGACTGGTGAATCTGCCAATGTAAATAATCCATTTCAGACGATTGAGCGTCAAAATGTAGGTATTTCCATGAGCGTTTTTCC
TGTTGCAATGGCTGGCGGTAATATTGTTCTGGATATTACCAGCAAGGCCGATAGTTTGAGTTCTTCTACTCAGGCAAGTGATGTTATTACTAATCAAAGAAGTATTGCTACAAC
GGTTAATTTGCGTGATGGACAGACTCTTTTACTCGGTGGCCTCACTGATTATAAAAACACTTCTCAGGATTCTGGCGTACCGTTCCTGTCTAAAATCCCTTTAATCGGCCTCC
TGTTTAGCTCCCGCTCTGATTCTAACGAGGAAAGCACGTTATACGTGCTCGTCAAAGCAACCATAGTACGCGCCCTGTAGCGGCGCATTAAGCGCGGCGGGTGTGGTGGT
TACGCGCAGCGTGACCGCTACACTTGCCAGCGCCCTAGCGCCCGCTCCTTTCGCTTTCTTCCCTTCCTTTCTCGCCACGTTCGCCGGCTTTCCCCGTCAAGCTCTAAATCG
GGGGCTCCCTTTAGGGTTCCGATTTAGTGCTTTACGGCACCTCGACCCCAAAAAACTTGATTTGGGTGATGGTTCACGTAGTGGGCCATCGCCC

Supplementary References:

1. E. Stahl, T. G. Martin, F. Praetorius, H. Dietz, Facile and scalable preparation of pure and dense DNA origami solutions. *Angewandte Chemie* **53**, 12735-12740 (2014).
2. F. A. S. Engelhardt *et al.*, Custom-Size, Functional, and Durable DNA Origami with Design-Specific Scaffolds. *ACS nano*, (2019).